A RULE BASED MISSILE EVASION METHOD FOR FIGHTER AIRCRAFTS

A THESIS SUBMITTED TO
THE GRADUATE SCHOOL OF NATURAL AND APPLIED SCIENCES
OF
MIDDLE EAST TECHNICAL UNIVERSITY

BY

MUHAMMET SERT

IN PARTIAL FULLFILLMENT OF THE REQUIREMENTS
FOR
THE DEGREE OF MASTER OF SCIENCE
IN
ELECTRICAL AND ELECTRONICS ENGINEERING

MAY 2008

Approval of the thesis:

A RULE BASED MISSILE EVASION METHOD FOR FIGHTER AIRCRAFTS

submitted by **MUHAMMET SERT** in partial fulfillment of the requirements for the degree of **Master of Science in Electrical and Electronics Engineering Department, Middle East Technical University** by,

Prof. Dr. Canan Özgen _____
Dean, Graduate School of **Natural and Applied Sciences**

Prof. Dr. İsmet Erkmen _____
Head of Department, **Electrical and Electronics Engineering**

Prof. Dr. M. Kemal Leblebicioğlu _____
Supervisor, **Electrical and Electronics Engineering Dept., METU**

Examining Committee Members:

Prof. Dr. Mübeccel Demirekler _____
Electrical and Electronics Engineering Dept., METU

Prof. Dr. M. Kemal Leblebicioğlu _____
Electrical and Electronics Engineering Dept., METU

Prof. Dr. M. Kemal Özgören _____
Mechanical Engineering Dept., METU

Assist. Prof. Dr. Afşar Saranlı _____
Electrical and Electronics Engineering Dept., METU

Dr. Özgür Ateşoğlu _____
MGEO-MD-SGSM, ASELSAN

Date: **06.05.2008**

I hereby declare that all information in this document has been obtained and presented in accordance with academic rules and ethical conduct. I also declare that, as required by these rules and conduct, I have fully cited and referenced all material and results that are not original to this work.

Name, Last name : Muhammet Sert

Signature :

ABSTRACT

A RULE BASED MISSILE EVASION METHOD FOR FIGHTER AIRCRAFTS

Sert, Muhammet

M. Sc., Department of Electrical and Electronics Engineering

Supervisor: Prof. Dr. M. Kemal Leblebicioğlu

May 2008, 142 pages

In this thesis, a new guidance method for fighter aircrafts and a new guidance method for missiles are developed. Also, guidance and control systems of the aircraft and the missile used are designed to simulate the generic engagement scenarios between the missile and the aircraft. Suggested methods have been tested under excessive simulation studies.

The aircraft guidance method developed here is a rule based missile evasion method. The main idea to develop this method stems from the maximization of the miss distance for an engagement scenario between a missile and an aircraft. To do this, an optimal control problem with state and input dependent inequality constraints is solved and the solution method is applied on different problems that represent generic scenarios. Then, the solutions of the optimal control problems are used to extract rules. Finally, a method that uses the interpolation of the extracted rules is given to guide the aircraft.

The new guidance method developed for missiles is formulated by modifying the classical proportional navigation guidance method using the position estimates. The position estimation is obtained by utilization of a Kalman based filtering method, called interacting multiple models.

Keywords: Proportional Navigation Guidance, Optimal Control, Kalman Filter, Interacting Multiple Models

ÖZ

SAVAŞ UÇAKLARI İÇİN FÜZELERDEN KURAL TABANLI BİR KAÇMA YÖNTEMİ

Sert, Muhammet

Yüksek Lisans, Elektrik Elektronik Mühendisliği Bölümü

Tez Yöneticisi: Prof. Dr. M. Kemal Leblebicioğlu

Mayıs 2008, 142 sayfa

Bu tezde, savaş uçakları ve füzeler için birer yeni güdüm yöntemi geliştirilmiştir. Ayrıca, füze ve uçak arasındaki jenerik angajman senaryolarının benzetimini yapmak için, füze ve uçağın güdüm ve kontrol sistemleri tasarlanmıştır. Önerilen yöntemler, benzetim çalışmaları ile yoğun bir şekilde test edilmiştir.

Uçak için geliştirilen güdüm yöntemi füzelerden kural tabanlı bir kaçma yöntemidir. Füze ve uçak arasındaki bir angajman senaryosunda füzenin kaçırma mesafesinin olabildiğince artırılması gereği, bu yöntemi geliştirmenin amacını oluşturmaktadır. Bunun için, durum değişkenlerine ve girdilere bağlı eşitsizlik sınırlamaları olan bir optimal kontrol problemi çözülerek, jenerik senaryoları temsil eden birçok değişik durum için uygulanmıştır. Daha sonra, bu optimal kontrol problemlerinin çözümlerinden yola çıkarak birtakım kurallar çıkarılmıştır. Son olarak da, çıkarılan kuralları, ara değerleme yöntemi kullanarak uçağın güdüm işlevini yerine getiren bir yöntem önerilmiştir.

Füzeler için geliştirilen yeni güdüm yöntemi, klasik orantısal seyrüsefer güdüm yönteminin, konum kestirim değerleri kullanılarak geliştirilmesiyle oluşturulmuştur. Konum kestirimi ise, Kalman süzgeci tabanlı, etkileşimli çoklu model yöntemi ile gerçekleştirilmiştir.

Anahtar Kelimeler: Orantısal Seyrüsefer Güdüm, Optimal Kontrol, Kalman Süzgeci, Etkileşen Çoklu Modeller

To My Family

and

My Darling

ACKNOWLEDGMENTS

I would like to express my deepest gratitude to my supervisor Prof. Dr. M. Kemal LEBLEBİCİOĞLU for his encouragement, guidance, advice, criticism and insight throughout the research.

I wish to thank ASELSAN Inc. for facilities provided for the completion of this thesis.

I am grateful to all of the thesis jury committee members who contributed to this thesis with their valuable comments.

I would also like to express my profound appreciation to my family and my dear girlfriend for their endless support, patience and understanding. Their love is the meaning of life.

TABLE OF CONTENTS

LIST OF TABLES

TABLES

LIST OF FIGURES

FIGURES

LIST OF SYMBOLS AND ABBREVIATIONS

Symbol	*Definition*	*Unit*
V_T	True air speed	m/s
α	Angle of attack	deg
β	Angle of sideslip	deg
ϕ	Roll angle	deg
θ	Pitch angle	deg
ψ	Yaw angle	deg
p	Body axis roll rate	deg/s
q	Body axis pitch rate	deg/s
r	Body axis yaw rate	deg/s
x_E	x-position w.r.t. earth fixed frame	m
y_E	y-position w.r.t. earth fixed frame	m
z_E	z-position w.r.t. earth fixed frame	m
h	Altitude w.r.t. earth fixed frame ($h = -z_E$)	m
pow	Power setting (%)	-
δ_{th}	Throttle setting (0-1)	-
δ_e	Elevator setting	deg
δ_a	Aileron setting	deg
δ_r	Rudder setting	deg
ρ	Air density	kg/m^3
b	Reference wing span	m
$\bar{c}$	Mean aerodynamic chord	m
C_{l_T}	Total rolling moment coefficient	-
C_{m_T}	Total pitching moment coefficient	-
C_{n_T}	Total yawing moment coefficient	-
C_{X_T}	Total force coefficient along body x-axis	-

Symbol	*Definition*	*Unit*
C_{Y_T}	Total force coefficient along body y-axis	-
C_{Z_T}	Total force coefficient along body z-axis	-
F_T	Total instantaneous engine thrust	N
g	Gravitational constant	m/s^2
h_{eng}	Engine angular momentum	$kg.m^2/s$
I_x	Roll moment of inertia	$kg.m^2$
I_y	Pitch moment of inertia	$kg.m^2$
I_z	Yaw moment of inertia	$kg.m^2$
I_{xz}	Product moment of inertia	$kg.m^2$
I_{xy}	Product moment of inertia	$kg.m^2$
I_{yz}	Product moment of inertia	$kg.m^2$
$\overline{L}$	Rolling moment	N.m
$\overline{M}$	Pitching moment	N.m
$\overline{N}$	Yawing moment	N.m
m	Total aircraft mass	kg
M	Mach number	-
p_s	Static pressure	Pa
$\overline{q}$	Dynamic pressure	Pa
S	Reference wing area	m^2
T	Temperature	K
u	Velocity component along body x-axis	m/s
v	Velocity component along body y-axis	m/s
w	Velocity component along body z-axis	m/s
x_{cg}	Center of gravity location	m
x_{cg_r}	Reference center of gravity location	m
$\overline{X}$	Body x-axis force component	N
$\overline{Y}$	Body y-axis force component	N
$\overline{Z}$	Body z-axis force component	N

Abbreviation	*Definition*
1-D	One Dimensional
3-D	Three Dimensional
6-DOF	Six Degrees of Freedom
BCS	Body Coordinate System
CA	Constant Acceleration
CAS	Control Actuation System
CM	Countermeasure
CCM	Counter-Countermeasure
CV	Constant Velocity
ECS	Earth-fixed Coordinate System
EOM	Equations of Motion
HPF	High Pass Filter
HPNG	Hybrid Proportional Navigation Guidance
HOT	Higher Order Terms
IMM	Interacting Multiple Models
IMM-KF	Interacting Multiple Models - Kalman Filter
IR	InfraRed
KF	Kalman Filter
LOS	Line of Sight
LPF	Low Pass Filter
LQC	Linear Quadratic Controller
LQR	Linear Quadratic Regulator
LTI	Linear Time Invariant
MIMO	Multiple Input Multiple Output
NED	North-East-Down
NL	Nonlinear
PID	Proportional-Integral-Derivative
PIDNG	PID Navigation Guidance
PNG	Proportional Navigation Guidance
RF	Radio Frequency

Abbreviation	*Definition*
SCS	Stability Coordinate System
SLQT	Suboptimal Linear Quadratic Tracker
TM	Transformation Matrix
UV	Ultraviolet
WCS	Wind Coordinate System

CHAPTER 1

INTRODUCTION

Modern electronic warfare necessitates the usage of intelligently guided missiles or aircrafts since CM and CCM techniques are developing day by day. In a warfare scenario, CM is a technique applied by the aircraft under missile threat. This technique either requires dispensing of a convenient decoy creating a false target that deceives the sensor of the missile, or an evasion maneuver that forces the missile to reach its physical limits and hence no more able to track the aircraft.

In a real warfare environment, development of such CM and CCM techniques require many trials by using the real systems that cost too much to design and produce. However, verification and validation of effectiveness of a CM or a CCM necessitates those high cost trials to collect data. In order not to make high cost trials for every development phase of such techniques, modeling of the warfare environment is done and then, the models are used on a software package that simulates many possible scenarios by batch runs. If the modeling is successful to represent the real world warfare scenario participants, such as a missile, an aircraft, a CM, a CCM, the atmospheric effects, etc., then so many trials may be done by the software with a low cost. Hence, collecting enough data by real trials in the field gives way to verify and validate the models and so resulting in a very cost effective way of developing new CM or CCM techniques.

In this thesis, some engagement scenarios between a missile and a fighter aircraft are used to evaluate the effectiveness of the guidance models developed for both the missile and the aircraft. If a real engagement between an IR guided SAM and a fighter aircraft flying at low altitude with relatively low speed is considered, the pilot must take a decision to guide the aircraft or apply a CM technique in such a way that he/she can deceive the missile. The time to react for the pilot and the range-to-go of the missile are the basic limitations that necessitate the usage of a rule based or intelligent guidance system as soon as the threat is detected. As a CCM technique, the missile may use a powerful tracking and guidance method that discards the false targets created by flares. So, the result of the engagement depends on both of the guidance methods used by the missile and the aircraft.

The development of the guidance models comes after the formulation of the flight dynamics and implementation of the flight control systems. The derivation of the flight dynamics and the implementation of the guidance and control systems require some assumptions resulting in the approximate models that represent the real world within an error bound. Effects that are neglected according to assumptions while modeling of warfare scenario participants can be cited as aerodynamic coefficient uncertainties, the change in the mass, inertia and the center of gravity, thrust misalignment, change of the gravitational acceleration due to the instantaneous position of the vehicle and atmospheric disturbance effects. In fact, all of these factors affect the resultant state trajectory of the missile and the aircraft and so their level of success changes.

A typical homing type IR guided missile can be modeled by designing seeker, guidance, autopilot, CAS, airframe, rigid body dynamics and sensor subsystems that are shown in the Figure 1-1. In this thesis, the seeker is not modeled as it is used in a real missile system. Instead, the target position measurements are assumed to be done. In some cases, in addition to the position measurements, position, velocity and acceleration of the target are estimated by a tracker that is using interacting multiple models via Kalman filtering. Then, measured or estimated position is used

to calculate the necessary inputs for the guidance subsystem. Also, the sensor models used here are a standard first order low pass filters (LPFs) that are modeled with a time constant. It is assumed that these sensors are able to measure every state of the missile dynamical model that is shown as airframe in the Figure 1-1.

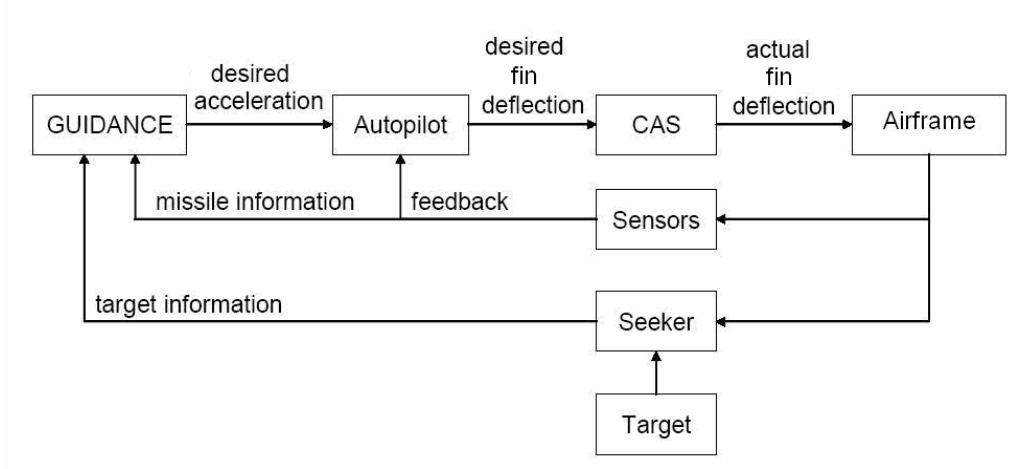

Figure 1-1: A generic homing type missile subsystems.

In the figure above, “missile information” represents the necessary states of the missile itself to use in the guidance subsystem, and “target information” represents the position information of the aircraft that is being tracked.

The states measured by the missile sensor are getting involved in the feedback loop of the autopilot and also they are fed to the guidance subsystem. Since the measured position of the missile fed to the guidance system is expressed in the BCS, it is transformed into the ECS in order to calculate the necessary guidance commands in this coordinate system. Then, these commands are transformed into the BCS and passed to the acceleration limiter and hence, the limited acceleration commands are used as the reference commands by the missile autopilot. The autopilot tracks the reference acceleration commands and hence it creates desired fin deflection

commands to the CAS. The CAS is modeled as a first order system by using a time constant value. Also, the CAS uses limitations for the demanded angles and rates so that the real world physical saturations are simulated.

Modeling of the aircraft subsystems has some similarities, as well as differences with the missile subsystems. The relative position of the missile with respect to the aircraft is determined by a warning sensor in terms of either measuring the LOS angles in azimuth and elevation and the range rate, or measuring the LOS rate in azimuth and elevation and estimating the range rate. The former is done by using RF sensors, whereas the latter is by IR or UV sensors. Also, the autopilot types used for an aircraft may not be acceleration autopilots. Instead, desired-height, desired-speed and desired-heading type autopilots may be used for the control of an aircraft. These autopilots are also called flight path control systems [2], [3], [14]. The rest of the subsystems can be modeled similar to the missile subsystems.

After briefly introducing the electronic warfare concept, the contents of the study is outlined in the following section.

1.1 Thesis Outline

Chapter 2: This chapter explains the derivation of EOM of aircraft with the necessary assumptions. First, the nonlinear EOM are derived. Then, the trim conditions, trim process and linearization are explained. Lastly, the decoupling of the state equations and brief information about the flight simulation of the aircraft are given.

Chapter 3: In this chapter, flight dynamics of a missile is summarized based on the study given in [13]. To do this, necessary assumptions are stated and the EOM of a skid-to-turn type missile are given.

Chapter 4: Autopilots designed for the aircraft are explained. For lateral and longitudinal autopilots, a classical control and a modern control technique are used.

The former is PID and the latter is LQR. By using these two techniques, local linear controllers are designed at some trim points in the flight envelope of the aircraft. Then, the control of nonlinear aircraft model is explained by using the local linear controllers via gain scheduling, by using LQR technique. Consequently, the performance results of these autopilot designs are given.

Chapter 5: In this chapter, the design of roll autopilot, normal acceleration and lateral acceleration autopilots are formulated. Consequently, the performances of these autopilots are illustrated.

Chapter 6: Applied missile guidance methods such as PNG, PIDNG and a new guidance method named as HPNG are formulated and their performances while tracking an aircraft are compared. The comparison method is based on three types of flight maneuvers whose details are given in the last section of the chapter.

Chapter 7: A rule based missile evasion method is formulated in the first part of this chapter. Then, a PNG based guidance (called anti-PNG) method is formulated to evaluate the performance of the rule-based method by comparing the miss distance obtained for some test scenarios that are given in chapter 8.

Chapter 8: Simulation studies to evaluate the performances of the proposed rule based missile evasion method and the anti-PNG method are given in this chapter. Also, the 3-D trajectories of the missile and the aircraft are given at the end of the chapter.

Chapter 9: A brief summary about the work done throughout the thesis studies is given as a conclusion and also some improvements are suggested as future work.

Appendix A: Modeling details of aerodynamics, engine, sensor, actuators and, mass and geometry properties for a fighter aircraft (F-16) are explained.

Appendix B: Missile design parameters such as the sensor and the actuators are given in this appendix.

CHAPTER 2

FLIGHT DYNAMICS OF AN AIRCRAFT

2.1 Introduction

In this chapter, nonlinear dynamical model of a fighter aircraft is derived. Derivation is based on [6], [16], [2] and [3]. Mass and metric data of the aircraft are given in Table A-3. Before getting into the detailed derivations, necessary definitions of coordinate systems and assumptions are explained.

2.1.1 Coordinate Systems

There are many types of coordinate systems used for modeling and simulation of aerospace vehicle dynamics. They are the inertial, the Earth, the geographic, the local-level, the velocity, the body, the stability and the wind coordinate systems. In this thesis, only four of these coordinate systems shown in Figure 2-1 are used to derive the model of an aircraft and a missile to do 6-DOF flight simulations in 3-D. Note that, all of the coordinate systems used are right handed. These coordinate systems are described as follows:

Earth-fixed Coordinate System (ECS): X_E and Y_E axes point to the North and East directions respectively and they are located on a plane tangent to the Earth's surface. As a consequence, Z_E axis points down to the center of the Earth, according

to the right-hand rule. In literature [2], [3], this coordinate system is also called as the local-level or the North-East-Down (NED) coordinate system.

Body Coordinate System (BCS): This coordinate system is assumed to be fixed to the center of gravity of the flight vehicle and moving with it. Its X_B axis points forward through the nose, Y_B axis through the starboard (right) wing and the Z_B axis downwards.

Stability Coordinate System (SCS): This coordinate system is obtained by a right handed rotation of the body coordinate axes around the Y_B axis at an amount of minus angle of attack, $-\alpha$. So, Y_S axis coincides with Y_B axis and X_S - Z_S axes are in the plane (which is called as the symmetry plane for most aircrafts) formed by X_B - Z_B axes. SCS is used for analyzing the effect of perturbations from steady-state flight.

Wind Coordinate System (WCS): Right handed rotation of the stability coordinate system around Z_S by an amount of sideslip angle, β, results in the wind coordinate system, so, Z_W axis coincides with Z_S, and X_W - Y_W axes lie in the plane formed by X_S - Y_S. Lift, drag and side forces are defined naturally in this coordinate system.

Remark:

Throughout the text, subscripts “E”, “B”, “S” and “W” are used on vectors or TMs in order to represent their relation with the ECS, BCS, SCS and WCS, respectively. In addition, TMs are represented with the capital letter “T” that has two capital letters as a subscript that determines related coordinate systems, i.e. T_{WB}.

The relations between these coordinate systems are shown in the following figure:

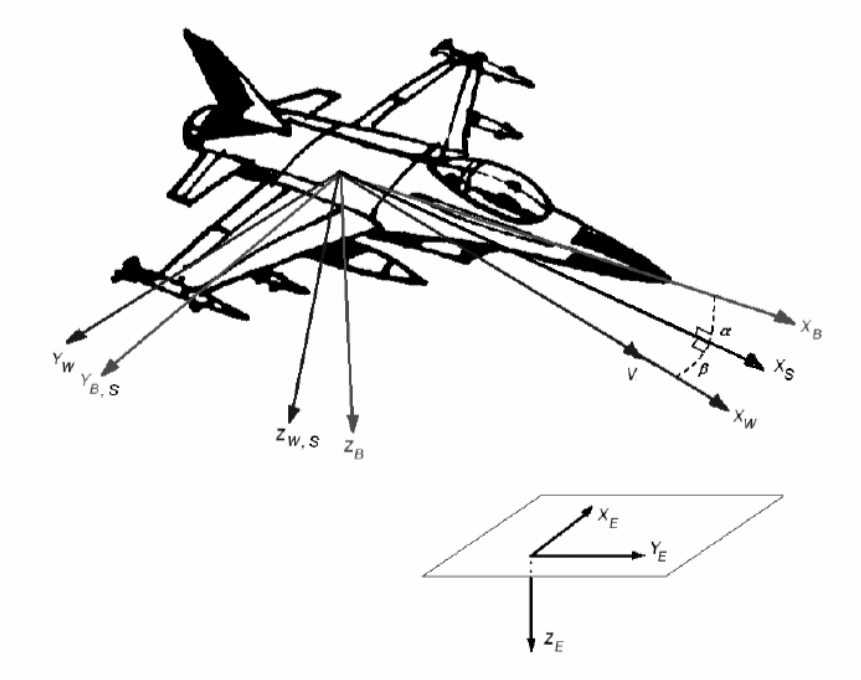

Figure 2-1: Earth-fixed, body, stability and wind coordinate systems

Coordinate TMs are used to transform a vector from one of the coordinate systems to another. These TMs are orthogonal and also taking their transpose corresponds to changing the sequence of transformation, i.e. $T_{WB}^{T} = T_{BW}$. Another property of TMs is that, consecutive transformations are contracted by canceling adjacent subscripts, i.e. $T_{BW} = T_{BS}T_{SW}$. For more properties, refer to [3].

The following TM is used to transform a vector expressed in ECS to BCS:

$$T_{BE} = \begin{bmatrix} \cos\psi\cos\theta & \sin\psi\cos\theta & -\sin\theta \\ \cos\psi\sin\theta\sin\phi - \sin\psi\cos\phi & \sin\psi\sin\theta\sin\phi + \cos\psi\cos\phi & \cos\theta\sin\phi \\ \cos\psi\sin\theta\cos\phi + \sin\psi\sin\phi & \sin\psi\sin\theta\cos\phi - \cos\psi\sin\phi & \cos\theta\cos\phi \end{bmatrix}, \quad (2\text{-}1)$$

where, ϕ, θ and ψ are called roll, pitch and yaw angles that define the orientation of the aircraft with respect to the ECS. These angles are known as Euler angles. In fact, T_{BE} is formed by multiplication of three planar rotation matrices:

$$T_{BE} = \begin{bmatrix} 1 & 0 & 0 \\ 0 & \cos\phi & \sin\phi \\ 0 & -\sin\phi & \cos\phi \end{bmatrix} \begin{bmatrix} \cos\theta & 0 & -\sin\theta \\ 0 & 1 & 0 \\ \sin\theta & 0 & \cos\theta \end{bmatrix} \begin{bmatrix} \cos\psi & \sin\psi & 0 \\ -\sin\psi & \cos\psi & 0 \\ 0 & 0 & 1 \end{bmatrix}. \quad (2\text{-}2)$$

It is apparent above that the sequence of the transformations is the yaw, pitch and roll when transforming a vector from ECS to BCS and vice versa. Briefly, starting from ECS, rotate about the Z_E axis by yaw (nose right), then rotate about the new Y-axis by pitch (nose up), and finally rotate about the new x-axis by roll (right wing down). Note that all of these rotations are positive according to the right hand rule.

The TMs that define the relation between BCS, SCS and WCS are formed by angle of attack α, and angle of sideslip β:

$$T_{SB} = \begin{bmatrix} \cos\alpha & 0 & \sin\alpha \\ 0 & 1 & 0 \\ -\sin\alpha & 0 & \cos\alpha \end{bmatrix}, \quad (2\text{-}3)$$

$$T_{WS} = \begin{bmatrix} \cos\beta & \sin\beta & 0 \\ -\sin\beta & \cos\beta & 0 \\ 0 & 0 & 1 \end{bmatrix}. \quad (2\text{-}4)$$

Since the transformation sequence between BCS and WCS is $BCS \xrightarrow{-\alpha} SCS \xrightarrow{\beta} WCS$, the TM that transforms a vector from BCS to WCS is given as follows:

$$T_{WB} = T_{WS} T_{SB} = \begin{bmatrix} \cos\alpha\cos\beta & \sin\beta & \sin\alpha\cos\beta \\ -\cos\alpha\sin\beta & \cos\beta & -\sin\alpha\sin\beta \\ -\sin\alpha & 0 & \cos\alpha \end{bmatrix}. \quad (2\text{-}5)$$

To define the angle of attack and sideslip, aircraft velocity vector components are used as:

$$\begin{aligned} V_T &= \sqrt{u^2 + v^2 + w^2} \\ \alpha &= \arctan\frac{w}{u} \\ \beta &= \arcsin\frac{v}{V_T} \end{aligned} \quad , \tag{2-6}$$

where, V_T is called as the true airspeed of the aircraft in BCS, and u, v and w are the components of velocity vector of the aircraft in BCS. Especially, V_T, α and β are useful to express the aerodynamic force and moment coefficients when multidimensional aerodynamic and thrust data look-up tables are given as function of these variables [2].

2.1.2 Assumptions

A number of assumptions have to be made before proceeding with the derivation of the EOM of the aircraft:

Assumption 1: The aircraft is a rigid body, which means that any two points on or within the airframe remain fixed with respect to each other. Mass change due to fuel consumption is neglected for the aircraft so its mass is taken as constant during the flight. This assumption is necessary to apply Newton's laws to derive the EOM.

Assumption 2: The Earth is flat and non-rotating and regarded as an inertial reference (that is non-rotating and non-accelerating relative to the average position of the fixed stars) [2]. This assumption is valid when dealing with the simulations of aircraft and missiles that fly with speed below Mach 5 [3]. So, the ECS is used as an inertial coordinate system for this flat Earth.

Assumption 3: Mass distribution of the aircraft is symmetric relative to the X_B - Z_B plane of BCS, meaning that the products of inertia I_{yz} and I_{xy} are equal to zero. This assumption is valid for most aircrafts.

Assumption 4: Angular momentum (h_{eng}) caused by the rotating machinery of the aircraft engine is assumed to act along the positive x-axis of the BCS.

Assumption 5: The engine of the aircraft is mounted so that the thrust point lies on the x-axis of the BCS.

Assumption 6: Gravity field is assumed to be uniform. In addition, the center of mass and the center of gravity of the aircraft are coincident.

Assumption 7: Still atmosphere i.e. no winds, no gusts.

Under the assumptions above, motion of the aircraft has 6-DOF (rotation and translation in three dimensions). The aircraft dynamics can be described by its position, orientation, velocity and angular velocity over time.

2.2 Nonlinear EOM

The EOM for an aircraft can be derived from Newton's 2nd Law of motion, which states that the summation of all external forces acting on a body must be equal to the time rate of change of its linear momentum relative to an inertial reference frame, and the summation of all external moments acting on a body must be equal to the time rate of change of its angular momentum relative to an inertial reference frame. According to **Assumption 2**, Newton's 2nd Law can be expressed in ECS by two vector equations:

$$\vec{F} = \frac{d}{dt}(m\vec{V})\Big|_E , \tag{2-7}$$

$$\vec{M} = \frac{d}{dt}(\vec{H})\Big|_E , \tag{2-8}$$

where, $\vec{F}$ represents the sum of all externally applied forces, m is the mass of the aircraft, $\vec{V}$ is the velocity vector, $\vec{M}$ represents the sum of all applied torques and $\vec{H}$ is the angular momentum. All of these four vectors are in BCS whereas the derivative is taken with respect to the ECS. In order to take the derivative in the BCS and express all the vectors in that coordinate system, Coriolis Theorem is used [2]. This theorem states that derivative of a vector relative to one reference frame is equal to derivative of the vector relative to a second reference frame plus cross product of rotation vector of the second reference frame relative to the first reference frame and the vector. For derivations of EOM, these two reference frames are represented with the BCS and the ECS.

The force equation above is used to derive the translational dynamics, and the moment equation is used to derive the rotational dynamics of the aircraft.

2.2.1 Translational Dynamics

Coriolis Theorem is applied to (2-7):

$$\vec{F} = \frac{d}{dt}(m\vec{V})\Big|_B + \vec{\omega} \times m\vec{V}, \tag{2-9}$$

where, $\vec{\omega}$ is the angular velocity of the aircraft with respect to the ECS, expressed in BCS. Formulating the vectors as the sum of their components with respect to the BCS gives:

$$\begin{aligned} \vec{V} &= u\vec{i} + v\vec{j} + w\vec{k} \\ \vec{\omega} &= p\vec{i} + q\vec{j} + r\vec{k} \end{aligned}, \tag{2-10}$$

where, $\vec{i}, \vec{j}$ and $\vec{k}$ are unit vectors along the aircraft's body axes X_B, Y_B and Z_B, respectively. Substituting (2-10) into (2-9) and considering **Assumption 1** results in:

$$\begin{aligned} F_x &= m(\dot{u} + qw - rv) \\ F_y &= m(\dot{v} + ru - pw) \\ F_z &= m(\dot{w} + pv - qu) \end{aligned}, \tag{2-11}$$

where, the external forces F_x, F_y and F_z depend on the weight vector $\vec{W}$, the aerodynamic force vector $\vec{R}$ and the thrust vector $\vec{T}$:

$$\vec{F} = \begin{bmatrix} F_x & F_y & F_z \end{bmatrix}^T = \vec{T} + \vec{W} + \vec{R}. \tag{2-12}$$

Thrust produced by the engine, F_T, acts along aircraft's X_B-axis (**Assumption 5**), which makes the thrust vector $\vec{T}$ equal to:

$$\vec{T} = \begin{bmatrix} T_x & T_y & T_z \end{bmatrix}^T = \begin{bmatrix} F_T & 0 & 0 \end{bmatrix}^T. \tag{2-13}$$

Weight vector points to the center of the Earth, lying along the Z_E axis of the ECS and the aerodynamic force vector has the components in all axes of the BCS:

$$\vec{W} = \begin{bmatrix} W_x & W_y & W_z \end{bmatrix}^T = T_{BE} \begin{bmatrix} 0 & 0 & mg \end{bmatrix}^T, \tag{2-14}$$

$$\vec{R} = \begin{bmatrix} X & Y & Z \end{bmatrix}^T, \tag{2-15}$$

where, g is the gravity constant. In Appendix A.1 the aerodynamic forces X, Y and Z are formulated by citing the effects that create these forces.

Hence, combining the last 4 equations results in the translational dynamic equations in BCS:

$$\begin{aligned} X + F_T - mg\sin\theta &= m(\dot{u} + qw - rv) \\ Y + mg\sin\phi\cos\theta &= m(\dot{v} + ru - pw) \\ Z + mg\cos\phi\cos\theta &= m(\dot{w} + pv - qu) \end{aligned}. \tag{2-16}$$

2.2.2 Rotational Dynamics

Using Coriolis Theorem, (2-8) can be written as:

$$\vec{M} = \frac{d}{dt}(\vec{H})\Big|_B + \vec{\omega} \times \vec{H} \,. \tag{2-17}$$

In the BCS, under **Assumption 1** and **Assumption 4**, angular momentum can be expressed as:

$$\vec{H} = I\vec{\omega} + \begin{bmatrix} h_{eng} & 0 & 0 \end{bmatrix}^T, \tag{2-18}$$

where, according to the **Assumption 3**, inertia matrix is defined as [2]:

$$\hat{I} = \begin{bmatrix} I_x & 0 & -I_{xz} \\ 0 & I_y & 0 \\ -I_{xz} & 0 & I_z \end{bmatrix}. \tag{2-19}$$

Expanding (2-17) using (2-18) results in:

$$\begin{aligned} M_x &= \dot{p}I_x - \dot{r}I_{xz} + qr(I_z - I_y) - pqI_{xz} \\ M_y &= \dot{q}I_y + pr(I_x - I_z) + (p^2 - r^2)I_{xz} + rh_{eng} \,, \\ M_z &= \dot{r}I_z - \dot{p}I_{xz} + pq(I_y - I_x) + qrI_{xz} - qh_{eng} \end{aligned} \tag{2-20}$$

where, the external moments M_x, M_y and M_z are the components of $\vec{M}$ along the body coordinate axes. These moments are due to aerodynamics and thrust since there is no moment caused by the gravity according to the **Assumption 6**. As a result, the external moments are:

$$\begin{aligned} M_x &= \overline{L} + L_T \\ M_y &= \overline{M} + M_T \,, \\ M_z &= \overline{N} + N_T \end{aligned} \tag{2-21}$$

where, $\overline{L}$, $\overline{M}$ *and* $\overline{N}$ are the aerodynamic moments and L_T, M_T and N_T are the moments due to the thrust. In **Assumption 5**, it is stated that there is no moment due to thrust, so:

$$L_T = M_T = N_T = 0. \tag{2-22}$$

Hence, combining (2-20) and (2-21), the rotational dynamic equations in BCS are formed as:

$$\begin{aligned} \overline{L} &= \dot{p}I_x - \dot{r}I_{xz} + qr(I_z - I_y) - pqI_{xz} \\ \overline{M} &= \dot{q}I_y + pr(I_x - I_z) + (p^2 - r^2)I_{xz} + rh_{eng} \\ \overline{N} &= \dot{r}I_z - \dot{p}I_{xz} + pq(I_y - I_x) + qrI_{xz} - qh_{eng} \end{aligned}. \tag{2-23}$$

2.2.3 Gathering the EOM

In addition to the translational and rotational acceleration equations, two more equations are needed to define the translational and rotational rates. These equations formulate the transformation of the velocity vector $\vec{V}$ from BCS to ECS and the transformation of the angular velocity vector $\vec{\omega}$ to the Euler rates $[\dot{\phi} \quad \dot{\theta} \quad \dot{\psi}]^T$ as follows:

$$[\dot{x}_E \quad \dot{y}_E \quad \dot{z}_E]^T = T_{EB}[u \quad v \quad w]^T, \tag{2-24}$$

$$\begin{bmatrix} \dot{\phi} \\ \dot{\theta} \\ \dot{\psi} \end{bmatrix} = \begin{bmatrix} 1 & \tan\theta\sin\phi & \tan\theta\cos\phi \\ 0 & \cos\phi & -\sin\phi \\ 0 & \dfrac{\sin\phi}{\cos\theta} & \dfrac{\cos\phi}{\cos\theta} \end{bmatrix} \begin{bmatrix} p \\ q \\ r \end{bmatrix}, \tag{2-25}$$

where, $[x_E \quad y_E \quad z_E]^T$ defines the position and $[\phi \quad \theta \quad \psi]^T$ defines the orientation of the aircraft with respect to ECS.

The EOM derived up to here are now written as a system of 12 scalar first order differential equations as follows:

$$\begin{aligned}
\dot{u} &= rv - qw - g\sin\theta + \frac{1}{m}(X + F_T) \\
\dot{v} &= pw - ru + g\sin\phi\cos\theta + \frac{1}{m}Y \\
\dot{w} &= qu - pv + g\cos\phi\cos\theta + \frac{1}{m}Z
\end{aligned} \quad , \tag{2-26}$$

$$\begin{aligned}
\dot{p} &= (c_1 r + c_2 p)q + c_3\bar{L} + c_4(\bar{N} + h_{eng}q) \\
\dot{q} &= c_5 pr - c_6(p^2 - r^2) + c_7(\bar{M} - h_{eng}r) \\
\dot{r} &= (c_8 p - c_2 r)q + c_4\bar{L} + c_9(\bar{N} + h_{eng}q)
\end{aligned}, \tag{2-27}$$

$$\begin{aligned}
\dot{\phi} &= p + \tan\theta(q\sin\phi + r\cos\phi) \\
\dot{\theta} &= q\cos\phi - r\sin\phi \\
\dot{\psi} &= \frac{q\sin\phi + r\cos\phi}{\cos\theta}
\end{aligned} \quad , \tag{2-28}$$

$$\begin{aligned}
\dot{x}_E &= u\cos\theta\cos\psi + u(\sin\phi\sin\theta\cos\psi - \cos\phi\sin\psi) + w(\sin\phi\sin\theta\cos\psi + \sin\phi\sin\psi) \\
\dot{y}_E &= u\cos\theta\sin\psi + v(\sin\phi\sin\theta\sin\psi + \cos\phi\cos\psi) + w(\cos\phi\sin\theta\sin\psi - \sin\phi\cos\psi) \\
\dot{z}_E &= -u\sin\theta + v\sin\phi\cos\theta + w\cos\phi\cos\theta
\end{aligned}, \tag{2-29}$$

where, the moment of inertia components are given as [2]:

$$\begin{aligned}
c_1 &= \frac{(I_y - I_z)I_z - I_{xz}^2}{I_x I_z - I_{xz}^2} & c_4 &= \frac{I_{xz}}{I_x I_z - I_{xz}^2} & c_7 &= \frac{1}{I_y} \\
c_2 &= \frac{(I_x - I_y + I_z)I_{xz}}{I_x I_z - I_{xz}^2} & c_5 &= \frac{I_z - I_x}{I_y} & c_8 &= \frac{I_x(I_x - I_y) + I_{xz}^2}{I_x I_z - I_{xz}^2} \\
c_3 &= \frac{I_z}{I_x I_z - I_{xz}^2} & c_6 &= \frac{I_{xz}}{I_y} & c_9 &= \frac{I_x}{I_x I_z - I_{xz}^2}
\end{aligned}. \tag{2-30}$$

2.2.4 Translational Dynamic Equations in WCS

For control system design, it is more convenient to express the force equations in the WCS instead of the BCS [2]. To do this, the derivative of α, β and V_T are used as a first step to get the following transformations:

$$\begin{aligned} \dot{V}_T &= \frac{u\dot{u} + v\dot{v} + w\dot{w}}{V_T} \\ \dot{\alpha} &= \frac{u\dot{w} - w\dot{u}}{u^2 + w^2} \\ \dot{\beta} &= \frac{\dot{v}V_T - v\dot{V}_T}{V_T^2 \cos\beta} \end{aligned} \quad . \tag{2-31}$$

Substituting (2-26) and (2-6) in (2-31) and neglecting some small terms gives the force equation in the WCS as [2]:

$$\begin{aligned} \dot{V}_T &= \frac{1}{m}(-D + F_T \cos\alpha\cos\beta + mg_1) \\ \dot{\alpha} &= q - (p\cos\alpha + r\sin\alpha)\tan\beta + \frac{1}{mV_T\cos\beta}(-L^* - F_T\sin\alpha + mg_3), \\ \dot{\beta} &= p\sin\alpha - r\cos\alpha + \frac{1}{mV_T}(Y^* - F_T\cos\alpha\sin\beta + mg_2) \end{aligned} \tag{2-32}$$

where, drag D, side force Y^* and lift force L^* are defined as:

$$\begin{bmatrix} -D & Y^* & -L^* \end{bmatrix}^T = T_{WB}\begin{bmatrix} X & Y & Z \end{bmatrix}^T, \tag{2-33}$$

and the gravity components g_1, g_2 and g_3 are defined as:

$$\begin{bmatrix} g_1 & g_2 & g_3 \end{bmatrix}^T = T_{WB}T_{BE}\begin{bmatrix} 0 & 0 & g \end{bmatrix}^T. \tag{2-34}$$

2.2.5 Nonlinear State-Space Model

For the aircraft model, the state vector whose components are associated with (2-27), (2-28), (2-29) and (2-32) is composed of the following states:

$$\bar{x} = \begin{bmatrix} V_T & \alpha & \beta & \phi & \theta & \psi & p & q & r & x_E & y_E & h & pow \end{bmatrix}^T, \qquad (2\text{-}35)$$

where, height h is used instead of $-z_E$ in order to work with the distances above the ground, and the last state, *pow,* represents actual engine power level since thrust response is also modeled for the nonlinear aircraft model [2]. The engine model is explained in Appendix A.3.

Dependency of aerodynamic force and moment components on the control surface deflections is used to determine the control vector of the nonlinear aircraft model as:

$$\bar{u} = \begin{bmatrix} \delta_{th} & \delta_e & \delta_a & \delta_r \end{bmatrix}^T. \qquad (2\text{-}36)$$

Note that, throttle setting δ_{th} is used as a control input to include the effect of the thrust produced by the engine.

Hence, the set of coupled, nonlinear, first-order ordinary differential equations that form the nonlinear aircraft model are represented by the vector equation:

$$\dot{\bar{x}} = \bar{f}(\bar{x}, \bar{u}), \qquad (2\text{-}37)$$

and the output equations are represented by the vector equation:

$$\bar{y} = \bar{h}(\bar{x}, \bar{u}), \qquad (2\text{-}38)$$

where, both $\bar{f}$ and $\bar{h}$ are nonlinear vector functions.

2.3 Trimming for the Steady-State Flight

In the theory of nonlinear systems, solution(s) of the following equation is (are) defined as the equilibrium point(s) of the autonomous (with no external control inputs) time-invariant system [2]:

$$\dot{\bar{x}}_{eq} = \bar{0} = \bar{f}(\bar{x}_{eq}, \bar{u}_{eq}), \tag{2-39}$$

where, $\bar{u}_{eq}$ is either zero or constant. At an equilibrium point, the system is said to be "at rest" since the derivatives of all the variables are zero. As a result, behavior of the system at rest is examined by slightly perturbing some of the variables. For example, if the state trajectory of an aircraft departs rapidly from an equilibrium point after a small perturbation of pitch attitude command given by a human pilot, then control of the aircraft by the pilot is said to be improbable.

Steady-state flight for an aircraft is defined as a condition in which all linear and angular velocity components are constant or zero, and all acceleration components are zero [2]. In other words, in equilibrium or a steady-state condition, vector sum of all the forces acting on the aircraft are equal to zero. Besides, the vector sum of all the moments acting on the aircraft is equal to zero in an equilibrium condition, which is also called as a trim condition.

The trim conditions for the nonlinear aircraft model used in this study are formulated with the following equations:

$$\begin{bmatrix} \dot{V}_T & \dot{\alpha} & \dot{\beta} & \dot{p} & \dot{q} & \dot{r} \end{bmatrix}^T = \bar{0}, \tag{2-40}$$

$$\begin{bmatrix} \delta_{th} & \delta_e & \delta_a & \delta_r \end{bmatrix}^T = const, \tag{2-41}$$

$$\begin{bmatrix} \dot{\phi} & \dot{\theta} & \dot{\psi} & \phi & p & q & r \end{bmatrix}^T = \bar{0}. \tag{2-42}$$

Note that, equations (2-40) and (2-41) are the result of the steady-state flight condition definition and equation (2-42) is the result of a special trim condition called as steady-state wings-level flight condition [2]. So, all the trim conditions of the nonlinear aircraft model referred in this text are the steady-state wings-level flight conditions. It is important to note that, the airspeed (V_T) and the altitude (h) are constant at the wings level flight.

In general, because of the nonlinearity in the equations that describe the trim conditions, it is too complicated to find a steady-state solution by solving these equations analytically. Instead, digital computers are used to apply numerical methods to find the solution(s). If multiple solutions exist, a feasible solution can be found by setting realistic constraints on the state and control variables [2]. Resulting steady-state values of the states and inputs are used as initial conditions for nonlinear simulations or as operating points for linearization of the nonlinear aircraft model [11].

A trim algorithm tries to find a solution for a user specified speed-altitude (V_T, h) pair by iteratively adjusting independent variables δ_{th}, δ_e, δ_a, δ_r, α and β so that following scalar cost function $J(\dot{\bar{x}})$ is minimized:

$$J(\dot{\bar{x}}) = k_1 \dot{V}_T^2 + k_2 \dot{\alpha}^2 + k_3 \dot{\beta}^2 + k_4 \dot{p}^2 + k_5 \dot{q}^2 + k_6 \dot{r}^2 . \tag{2-43}$$

Throughout the minimization, weight coefficients k_1 to k_6 are chosen as 1, 100, 100, 10, 10 and 10, respectively [2]. It is also important to note that, equation (2-42) and the following flight path constraint condition

$$\gamma\big|_{\phi=\beta=0} = \theta - \alpha = 0 , \tag{2-44}$$

are all used as the constraints to find a feasible solution where γ is the flight path angle. Note that, if the minimization is successfully done with a suitable termination condition, β takes a value very close to zero in order to zero out any side force and as a result, flight path angle condition is satisfied [2].

For the minimization, simplex algorithm is used as the multivariable numerical optimization algorithm since it performs well on this problem [2]. Details and implementation of this algorithm can be found in [2] and [8].

2.4 LTI State-Space Model

A linear state-space equivalent of the nonlinear state-space model about a trim point is obtained using a first-order multivariable Taylor series expansion about that trim point. The resulting linear LTI system that represents aircraft dynamics for small perturbations about the trim condition is given by the state and output equations:

$$\begin{aligned} \delta\dot{\bar{x}} &= A\,\delta\bar{x} + B\,\delta\bar{u} \\ \delta\bar{y} &= C\,\delta\bar{x} + D\,\delta\bar{u} \end{aligned} . \tag{2-45}$$

Elements of the constant coefficient matrices in the linearized dynamic equations are the gradients evaluated at the trim values $\bar{x}_{eq}$ and $\bar{u}_{eq}$:

$$\begin{aligned} A &\equiv \left.\frac{\partial \bar{f}(\bar{x},\bar{u})}{\partial \bar{x}}\right|_{\substack{\bar{x}=\bar{x}_{eq} \\ \bar{u}=\bar{u}_{eq}}} = n\times n\ matrix \qquad B \equiv \left.\frac{\partial \bar{f}(\bar{x},\bar{u})}{\partial \bar{u}}\right|_{\substack{\bar{x}=\bar{x}_{eq} \\ \bar{u}=\bar{u}_{eq}}} = n\times m\ matrix \\ C &\equiv \left.\frac{\partial \bar{h}(\bar{x},\bar{u})}{\partial \bar{x}}\right|_{\substack{\bar{x}=\bar{x}_{eq} \\ \bar{u}=\bar{u}_{eq}}} = l\times n\ matrix \qquad D \equiv \left.\frac{\partial \bar{h}(\bar{x},\bar{u})}{\partial \bar{u}}\right|_{\substack{\bar{x}=\bar{x}_{eq} \\ \bar{u}=\bar{u}_{eq}}} = l\times m\ matrix \end{aligned} , \tag{2-46}$$

where n is the number of the elements in the state vector, m is the number of elements in the control vector and l is the number of elements in the output vector. The gradients are obtained numerically by perturbing each state and control input independently and recording the changes in the trimmed state and output equations. The matrices A, B, C and D are called as the LTI state-space coefficient matrices.

Derivation of the LTI state-space model that represents the nonlinear aircraft state-space model about the trim point ($\bar{x}_{eq}, \bar{u}_{eq}$) can be summarized as follows:

First, define the states and inputs as the sum of the trim and the small perturbation components:

$$\begin{aligned} \bar{x} &\cong \bar{x}_{eq} + \delta\bar{x} \\ \bar{u} &\cong \bar{u}_{eq} + \delta\bar{u} \\ \dot{\bar{x}} &= \bar{f}(\bar{x}, \bar{u}) \\ \dot{\bar{x}}_{eq} &= \bar{f}(\bar{x}_{eq}, \bar{u}_{eq}) \end{aligned} \quad . \tag{2-47}$$

Then, derivative of the perturbed state is taken:

$$\begin{aligned} \delta\dot{\bar{x}} &= \dot{\bar{x}} - \dot{\bar{x}}_{eq} = \bar{f}(\bar{x}, \bar{u}) - \bar{f}(\bar{x}_{eq}, \bar{u}_{eq}) \\ &= \bar{f}(\bar{x} - \bar{x}_{eq} + \bar{x}_{eq}, \bar{u} - \bar{u}_{eq} + \bar{u}_{eq}) - \bar{f}(\bar{x}_{eq}, \bar{u}_{eq}) . \\ &= \bar{f}(\bar{x}_{eq} + \delta\bar{x}, \bar{u}_{eq} + \delta\bar{u}) - \bar{f}(\bar{x}_{eq}, \bar{u}_{eq}) \end{aligned} \tag{2-48}$$

After that, the Taylor series expansion around the equilibrium point $(\bar{x}_{eq}, \bar{u}_{eq})$ for the first expression on the right hand side of the equation above is used:

$$\delta\dot{\bar{x}} = \bar{f}(\bar{x}_{eq}, \bar{u}_{eq}) + \frac{\partial\bar{f}(\bar{x}, \bar{u})}{\partial\bar{x}}\bigg|_{\substack{\bar{x}=\bar{x}_{eq} \\ \bar{u}=\bar{u}_{eq}}} \delta\bar{x} + \frac{\partial\bar{f}(\bar{x}, \bar{u})}{\partial\bar{u}}\bigg|_{\substack{\bar{x}=\bar{x}_{eq} \\ \bar{u}=\bar{u}_{eq}}} \delta\bar{u} + H.O.T. - \bar{f}(\bar{x}_{eq}, \bar{u}_{eq}) . \tag{2-49}$$

After cancellation and ignoring the HOT, equation takes the form of:

$$\delta\dot{\bar{x}} \approx \frac{\partial\bar{f}(\bar{x}, \bar{u})}{\partial\bar{x}}\bigg|_{\substack{\bar{x}=\bar{x}_{eq} \\ \bar{u}=\bar{u}_{eq}}} \delta\bar{x} + \frac{\partial\bar{f}(\bar{x}, \bar{u})}{\partial\bar{u}}\bigg|_{\substack{\bar{x}=\bar{x}_{eq} \\ \bar{u}=\bar{u}_{eq}}} \delta\bar{u} . \tag{2-50}$$

Let

$$A \cong \frac{\partial\bar{f}(\bar{x}, \bar{u})}{\partial\bar{x}}\bigg|_{\substack{\bar{x}=\bar{x}_{eq} \\ \bar{u}=\bar{u}_{eq}}} \quad and \quad B \cong \frac{\partial\bar{f}(\bar{x}, \bar{u})}{\partial\bar{u}}\bigg|_{\substack{\bar{x}=\bar{x}_{eq} \\ \bar{u}=\bar{u}_{eq}}} , \tag{2-51}$$

then,

$$\delta\dot{\bar{x}} \approx A\delta\bar{x} + B\delta\bar{u} . \tag{2-52}$$

Similarly, C and D matrices can be found by applying the Taylor series expansion to the vector function $\bar{h}$ about the same trim point.

Hence, the following LTI model is obtained if only the states variables are used as outputs, since C matrix turns out to be the identity matrix and D matrix is of no use:

$$\begin{aligned} \delta\dot{\bar{x}} &\approx A\delta\bar{x} + B\delta\bar{u} \\ \delta\bar{y} &= \delta\bar{x} \end{aligned} . \tag{2-53}$$

A useful subroutine to calculate the A, B, C and D matrices can be found in [2] and [8]. If the EOM of the aircraft are implemented in Matlab/Simulink, an alternative way to find the trim points and the linearized model of the aircraft is to use built-in functions "trim" and "linmod" that are available in Matlab/Simulink [11], [9] and [12]. Here, the former method given in [2] is used to find the matrices A and B.

2.5 Decoupling of the State-Space Models

Decoupling refers to the separation of EOMs into two independent sets. One set describes longitudinal motion (pitching, and translation in the x-z plane) and the other set describes lateral-directional motion (rolling, and side-slipping and yawing) of the aircraft. In analytical studies, decoupled equations are very much easier to work with. Decoupling occurs in both nonlinear and LTI state-space equations. Here, only the decoupling of the LTI state-space equations just after the trim and the linearization processes is used. If the entries of the LTI state-space coefficient matrices that represent the relation of lateral state/input variables with longitudinal state/input variables are small enough to be neglected, then the longitudinal and the lateral-directional equations are decoupled (see *Remark-2* below). So, the longitudinal states and controls are:

$$\begin{aligned} \bar{x}_{long} &= \begin{bmatrix} V_T & h & \alpha & \theta & q & pow \end{bmatrix}^T \\ \bar{u}_{long} &= \begin{bmatrix} \delta_{th} & \delta_e \end{bmatrix}^T \end{aligned} , \tag{2-54}$$

and the lateral-directional states and controls are:

$$\begin{aligned} \bar{x}_{lat} &= [\beta \quad \phi \quad p \quad r \quad \psi]^T \\ \bar{u}_{lat} &= [\delta_a \quad \delta_r]^T \end{aligned} \quad . \tag{2-55}$$

Remark-1: Although the LTI state-space models given above represent an aircraft dynamics for small perturbations about a trim condition, the symbol "δ" is not used in front of the state and control variables from now on. Since, the LTI models are used for the design purposes of the aircraft flight control systems, the symbol "δ" representing the small signal value of a state or a control variable is discarded. Also, throughout the aircraft autopilot design processes, the word "lateral" is used instead of the expression "lateral-directional".

Remark-2: An example of the coupling between the lateral-directional and longitudinal motions are represented with the orange colored entries of the system matrix that are shown in Table 2-1. Here, the state and the control variables of the coupled LTI model that is obtained by equation (2-53) are given as follows:

$$\begin{aligned} \bar{x} &= [V_T \quad h \quad \alpha \quad \theta \quad q \quad pow \quad \beta \quad \phi \quad p \quad r \quad \psi]^T \\ \bar{u} &= [\delta_{th} \quad \delta_e \quad \delta_a \quad \delta_r] \end{aligned} \quad . \tag{2-56}$$

Table 2-1: System matrix, A, for the trim point given in Figure 4-3

-0.019	0	57.710	-31.694	-0.353	0.382	0	0	0	0	0
0	0	-565.601	565.601	0	0	0	0	0	0	0
0	0	-1.253	0	0.914	0	0	0	0	0	0
0	0	0	0	1.000	0	0	0	0	0	0
0	0	-2.032	0	-1.436	0	0	0	0	-0.003	0
0	0	0	0	0	-1.000	0	0	0	0	0
0	0	0	0	0	0	-0.320	0.055	0.029	-0.993	0
0	0	0	0	0	0	0	0	1.000	0.029	0
0	0	0	0	0.0003	0	-26.330	0	-3.838	0.649	0
0	0	0	0	0.003	0	11.844	0	-0.017	-0.517	0
0	0	0	0	0	0	0	0	0	1.000	0

Note that, after decoupling, the upper left 6-by-6 matrix shown with the yellow color in Table 2-1 is the longitudinal system matrix, and the lower right 5-by-5 matrix shown with turquoise color is the lateral-directional system matrix.

It is obvious that there is a coupling between roll rate (p) and pitch rate (q), and also between yaw rate (r) and pitch rate (q). However, these couplings can be neglected since magnitudes of the entries (orange colored) of the system matrix that represent the coupled variables are small enough. On the other hand, there is no coupling between LTI models for the input matrix (see Table 2-2).

Table 2-2: Input matrix, B, for the trim point given in Figure 4-3

0	0.219	0	0
0	0	0	0
0	-0.002	0	0
0	0	0	0
0	-0.217	0	0
33.792	0	0	0
0	0	0	0.001
0	0	0	0
0	0	-0.870	0.157
0	0	-0.039	-0.076
0	0	0	0

Although this example illustrates the decoupling of the lateral-directional and longitudinal LTI models found for the trim point # 5 (see Figure 4-3), similar assumption is also applicable for the rest of the 11 trim points.

2.6 Flight Simulation

In order to simulate the flight of the aircraft to have an idea about how the state trajectory (i.e. the position and the orientation of the aircraft in 3-D) evolves, a numerical integration method is used. Both the linear and the nonlinear state-space

equations that are in the form of an initial value problem can be solved with a numerical integration method. As mentioned before, initial values of the states and controls can be found by the trimming process.

The state trajectory of the aircraft model changes continuously since the model belongs to a physical system and the stored energy of this system is described by the state variables. However, the numerical solution to the initial value problem by the numerical integration method implies calculating discrete sequential values of the state trajectory. Discrete time instants can be chosen based on either fixed time step or variable time step. If the fixed time step is not specified properly by considering stiffness of the equations, then the solution may not converge or error made by the approximation method of the algorithm is magnified.

By considering spread of time constants in the system that models the aircraft, the flight simulations are done based on an appropriate fixed time step by using Runge-Kutta method ("Runge's fourth-order rule") as the numerical integration algorithm. Details of this algorithm can be found in [2] and also in Matlab/Simulink documentation [12].

CHAPTER 3

FLIGHT DYNAMICS OF A MISSILE

3.1 Introduction

Derivation of flight dynamics of a missile is similar to the derivation of an aircraft's flight dynamics. Important differences stem from the symmetry axes of the vehicle.

In the first part of this chapter, assumptions and the important points to derive the flight dynamics of a canard controlled, skid-to-turn type missile that are formulated in [13] are summarized. Since a detailed derivation of flight dynamics of an aircraft has been given in Chapter 2, only the resultant LTI state-space models obtained after trimming, linearization and decoupling processes are given here.

In the second part of the chapter, based on the LTI state-space models derived in [13], missile flight control system design details are explained.

It is important to note that, the same coordinate systems defined for the aircraft are also applicable for the missile. In addition, **Assumption 1**, **Assumption 2**, **Assumption 6** and

Assumption 7 holds for the missile, whereas **Assumption 4** and **Assumption 5** are not applicable. Besides, **Assumption 3** is modified such that the missile has three symmetry axes that coincide with its body axes, so $I_{xy} = I_{xz} = I_{yz} = 0$. Also, due to

the symmetry of the missile used in this study, $I_y = I_z$. As a result, inertia matrix is simplified with these equations.

3.2 LTI State-Space Model

As illustrated with a design example in [13], the numerical values of the matrices that construct the linear state-space model for the missile used throughout this thesis are calculated at a single trim condition where Mach = 0.86 and h = 5000 m.

In order to derive the linearized and decoupled state-space model, some extra assumptions are also needed [13]:

- Angle of attack and sideslip and the fin deflection angles are assumed to be small ($\alpha, \beta, \delta_a, \delta_e \delta_r < 15^\circ$),
- Rolling motion is constant and very small ($\phi \le 5^\circ$, $p \le 5^\circ / s$),
- Gravitational acceleration components in the translational dynamic equations are assumed to be external disturbances.

Considering these assumptions with the small angle approximations and ignoring the HOT, linearized and decoupled state space representations are given as follows:

Roll Plane State Equations:

$$\begin{bmatrix} \dot{\phi} \\ \dot{p} \end{bmatrix} = \begin{bmatrix} 0 & 1 \\ 0 & -0.10236 \end{bmatrix} \begin{bmatrix} \phi \\ p \end{bmatrix} + \begin{bmatrix} 0 \\ 132.89 \end{bmatrix} \delta_a . \tag{3-1}$$

Pitch Plane State Equations:

$$\begin{bmatrix} \dot{w} \\ \dot{q} \end{bmatrix} = \begin{bmatrix} -0.41362 & 275.12 \\ -0.057149 & -1.0471 \end{bmatrix} \begin{bmatrix} w \\ q \end{bmatrix} + \begin{bmatrix} 21.51 \\ -29.201 \end{bmatrix} \delta_e . \tag{3-2}$$

Yaw Plane State Equations:

$$\begin{bmatrix} \dot{v} \\ \dot{r} \end{bmatrix} = \begin{bmatrix} -0.41362 & -275.12 \\ 0.057149 & -1.0471 \end{bmatrix} \begin{bmatrix} v \\ r \end{bmatrix} + \begin{bmatrix} 21.51 \\ 29.201 \end{bmatrix} \delta_r \, . \tag{3-3}$$

Remark: Although the LTI state-space models given above represent missile dynamics for small perturbations about the trim condition, the symbol "δ" is not used in front of the state and control variables of the missile. However, that symbol is used to discriminate the state and control variables of the LTI and the nonlinear state-space models of aircraft. Since, only the LTI models are used for the design purposes of missile flight control systems and missile guidance systems, the symbol "δ" is discarded.

Normally, there are 12 nonlinear state equations that model the dynamics of the missile. The linear equations given at (3-1), (3-2) and (3-3) represent 6 of the nonlinear state equations. The rest of them considering the assumptions and the linearization process are given as follows:

$$\begin{aligned} \dot{y} &= u\cos\theta\sin\psi + v\cos\psi + w\sin\theta\sin\psi \\ \dot{z} &= -u\sin\theta + w\cos\theta \\ \dot{\theta} &= q \\ \dot{\psi} &= \frac{r}{\cos\theta} \\ u &= const. \\ \dot{x} &= u\cos\theta\cos\psi - v\sin\psi \end{aligned} \quad . \tag{3-4}$$

Note that, equations (3-1), (3-2), (3-3) and (3-4) are used in flight simulations to get the state trajectory of the missile.

CHAPTER 4

AUTOPILOT OF THE AIRCRAFT

4.1 Introduction

Autopilot of an aircraft can be designed via classical or modern control techniques. The former requires closure of one-loop-at-a-time by such tools as root locus, Bode and Nyquist plots and so on, whereas by using the latter, all the control gains are calculated simultaneously and hence all the loops are closed at once.

Generally, a classical control technique such as PID necessitates the tuning of its parameters for each control loop by trial-and-error. Although Ziegler-Nichols tuning of a PID compensator works for a large class of industrial systems, the design procedure becomes more complex as more loops are existing. As a result, often PID technique is not preferred for controlling MIMO systems. However, a modern control technique such as LQR is fundamentally a time-domain design technique useful in shaping the closed-loop response in contrast to the classical controls, where most techniques are in the frequency domain [2]. By using LQR, one can design a controller for a MIMO system satisfying the performance specifications like rise time, overshoot and settling time, by selecting the precise performance criterion. As a consequence, this technique is mostly used in the design of stability augmentation systems and autopilots.

For the design of lateral and longitudinal aircraft autopilots, both LQR and PID techniques are used in this study. Tuning of the PID parameters are done via an optimization technique choosing a suitable cost function to satisfy the closed loop stability and the performance specifications.

Finally, it is important to note that, both of the controller design techniques are applied on lateral and longitudinal LTI state-space models derived in section 2.5 for each of 12 trim points that are chosen in the flight envelope of the aircraft. Then, the resultant lateral and longitudinal controllers are used on the nonlinear aircraft model by gain scheduling depending on the speed and the altitude of the aircraft. Note that the local controller gains found for each trim point are linearly interpolated within the flight envelope to find the global controller gains.

4.2 Linear Quadratic Controller (LQC) Design

4.2.1 Linear Quadratic Regulator (LQR)

The LQR is an optimal control method used on a linear system so that the states of this linear system are regulated to zero by minimizing a quadratic cost function as follows:

$$J(\bar{x}(t),\bar{u}(t)) = \frac{1}{2}\int_0^\infty \left(\bar{x}(t)^T Q\bar{x}(t) + \bar{u}(t)^T R\bar{u}(t)\right)dt, \qquad (4\text{-}1)$$

where, $\bar{x} \in R^n$ is the state vector, $\bar{u} \in R^r$ is the control vector, and $Q \in R^{n\times n}$ is a positive semi-definite matrix, $R \in R^{r\times r}$ is a positive definite matrix and J is the performance index.

By minimizing the performance index with the selection of suitable Q and R, a feedback gain "K" can be found such that the control is optimal in order to satisfy the time-domain performance criteria, such as settling time, overshoot and rise time.

$$\bar{u}(t) = -K\bar{x}(t)\,. \tag{4-2}$$

If all of the states are available, then an LQR with full-state feedback design is used, as in our case throughout this thesis. But if all the states are not available, then an LQR with output feedback design is used. The output feedback design is not in the scope of this study. More information about these techniques can be found in [2] and [1].

For a linear system described by:

$$\begin{aligned} \dot{\bar{x}}(t) &= A\bar{x}(t) + B\bar{u}(t) \\ \bar{y}(t) &= \bar{x}(t) \end{aligned}, \tag{4-3}$$

controllability of the pair (A, B) and observability of the pair (H, A) guarantee the closed loop stability of this LQR with state feedback [2]. Here, H is any matrix such that $Q = H^T H$.

Substituting (3-2) into (3-3) results in the following closed loop system:

$$\begin{aligned} \dot{\bar{x}}(t) &= (A - BK)\bar{x}(t) = A_C\bar{x}(t) \\ \bar{y}(t) &= \bar{x}(t) \end{aligned}. \tag{4-4}$$

In fact, finding the Q and R matrices requires trial-and-error, so, engineering comes into play to find suitable values for them. The next section briefly describes how to select these parameters.

For a selected (Q,R) pair, the feedback gain K is found by solving the LQR problem via the function "lqr" in Matlab. By using "lqr", the closed loop stability of the system is obtained, since the controllability of the pair (A, B) and the observability of the pair (H, A) are checked as an initial step. More details on the analytical solution to the problem can be found in [17], [2], [18] and [10].

4.2.2 Selection of Quadratic Weights: Q and R

The selection of Q and R necessitates the engineering judgment. In different designs, they may be selected for different performance requirements. If they are both chosen nonsingular, then all of the state vector $\bar{x}(t)$ and control vector $\bar{u}(t)$ will eventually go to zero if J has a finite value. Since the minimization of J is a type of minimum energy problem, the aim of this optimal control method, LQR, is to minimize the energy in the states without using too much control energy [2].

The relative magnitudes of Q and R determine smallness of the states relative to those of the controls. For example, a larger R penalizes the controls more so that the state vector will be in greater norm relative to the control vector. On the other hand, Q is chosen larger in order to make the states go to zero quickly.

It is worth noting that the selection of Q and R determines the closed-loop pole positions which, in fact, shape the time response of the closed-loop system.

4.2.3 Suboptimal Linear Quadratic Tracker (SLQT)

Flight control systems generally require the direct application of the LQR for the inner control loops that determine the stability of the system. These inner loops are the rate loops. However, the controller specifications may require not always the regulation of the states to zero, but also some of them may be wanted to track a nonzero reference command signal, *r(t)*. This type of a problem is called as servo design problem and it has many implementations in the design of control augmentation systems that contain stability augmentation systems as inner loops.

The optimal linear quadratic tracker is not a causal system. It depends on solving an adjoint system of differential equations backward in time, and so is impossible to be implemented. Instead, a suboptimal "steady-state" tracker is used [2]. Then, the design problem turns out to be a suboptimal linear quadratic tracker problem with the following cost function (or performance index):

$$J\left(e(t),u(t)\right)=\frac{1}{2}\int_{0}^{\infty}\left(e(t)^{T}\,Q\,e(t)+u(t)^{T}\,R\;u(t)\right)dt\,, \tag{4-5}$$

where, the tracking error and the performance output are formulated respectively as:

$$e\,(t)=r\,(t)-y\,(t)\,, \tag{4-6}$$

$$y\,(t)=C\,x\,(t)\,. \tag{4-7}$$

The sub-optimality stems from the fact that, the performance index does not necessarily minimize a quadratic function of the total tracking error [2].

Solution to the steady-state tracker problem is similar to the one defined previously for the LQR. Depending on the type of the LTI system on which the SLQT is applied, one of the two different techniques is used as explained in the preceding sections.

4.2.3.1 SLQT Design for Type 0 LTI System

An SLQT for an LTI system that has no integrator, that is to say type 0, can be constructed as follows [1]:

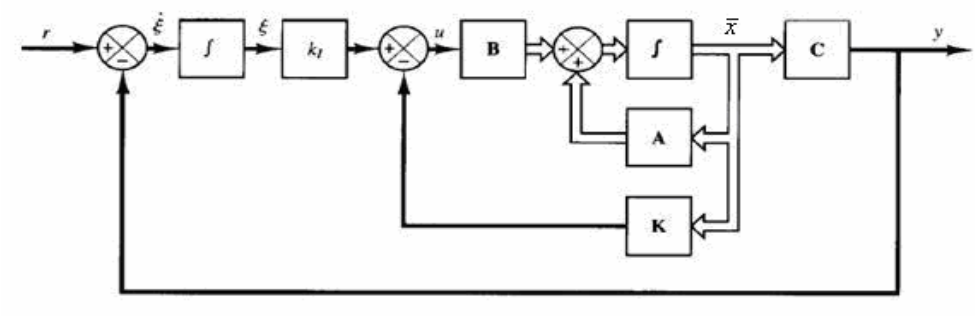

Figure 4-1: Servomechanism for a type 0 LTI system [1].

Here, the control signal u, the output signal y and the reference step signal r are scalars, and $A \in R^{n\times n}$, $B \in R^{n\times 1}$, $C \in R^{1\times n}$, $K \in R^{1\times n}$. From the diagram above, following equations are obtained:

$$\dot{\bar{x}} = A\bar{x} + Bu\,, \tag{4-8}$$

$$y = C\bar{x}\,, \tag{4-9}$$

$$u = -K\bar{x} + k_I\xi\,, \tag{4-10}$$

$$\dot{\xi} = r - y = r - C\bar{x}\,. \tag{4-11}$$

The pair (A, B) is assumed to be controllable and also $C(sI - A)^{-1}B$ is assumed to have no zero at the origin to avoid the pole zero cancellation due to the integrator inserted in the feed-forward path. Suppose that the reference step input is applied at $t = 0$. Then, by combining the equations (4-8) and (4-11) for $t > 0$, the system dynamics takes the form:

$$\begin{bmatrix}\dot{\bar{x}}(t)\\ \dot{\xi}(t)\end{bmatrix} = \begin{bmatrix} A & 0\\ -C & 0\end{bmatrix}\begin{bmatrix}\bar{x}(t)\\ \xi(t)\end{bmatrix} + \begin{bmatrix}B\\ 0\end{bmatrix}u(t) + \begin{bmatrix}0\\ 1\end{bmatrix}r(t)\,. \tag{4-12}$$

At steady state, (4-12) turns into:

$$\begin{bmatrix}\dot{\bar{x}}(\infty)\\ \dot{\xi}(\infty)\end{bmatrix} = \begin{bmatrix} A & 0\\ -C & 0\end{bmatrix}\begin{bmatrix}\bar{x}(\infty)\\ \xi(\infty)\end{bmatrix} + \begin{bmatrix}B\\ 0\end{bmatrix}u(\infty) + \begin{bmatrix}0\\ 1\end{bmatrix}r(\infty)\,. \tag{4-13}$$

An asymptotically stable system can be designed such that $\bar{x}(\infty), u(\infty)$ and $\xi(\infty)$ converge to constant values and hence, $\dot{\xi}(\infty) = 0$ and $y(\infty) = r$.

By defining:

$$\begin{aligned}\bar{x}_e(t) &= \bar{x}(t) - \bar{x}(\infty)\\ \xi_e(t) &= \xi(t) - \xi(\infty)\,,\\ u_e(t) &= u(t) - u(\infty)\end{aligned} \tag{4-14}$$

and subtracting (4-13) from (4-12), using $r(t) - r(\infty) = 0$ since r is constant for $t > 0$, the following form is obtained:

$$\begin{bmatrix} \dot{\bar{x}}_e(t) \\ \dot{\xi}_e(t) \end{bmatrix} = \begin{bmatrix} A & 0 \\ -C & 0 \end{bmatrix} \begin{bmatrix} \bar{x}_e(t) \\ \xi_e(t) \end{bmatrix} + \begin{bmatrix} B \\ 0 \end{bmatrix} u_e(t), \tag{4-15}$$

where

$$u_e(t) = -K\bar{x}_e(t) + k_I \xi_e(t). \tag{4-16}$$

If a new, (n+1)th order error vector is defined as $\bar{e}(t) = \begin{bmatrix} \bar{x}_e(t) & \xi_e(t) \end{bmatrix}^T$, then (4-16) becomes:

$$\dot{\bar{e}} = \hat{A}\bar{e} + \hat{B}u_e, \tag{4-17}$$

where

$$\hat{A} = \begin{bmatrix} A & 0 \\ -C & 0 \end{bmatrix}, \quad \hat{B} = \begin{bmatrix} B \\ 0 \end{bmatrix}. \tag{4-18}$$

Then, (4-16) becomes:

$$u_e = -\begin{bmatrix} K & -k_I \end{bmatrix} \bar{e}. \tag{4-19}$$

If (4-19) is substituted into (4-17), then the following state error equation is obtained:

$$\dot{\bar{e}} = (\hat{A} - \hat{B}\hat{K})\bar{e}, \tag{4-20}$$

where, $\hat{K} = \begin{bmatrix} K & -k_I \end{bmatrix}$.

Finally, the new feedback gain matrix $\hat{K}$ can be found by using LQR technique that is explained in section 4.2.1.

4.2.3.2 SLQT Design for Type 1 LTI System

If the LTI system defined by (4-8) has an integrator, then there is no need to add an integrator to the feed-forward path shown in Figure 4-1, so the resultant block diagram of the controller is as follows:

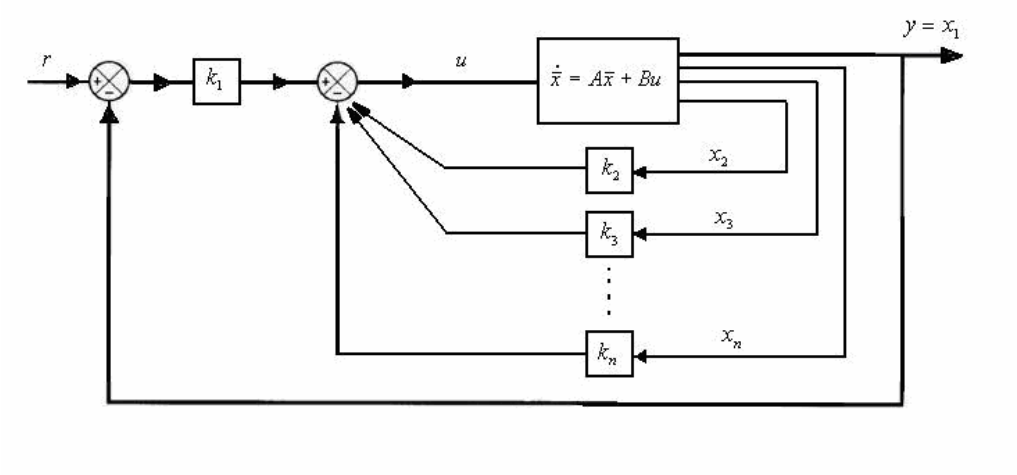

Figure 4-2: Servomechanism for a type 1 LTI system [1].

According to the state-feedback control scheme shown above,

$$u = -K\bar{x} + k_I r\,, \tag{4-21}$$

where, K is the feedback gain matrix defined by $K = \begin{bmatrix} k_1 & k_2 & \cdots & k_n \end{bmatrix}$. Then, the state dynamics can be described by:

$$\dot{\bar{x}}(t) = A\bar{x} + Bu = (A - BK)\bar{x} + Bk_I r\,. \tag{4-22}$$

After defining $\bar{e}(t) = \bar{x}(t) - \bar{x}(\infty)$ and using the similar steps used in the previous section, the error dynamics can be described by:

$$\dot{\bar{e}} = (A - BK)\bar{e}\,. \tag{4-23}$$

Hence, the feedback gain matrix K can be found by using LQR technique that is explained in section 4.2.1.

4.2.4 Gain Scheduling

The trimming process explained in section 2.3 is used to obtain the trim points in flight envelope of the aircraft. Borders of the flight envelope are given roughly in Appendix A.1. In order to see the trimming performance at the trim points, the trim values of the state and control variables are used as initial conditions for the nonlinear model and tested with zero input to check if the linear and angular accelerations are close to zero. Also, maximum value of the cost function of the trim process which is given in equation (2-43) is checked if it is close to zero.

In order to design the lateral and longitudinal autopilots of the aircraft by using LQC technique, 12 trim points shown in the Figure 4-3 are used:

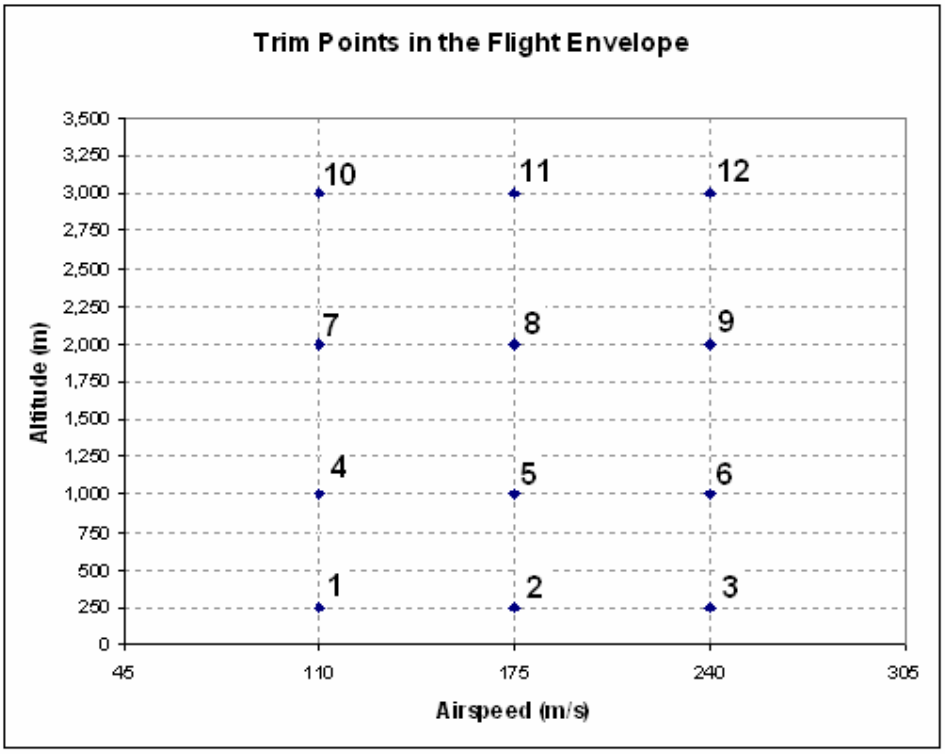

Figure 4-3: Trim points used for the controller design.

LQC technique is applied on lateral and longitudinal LTI state-space models derived in section 2.5 for each of 12 trim points shown above. The trim values obtained for these 12 trim points are given in the following table:

Table 4-1: Trim values of the state and the control variables

	Trim Point #					
State Variables	**1**	**2**	**3**	**4**	**5**	**6**
Vt (m/s)	110	175	240	110	175	240
alpha (deg)	5.878	1.451	0.090	6.430	1.669	0.206
beta (deg)	0	0	0	0	0	0
phi (deg)	0	0	0	0	0	0
theta (deg)	5.878	1.451	0.090	6.430	1.669	0.206
psi (deg)	0	0	0	0	0	0
p (deg/s)	0	0	0	0	0	0
q (deg/s)	0	0	0	0	0	0
r (deg/s)	0	0	0	0	0	0
npos (m)	0	0	0	0	0	0
epos (m)	0	0	0	0	0	0
alt (m)	250	250	250	1000	1000	1000
pow (%)	7.886	12.453	24.184	8.734	12.555	23.706
Control Variables	**1**	**2**	**3**	**4**	**5**	**6**
thtl (0-1)	0.121	0.192	0.372	0.135	0.193	0.365
el (deg)	-2.881	-1.738	-1.415	-3.063	-1.791	-1.442
ail (deg)	0	0	0	0	0	0
rdr (deg)	0	0	0	0	0	0
Max. Trim Cost*	5e-30	4e-30	1e-23	2e-27	1e-24	3e-23

Table 4-2: Trim values of the state and the control variables – cont'd

	Trim Point #					
State Variables	**7**	**8**	**9**	**10**	**11**	**12**
Vt (m/s)	110	175	240	110	175	240
alpha (deg)	7.245	1.994	0.379	8.162	2.361	0.575
beta (deg)	0	0	0	0	0	0
phi (deg)	0	0	0	0	0	0
theta (deg)	7.245	1.994	0.379	8.162	2.361	0.575
psi (deg)	0	0	0	0	0	0
p (deg/s)	0	0	0	0	0	0
q (deg/s)	0	0	0	0	0	0
r (deg/s)	0	0	0	0	0	0
npos (m)	0	0	0	0	0	0
epos (m)	0	0	0	0	0	0
alt (m)	2000	2000	2000	3000	3000	3000
pow (%)	10.269	12.819	23.103	12.430	13.274	22.540
Control Variables	**7**	**8**	**9**	**10**	**11**	**12**
thtl (0-1)	0.158	0.197	0.356	0.191	0.204	0.347
el (deg)	-3.332	-1.868	-1.484	-3.633	-1.956	-1.530
ail (deg)	0	0	0	0	0	0
rdr (deg)	0	0	0	0	0	0
Max. Trim Cost*	1e-29	6e-29	3e-25	1e-29	4e-30	3e-25

*: This value is obtained after testing of the trim values on the nonlinear aircraft model within 100 seconds.

The resultant lateral and longitudinal controller gains are scheduled with respect to the airspeed and the altitude, and the controllers are applied on the nonlinear aircraft model to check the design performance as shown below:

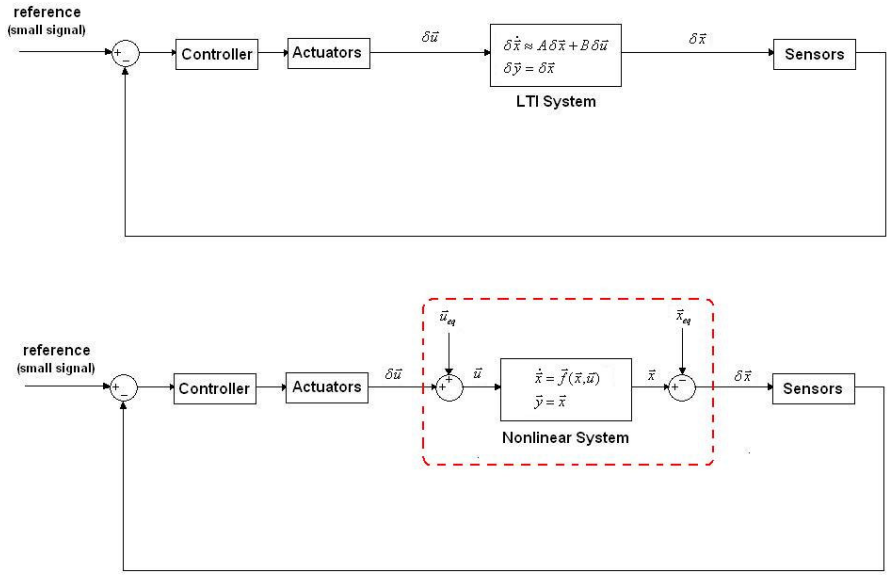

Figure 4-4: Block diagram used to test the performance of the autopilot designed for an LTI system at a single trim point

The controller gains for the points in the flight envelope that do not correspond to the trim points, are calculated by using the linear interpolation method. Built-in interpolation algorithm of Simulink is used for this purpose.

4.2.5 Gain Scheduled LQC Design

4.2.5.1 Longitudinal LQC Design

The LTI longitudinal system for the aircraft is composed of the states and controls defined in (2-54). For the 12 trim points given in the previous section, controller structure formulated in section 4.2.3.1 is used to design the longitudinal flight

control system of the aircraft. The following figure illustrates the block diagrams used for the design process.

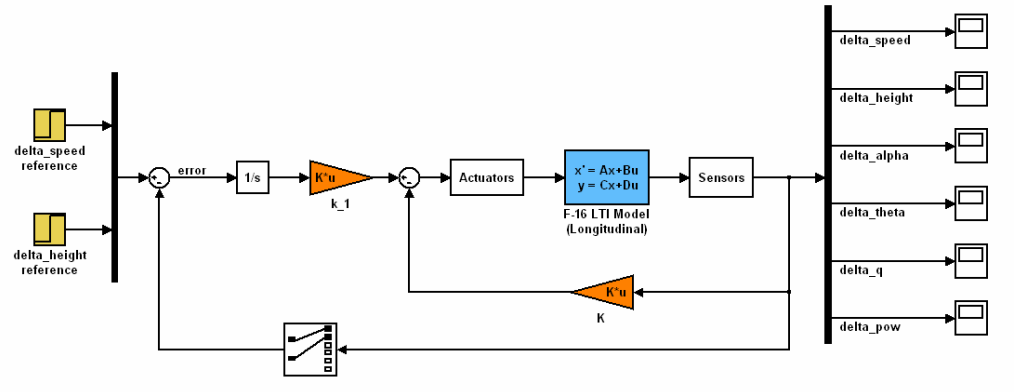

Figure 4-5: Longitudinal autopilot of the aircraft designed with SLQT

Table 4-3 shows the selection of Q and R matrices for the longitudinal LQC design. These values are determined by trial and error. It is important to note that, the closed loop stability is satisfied even if the reference signal magnitudes given in the next table are applied to the nonlinear (NL) system.

Note that, the reason of choosing some of the delta speed reference signal amplitudes smaller than the others (in Table 4-4) is the maximum speed constraint (which is 270 m/s) for the flight envelope. Also, note that the diagonal entries of the diagonal Q and R matrices are shown as they are represented in Matlab in order to save space.

Table 4-3: Selection of Q and R for the longitudinal LQC design

Trim Point #	Weighting Matrices	Values
1	Q	diag(1, 1, 1, 1, 1, 1, 2000, 20)
	R	diag(300000000, 150000)
2	Q	diag(1, 1, 1, 1, 1, 1, 300, 1)
	R	diag(25000000, 10000)
3	Q	diag(1, 1, 1, 1, 1, 1, 1500, 1)
	R	diag(10000000, 30000)
4	Q	diag(1, 1, 1, 1, 1, 1, 2000, 20)
	R	diag(500000000, 3000000)
5	Q	diag(1, 1, 1, 1, 1, 1, 300, 1)
	R	diag(30000000, 50000)
6	Q	diag(1, 1, 1, 1, 1, 1, 2000, 1)
	R	diag(10000000, 80000)
7	Q	diag(1, 1, 1, 1, 1, 1, 20, 1)
	R	diag(10000000, 1000000)
8	Q	diag(1, 1, 1, 1, 1, 1, 100, 1)
	R	diag(50000000, 500000)
9	Q	diag(1, 1, 1, 1, 1, 1, 2000, 1)
	R	diag(20000000, 80000)
10	Q	diag(1, 1, 1, 1, 1, 1, 50, 1)
	R	diag(20000000, 1000000)
11	Q	diag(1, 1, 1, 1, 1, 1, 200, 1)
	R	diag(50000000, 200000)
12	Q	diag(1, 1, 1, 1, 1, 1, 1000, 1)
	R	diag(50000000, 100000)

Table 4-4: Longitudinal LQC design

Trim Point #	Max. Reference Step Commands	
	delta_V (m/s)	delta_h (m)
1	65	750
2	65	750
3	30	750
4	65	1000
5	65	1000
6	30	1000
7	65	1000
8	65	1000
9	30	1000
10	65	1000
11	65	1000
12	30	1000

4.2.5.2 Lateral LQC Design

The LTI lateral system for the aircraft is composed of the states and controls defined in (2-55). For the 12 trim points, the controller structure formulated in section 4.2.3.2 is used to design the lateral flight control system. The following figure illustrates the block diagrams used for the design process:

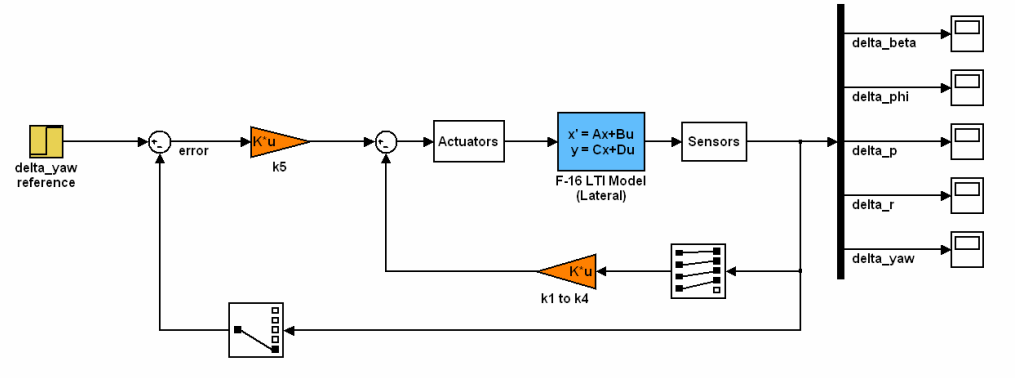

Figure 4-6: Lateral autopilot of the aircraft designed with SLQT

Table 4-5 shows the selection of Q and R matrices for the lateral LQC design. These values are determined by trial and error. It is important to note that, the closed loop stability is satisfied even if the reference signal magnitudes given in the next table are applied to the nonlinear (NL) system.

Table 4-5: Selection of Q and R for the lateral LQC design

Trim Point #	Weighting Matrices	Values
1	Q	diag(1, 1, 1, 1, 1000)
	R	diag(100000, 8)
2	Q	diag(1, 1, 1, 1, 2000)
	R	diag(5000000, 5)
3	Q	diag(1, 1, 1, 1, 10)
	R	diag(200, 1)
4	Q	diag(1, 1, 1, 1, 1000)
	R	diag(100000, 10)
5	Q	diag(1, 1, 1, 1, 5000)
	R	diag(10000000, 30)
6	Q	diag(1, 1, 1, 1, 10)
	R	diag(150, 1)
7	Q	diag(1, 1, 1, 1, 400)
	R	diag(100000, 30)
8	Q	diag(1, 1, 1, 1, 2000)
	R	diag(10000000, 10)
9	Q	diag(1, 1, 1, 1, 10)
	R	diag(100, 7)
10	Q	diag(1, 1, 1, 1, 600)
	R	diag(100000, 40)
11	Q	diag(1, 1, 1, 1, 1000)
	R	diag(5000000, 10)
12	Q	diag(1, 1, 1, 1, 30)
	R	diag(500, 1)

Table 4-6: Lateral LQC design

	Max. Reference Step Command
Trim Point #1 to #12	**delta_yaw (deg)**
	179

4.2.6 Gain Scheduled LQC Design Performance

The resultant lateral and longitudinal autopilots designed by gain scheduled LQC method are combined and then tested by applying reference signals (i.e. delta speed, delta height and delta yaw, simultaneously) to the nonlinear system. In order to illustrate the performance of the resultant autopilot, the following case is given:

Test Case: The state and input trim values for the initial point at which V_0=175 m/s and h_0=2000 m are found by the trimming algorithm given in section 2.3. Then, delta speed, delta height and delta yaw step reference signals are applied simultaneously; that is to say, the height and the speed of the aircraft are increased, while making a coordinated turn in the horizontal plane. The step responses of the gain scheduled autopilot are given with the following figures:

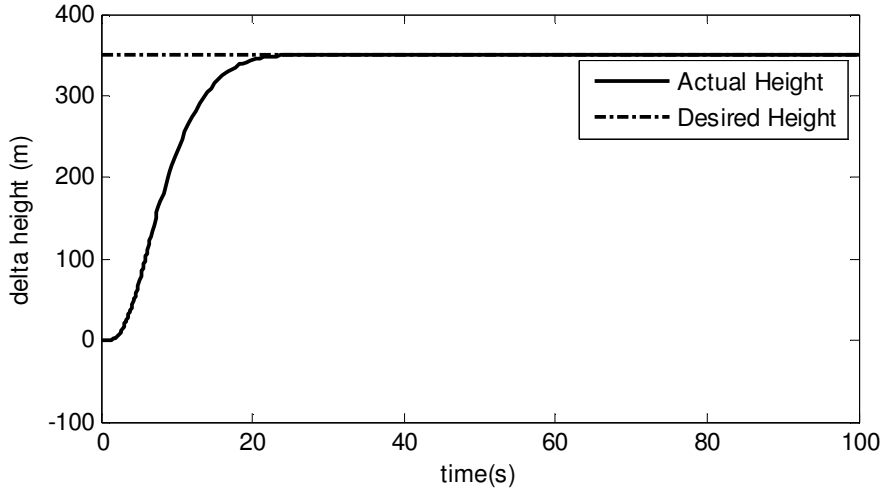

Figure 4-7: Height response of the LQC from the point A to the point B

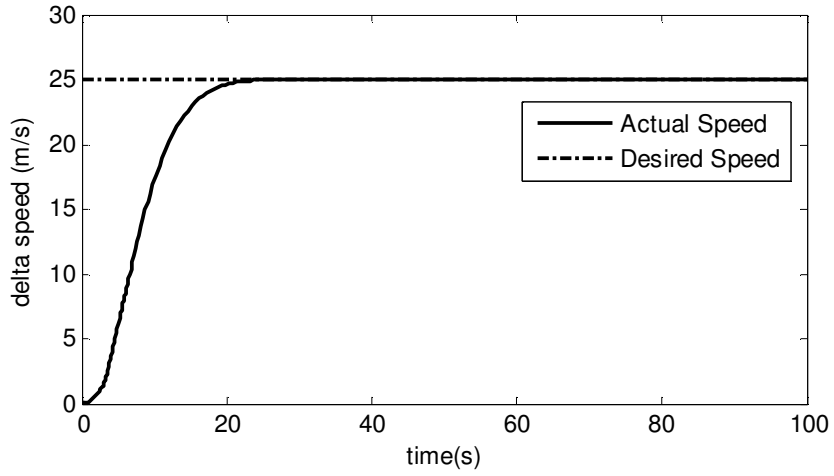

Figure 4-8: Speed response of the LQC from the point A to the point B

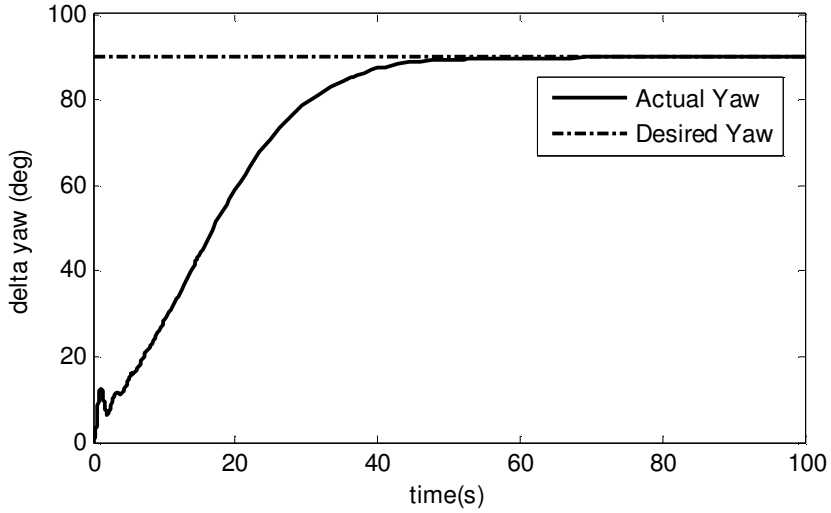

Figure 4-9: Yaw response of LQC from the point A to the point B

4.3 Proportional Integral Derivative (PID) Controller Design

For the longitudinal and lateral autopilots, the controller structures are given in Figure 4-10 and Figure 4-11. In order to tune the proportional, integral and derivative coefficients of each PID controller, the optimization algorithm "fmincon" of the Matlab Optimization Toolbox is used. By defining necessary bounds for the coefficients to be tuned and also a suitable cost function, the optimization algorithm finds a solution that satisfies a user defined stopping criteria, for example, the directional derivative, 1-D search step length, change in the cost function value or change in the magnitude of the coefficient vector to be tuned.

Lateral and longitudinal autopilot structures used for the PID controller are shown in the figures below.

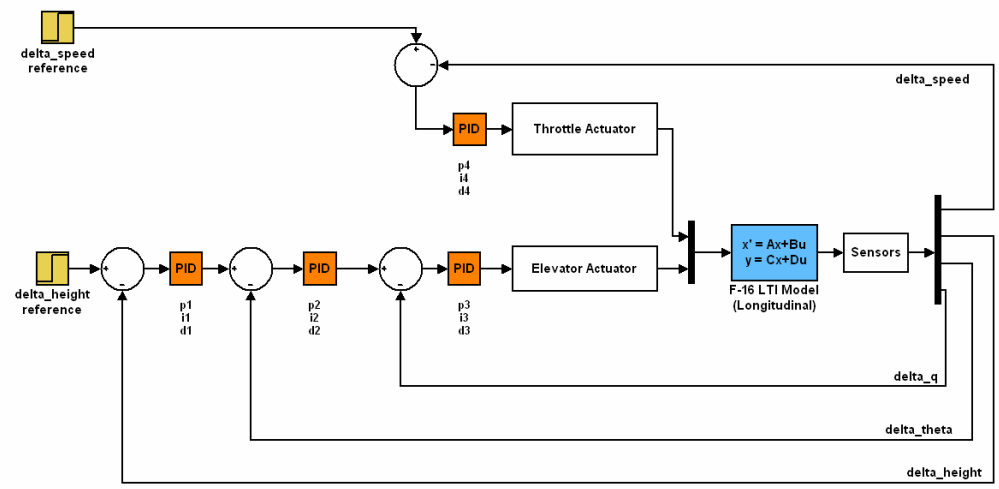

Figure 4-10: Longitudinal autopilot of the aircraft designed with PID

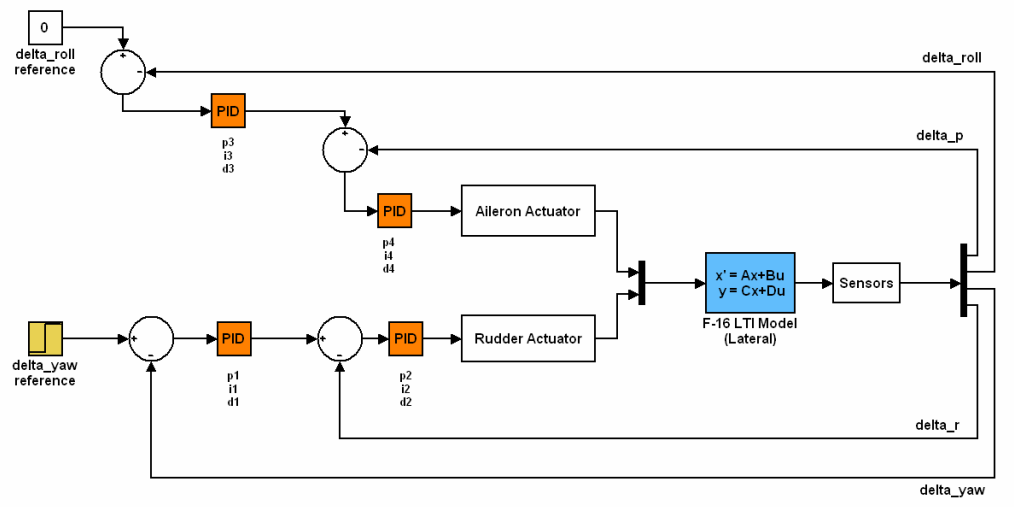

Figure 4-11: Lateral autopilot of the aircraft designed with PID

The application of "fmincon" to our problem requires the following cost function definitions for the longitudinal and lateral autopilots, respectively:

$$
\begin{aligned}
J_{long} &= \sqrt{\frac{1}{N}(k_V A + k_h B + k_\alpha C + k_\theta D + k_q E)} \\
A &= (\Delta\overline{V}_{ref} - \Delta\overline{V})^T (\Delta\overline{V}_{ref} - \Delta\overline{V}) \\
B &= (\Delta\overline{h}_{ref} - \Delta\overline{h})^T (\Delta\overline{h}_{ref} - \Delta\overline{h}) \\
C &= (\Delta\overline{\alpha}_{ref} - \Delta\overline{\alpha})^T (\Delta\overline{\alpha}_{ref} - \Delta\overline{\alpha}) \\
D &= (\Delta\overline{\theta}_{ref} - \Delta\overline{\theta})^T (\Delta\overline{\theta}_{ref} - \Delta\overline{\theta}) \\
E &= (\Delta\overline{q}_{ref} - \Delta\overline{q})^T (\Delta\overline{q}_{ref} - \Delta\overline{q})
\end{aligned}
\quad , \qquad (4\text{-}24)
$$

$$
\begin{aligned}
J_{lat} &= \sqrt{\frac{1}{N}(k_\beta A + k_\phi B + k_p C + k_r D + k_\psi E)} \\
A &= (\Delta\overline{\beta}_{ref} - \Delta\overline{\beta})^T (\Delta\overline{\beta}_{ref} - \Delta\overline{\beta}) \\
B &= (\Delta\overline{\phi}_{ref} - \Delta\overline{\phi})^T (\Delta\overline{\phi}_{ref} - \Delta\overline{\phi}) \\
C &= (\Delta\overline{p}_{ref} - \Delta\overline{p})^T (\Delta\overline{p}_{ref} - \Delta\overline{p}) \\
D &= (\Delta\overline{r}_{ref} - \Delta\overline{r})^T (\Delta\overline{r}_{ref} - \Delta\overline{r}) \\
E &= (\Delta\overline{\psi}_{ref} - \Delta\overline{\psi})^T (\Delta\overline{\psi}_{ref} - \Delta\overline{\psi})
\end{aligned}
\quad , \qquad (4\text{-}25)
$$

where, N is the number of total time steps and the vector $\Delta\overline{V}_{ref} - \Delta\overline{V}$ is an Nx1 vector that stores the delta speed error value for each time step.

Also note that, the reference values of the variables other than the controlled ones are taken as zero for the applications given below. Only the weight values (k's) of the error for each state variable change as indicated for each of the application (see the example below).

By choosing a suitable initial condition for the coefficients, the algorithm is run at fixed step size for t_{final} seconds for each iteration steps of the "fmincon". Finally, the solution is found for the user specified termination condition.

4.3.1 PID Controller Design Example

In order to illustrate the utilization of the optimization algorithm on our problem, the state trim values and input trim values are used that are the solution of the trim algorithm given in section 2.3 for the speed of 150 m/s and the altitude of 680 m, (for the lateral and longitudinal autopilots of the following example).

4.3.1.1 Longitudinal Autopilot

The parameter selection for this design is given as follows:

$$\begin{aligned}
&\Delta V_{ref} = 1\ m/s \\
&\Delta h_{ref} = 1\ m \\
&t_{final} = 100\ s \\
&\Delta t = 0.01\ s \\
&\begin{bmatrix} k_V & k_h & k_\alpha & k_\theta & k_q \end{bmatrix} = \begin{bmatrix} 10 & 10 & 0 & 0 & 1 \end{bmatrix}
\end{aligned} \quad . \qquad (4\text{-}26)$$

The optimization process is completed in 75 iterations after reaching the directional derivative of 6e-8 and the final cost value is 0.438675. So, the final values of the PID coefficients are given in the following table (note that, the first row corresponds to the initial conditions):

p1	i1	d1	p2	i2	d2	p3	i3	d3	p4	i4	d4
0.003	0	0	1	0	0	-1	0	0	1	1	1
0.693	0.034	0.130	34.976	0	4.593	-0.203	-3.942	-0.106	13.861	0	16.036

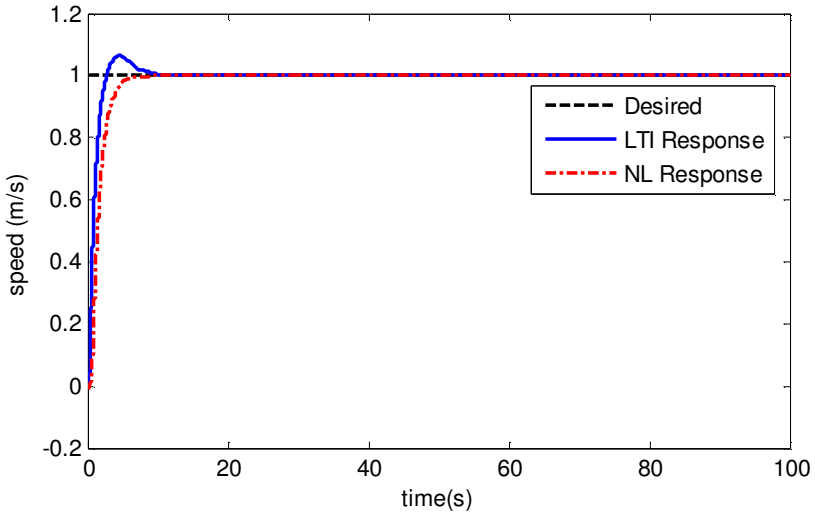

Figure 4-12: Step response of the longitudinal autopilot for delta speed command

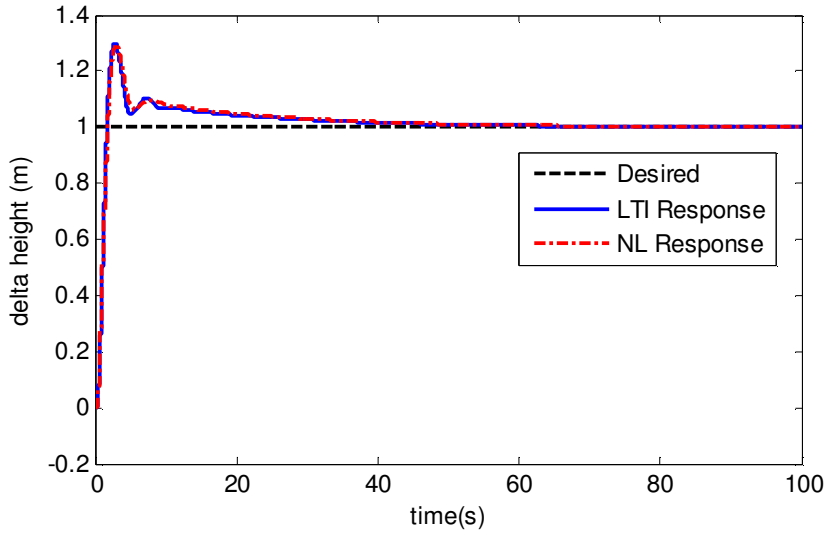

Figure 4-13: Step response of the longitudinal autopilot for delta height command

PID coefficients found by the optimization algorithm for the given parameter set (initial condition, weights of the states in the cost function) can further be tuned manually (by trial and error) in order to have a better step response. For example, if the p1, i1 and d1 coefficients are changed to the values of 1, 0.1 and 0.03, respectively, then the following step responses are obtained. Although the settling time of the height response is improved, its overshoot is larger than the previous one. Therefore, there is a compromise between the time response characteristics (i.e.: settling time and overshoot for this case) of the designed autopilot.

It is important to note that among all the responses obtained by the PID coefficient tuning trials (first by using the optimization, then manually tuning), following responses are the best ones:

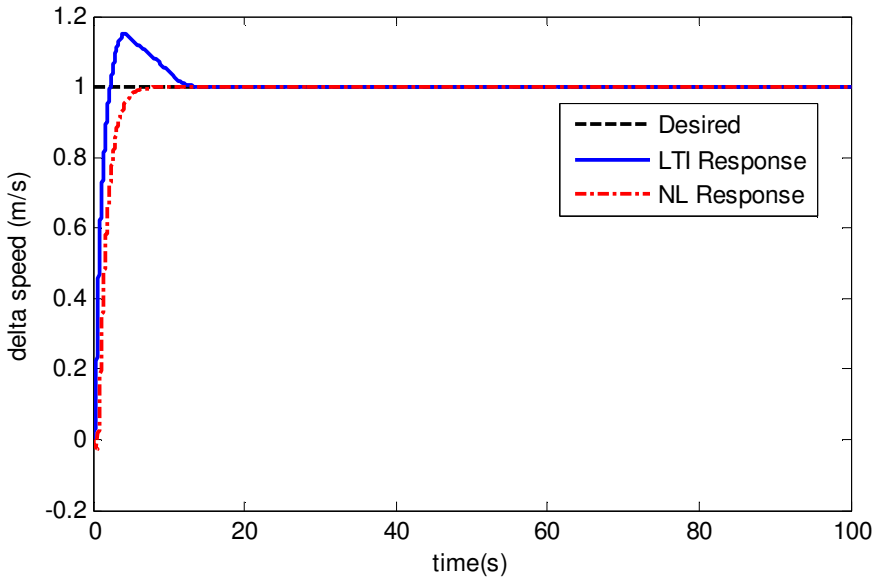

Figure 4-14: Step response of the longitudinal autopilot after manual tuning - 1

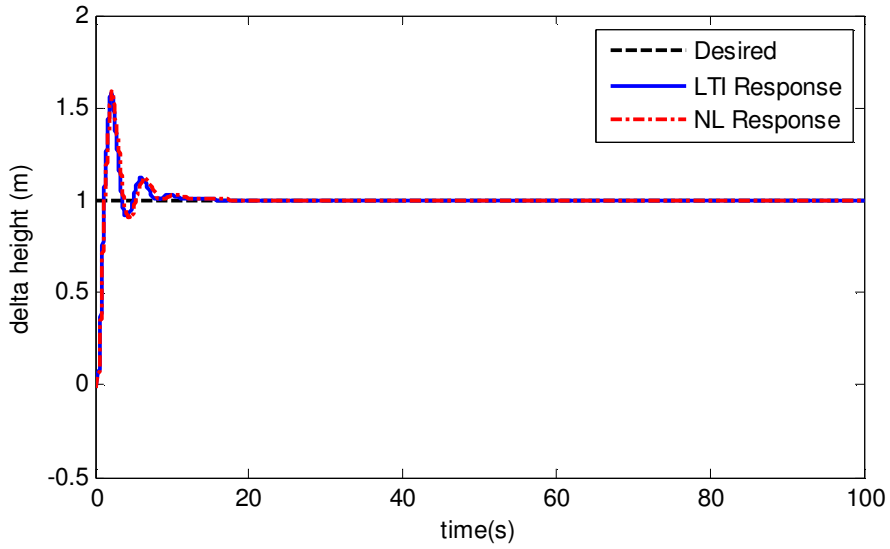

Figure 4-15: Step response of the longitudinal autopilot after manual tuning – 2

4.3.1.2 Lateral Autopilot

The parameter selection for this design is given as follows:

$$\begin{aligned} &\Delta\psi_{ref} = 1^{\circ} \\ &t_{final} = 100\ s \\ &\Delta t = 0.01\ s \\ &\begin{bmatrix} k_\beta & k_\phi & k_p & k_r & k_\psi \end{bmatrix} = \begin{bmatrix} 1 & 1 & 5 & 5 & 5 \end{bmatrix} \end{aligned} \quad . \tag{4-27}$$

The optimization process is completed in 42 iterations after reaching the directional derivative of -1e-9 and the final cost value is 0.256912. So, the final values of the PID coefficients are given in the following table (note that, the first row corresponds to the initial conditions):

p1	i1	d1	p2	i2	d2	p3	i3	d3	p4	i4	d4
1	0	0	-1	0	0	1	0	0	-1	0	0
5.514	0.004	4.061	-4.445	0	-0.350	0.318	0	0	-1.948	-0.002	-1.397

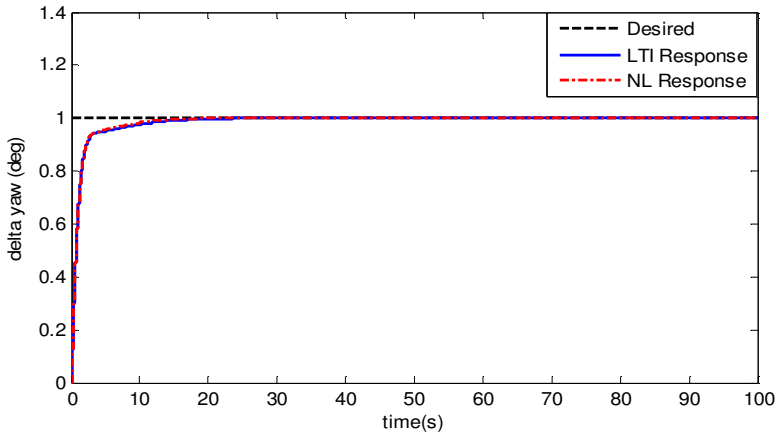

Figure 4-16: Step response of the lateral autopilot for delta yaw command

4.4 Comparison of LQC and PID Controller Performances

In this section, a longitudinal and a lateral LQC design example are given in order to compare their performance with the PID controller designs given in the previous section. Necessary LTI state space matrices, input trim and state trim values are used same as in the case of the PID designs. Selection of Q and R matrices for the longitudinal and the lateral autopilot designs are given respectively as follows:

$$\begin{aligned} Q_{long} &= diag(1,1,1,1,1,1,3,3) \\ R_{long} &= diag(0.01,1) \end{aligned} . \tag{4-28}$$

$$\begin{aligned} Q_{lat} &= diag(1,1,1,1,70) \\ R_{lat} &= diag(0.01,0.01) \end{aligned} . \tag{4-29}$$

With these parameters, the following unit step responses are obtained for the longitudinal and lateral autopilots:

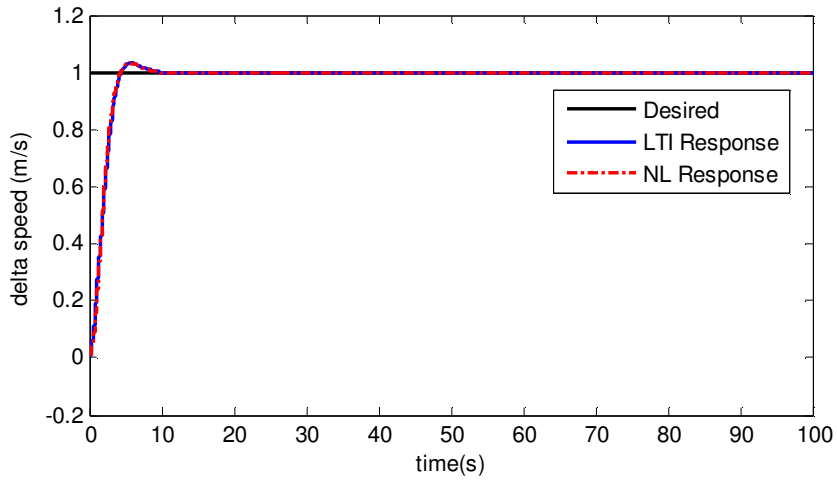

Figure 4-17: Step response of the longitudinal autopilot for delta speed command

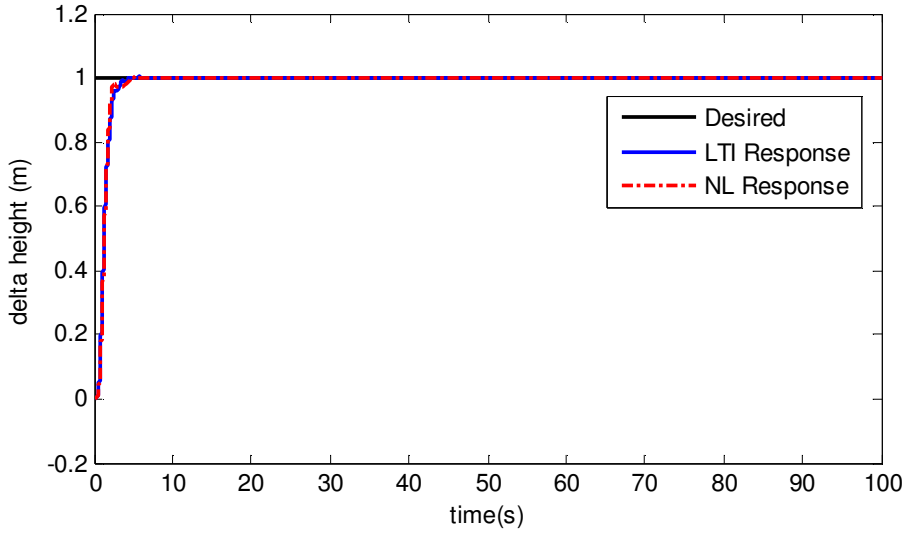

Figure 4-18: Step response of the longitudinal autopilot for delta height command

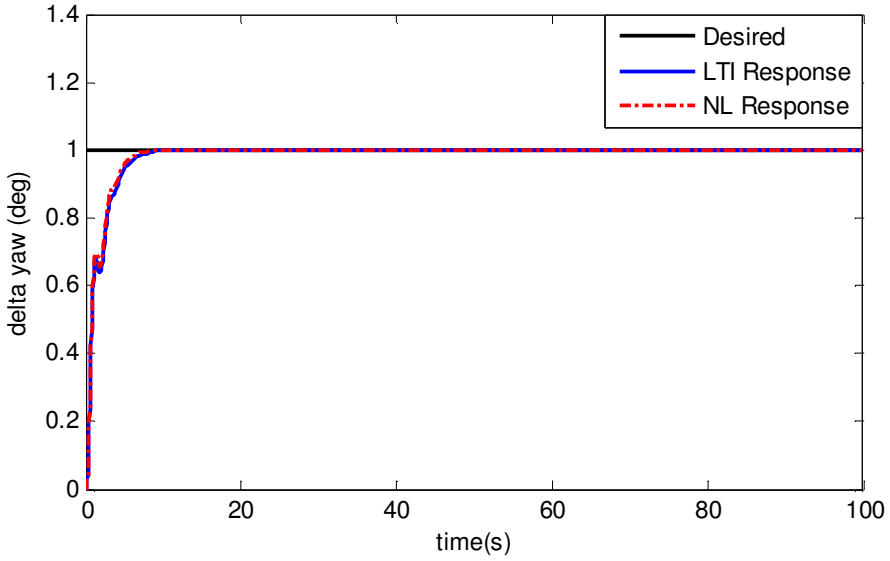

Figure 4-19: Step response of the lateral autopilot for delta yaw command

If the above graphs are compared with the ones obtained for the PID controller design method considering the rise time, settling time and overshoot criteria, the LQ controllers perform better than the PID controllers. Although for each of the two controller design methods there is a parameter selection and a tuning process, LQ controller method gives better results and therefore, it is used for the gain scheduled controller design (see sections 4.2.5 and 4.2.6).

CHAPTER 5

AUTOPILOT OF THE MISSILE

5.1 Introduction

In this chapter, missile autopilot design is explained first. Then, the design parameters and the autopilot structures are given. Finally, the unit step responses of the designed autopilots are given.

Missile autopilots are designed applying the SLQT methods that are explained in section 4.2.3. Three different autopilots are used here, such as roll autopilot, normal acceleration autopilot and lateral acceleration autopilot.

5.2 Autopilot Design

Roll autopilot is designed using the approach given in section 4.2.3.2 using the state space formulation given in the equation (3-1) with the following weight matrices for the application of the SLQT method:

$$Q = \begin{bmatrix} 5000 & 0 \\ 0 & 30 \end{bmatrix}, \quad R = 10000. \tag{5-1}$$

The following figure shows the roll autopilot design:

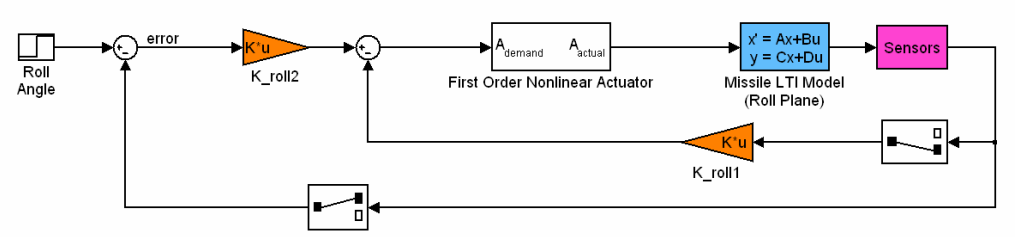

Figure 5-1: Missile roll autopilot

Normal and lateral acceleration autopilots are designed using the approach given in section 4.2.3.1 with the state space formulations given in the equations (3-2) and (3-3), respectively. It is important to note that, since the normal and lateral accelerations are not present as state variables in the state space formulation, they can be obtained as follows, by assuming the roll rate is negligibly small [13]:

$$\begin{aligned} a_y &= \dot{v} + ur \\ a_z &= \dot{w} - uq \end{aligned}. \tag{5-2}$$

The weight matrices used to apply SLQT method for the normal acceleration and lateral acceleration autopilots are given, respectively, as follows:

$$Q = \begin{bmatrix} 0 & 0 & 0 \\ 0 & 0 & 0 \\ 0 & 0 & 20 \end{bmatrix}, \quad R = 0.5, \tag{5-3}$$

$$Q = \begin{bmatrix} 0 & 0 & 0 \\ 0 & 0 & 0 \\ 0 & 0 & 4 \end{bmatrix}, \quad R = 0.5. \tag{5-4}$$

In the Q matrices given above, diagonal entries in the third rows represent the normal acceleration error and the lateral acceleration error, respectively. These error states are also shown in the following figures:

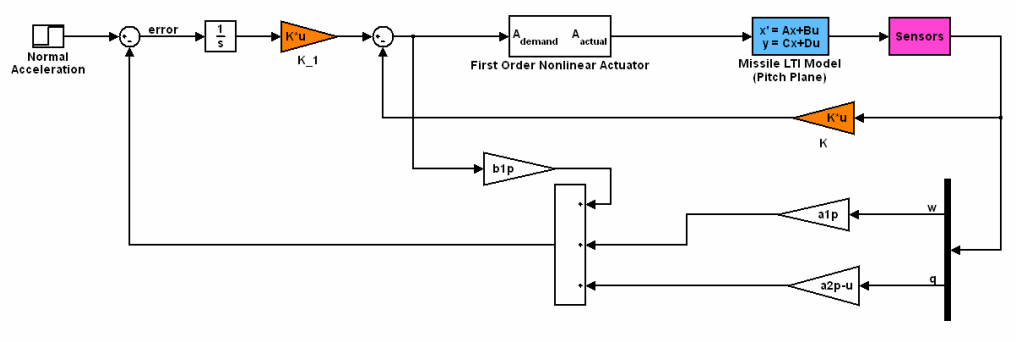

Figure 5-2: Missile normal acceleration autopilot

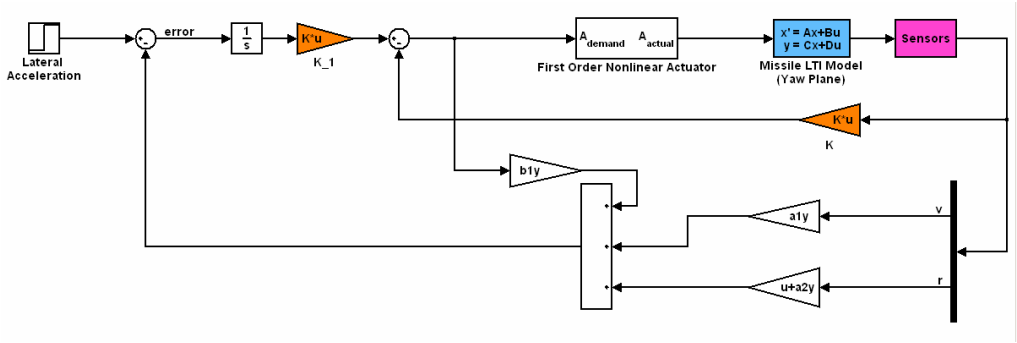

Figure 5-3: Missile lateral acceleration autopilot

In the figures given above, variables “a1p”, “a2p” and “b1p” represent the entries in the first row of the equation (3-2), whereas “a1y”, “a2y” and “a3y” represent the entries in the first row of the equation (3-3) [13]. In addition, the details of the sensors and the actuators used for the missile autopilot designs are given in Appendix B.

Finally, the unit step response of each autopilot is given in Figure 5-4 as:

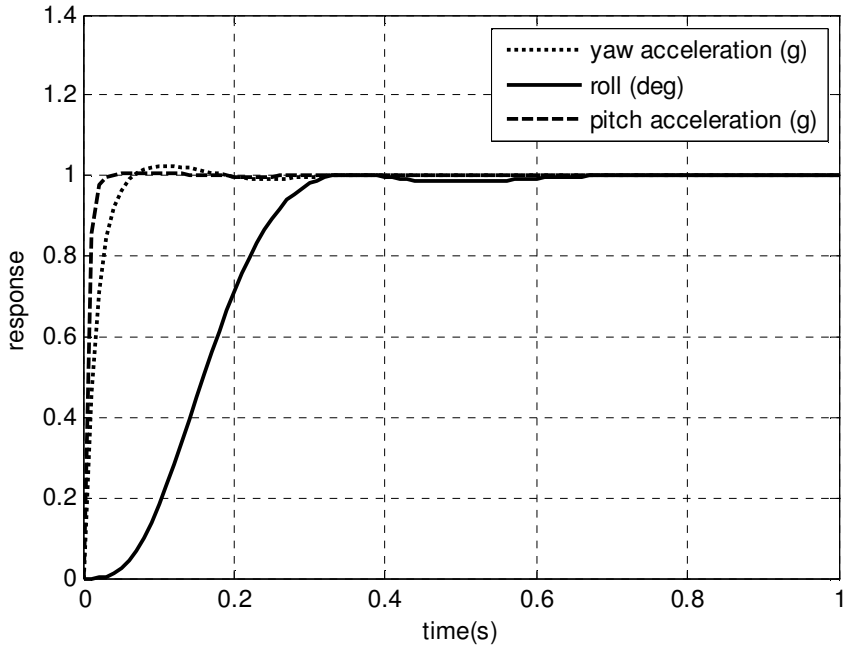

Figure 5-4: Unit step responses of the missile autopilots

CHAPTER 6

GUIDANCE OF THE MISSILE

6.1 Introduction

In this chapter, formulations of three different missile guidance methods, one of which is developed throughout this study, are given. In addition to the formulations, these methods require some parameters to be selected before using them in the simulation studies. Therefore, parameter selection processes and the necessary assumptions are also given. Consequently, the engagement scenarios used for the performance comparison of the guidance methods and the simulation results are also given.

6.2 Proportional Navigation Guidance (PNG)

Theoretically, PNG guidance law gives out an acceleration command that is proportional to LOS rate $\dot{\lambda}$ and the missile-target closing velocity V_c [5]. The acceleration command produced by PNG that is perpendicular to the instantaneous missile-target LOS, can be stated as:

$$n_c = NV_c\dot{\lambda}\,, \tag{6-1}$$

where, n_c is the normal acceleration command, N is a unitless, designer chosen gain (usually in the range of 3-5) known as the proportional navigation ratio, V_c is the missile-target closing velocity, and λ is the LOS angle.

In tactical IR missile applications of PNG, LOS rate is measured; whereas the closing velocity is estimated [10] or taken as constant [3]. For the model used in this thesis, LOS rate is calculated after the measurement of the position of the target. The position measurement is obtained by adding a Gaussian noise with a specified rms value to the position of the target since a seeker model does not exist in this study.

Following figure shows two-dimensional missile-target engagement geometry to illustrate how PNG works:

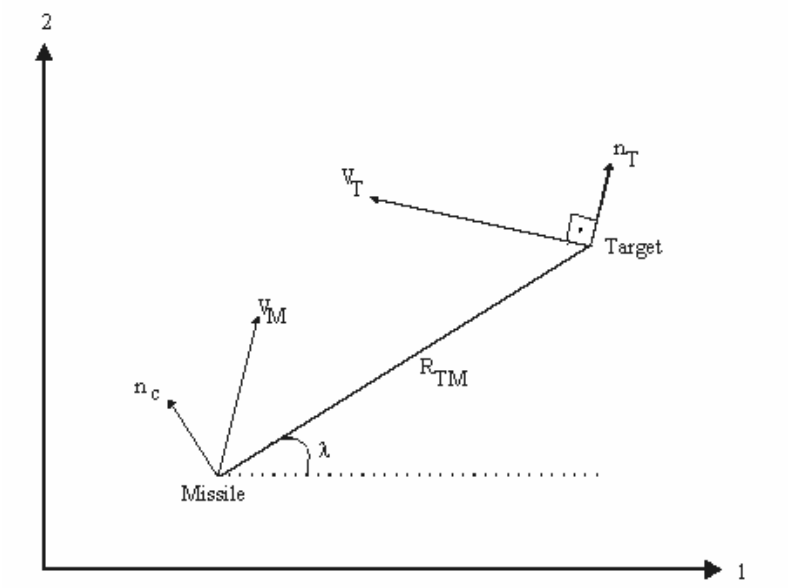

Figure 6-1: Two-dimensional missile-target engagement geometry

To derive relative kinematics between a missile and a target in the ECS, inertial azimuth and elevation LOS angles are expressed respectively as:

$$\lambda_{EL} = a\tan\left(\frac{-Z_r}{\sqrt{X_r^2 + Y_r^2}}\right), \tag{6-2}$$

$$\lambda_{AZ} = a\tan 2\left(Y_r, X_r\right), \tag{6-3}$$

where, Y_r and Z_r denote the relative position errors and R_{TM} stands for target-to-missile range that can be expressed as:

$$R_{TM} = \sqrt{X_r^{\,2} + Y_r^{\,2} + Z_r^{\,2}}\,. \tag{6-4}$$

In order to use equation (6-1) to compute the accelerations in a non-rotating fixed frame, V_c should be clarified as:

$$V_c = -\dot{R}_{TM}\,. \tag{6-5}$$

Once the equalities above are given, the guidance commands in the horizontal and vertical frames can be stated respectively as:

$$a_H = N\,\dot{\lambda}_{AZ}\,V_c\,, \tag{6-6}$$

$$a_V = N\dot{\lambda}_{EL}\,V_c\,. \tag{6-7}$$

Proportional navigation ratio (*N*) is taken as 4 in this study.

6.3 Proportional Integral Derivative Navigation Guidance (PIDNG)

6.3.1 PIDNG Method Formulation

The PID controller design method can be applied from a different perspective to the missile guidance problem [10]. It has a transfer function of the form:

$$G_c(s) = k_p + \frac{k_i}{s} + k_d s\,, \tag{6-8}$$

with the control input produced as:

$$u(s) = G_c(s)\,e(s)\,, \tag{6-9}$$

where, $e(s)$ stands for the error to be regulated to zero. In the equation stated above, controller input surely corresponds to steering command and error is the LOS rate in order for the missile to hit the target.

By using the idea in equations (6-8) and (6-9) with the rule that LOS rate is the variable to be nullified in guidance applications, the acceleration commands in the vertical and horizontal planes of the inertial frame can be stated as follows:

$$a_V = k_p \dot{\lambda}_{EL} + k_i \int \dot{\lambda}_{EL} dt + k_d \frac{d}{dt} \dot{\lambda}_{EL}\,. \tag{6-10}$$

$$a_H = k_p \dot{\lambda}_{AZ} + k_i \int \dot{\lambda}_{AZ} dt + k_d \frac{d}{dt} \dot{\lambda}_{AZ}\,. \tag{6-11}$$

Here, the proportional (k_p), integral (k_i) and derivative (k_d) navigation ratios are the design parameters chosen by the user via trial-and-error. The following section describes how these parameters were selected for the simulations done by PIDNG method throughout the thesis.

6.3.2 Parameter (k_p, k_i, k_d) Selection

In order to determine the proportional, integral and derivative navigation ratio parameters of the PIDNG method, a fast maneuvering target scenario (S3, given in the section 6.5.1.3) with a measurement rms value of 1 m is used. Also, for guidance in the horizontal and the vertical planes of the inertial frame, the same parameter set (k_p, k_i, k_d) is used.

Table 6-1 shows the performance of the 13 different parameter sets. Considering the results given in this table, if the miss distance is taken as the performance criterion, the best values of the parameters are obtained at case 11. Therefore, for the rest of the simulations where PIDNG is used in this thesis, proportional (k_p), integral (k_i) and derivative (k_d) navigation ratio parameters are used as 500, 10 and 0.1, respectively. To illustrate the effect of these parameters on the trajectory of the missile, three cases are chosen. The following figures give a feeling about how the integral and derivative navigation ratios affect the trajectory and hence the miss distance.

Table 6-1: Examples for PID parameter selection

Case	**k_p**	**k_i**	**k_d**	**Miss Distance (m)**	**Time (s)**
1	400	0	0	200.7	50.0
2	500	0	0	8.6	49.3
3	1000	0	0	53.9	41.4
4	1500	0	0	105.6	38.9
5	500	0.1	0	8.2	49.3
6	500	1	0	4.0	49.1
7	500	5	0	18.6	48.5
8	500	10	0	3.6	48.2
9	500	15	0	16.8	48.1
10	500	10	0.01	3.2	48.2
11	**500**	**10**	**0.1**	**0.9**	**48.3**
12	500	10	1	15.0	48.6
13	500	10	5	15.9	48.1

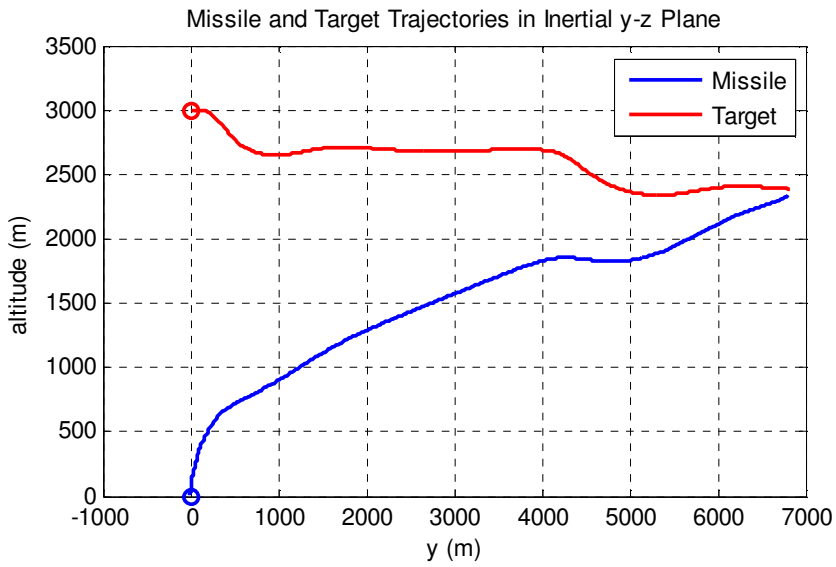

Figure 6-2: Case 4

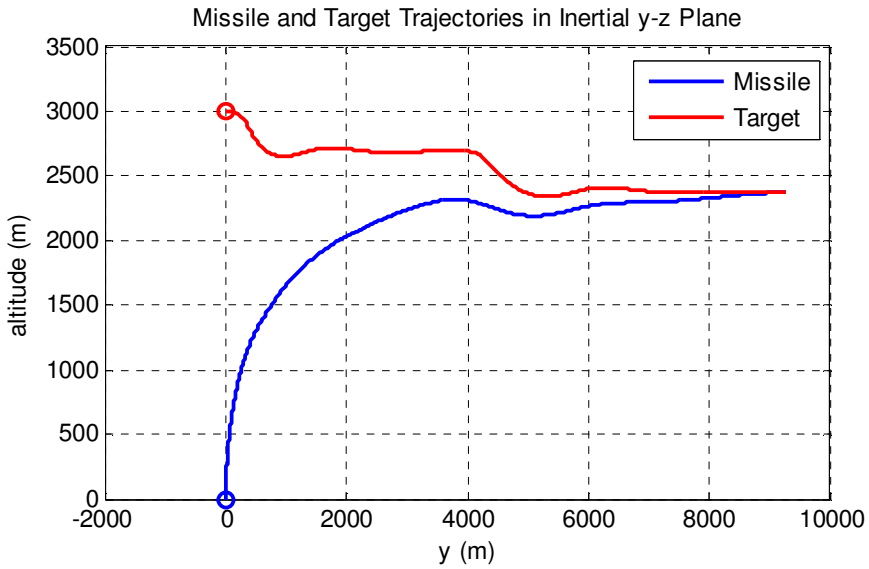

Figure 6-3: Case 7

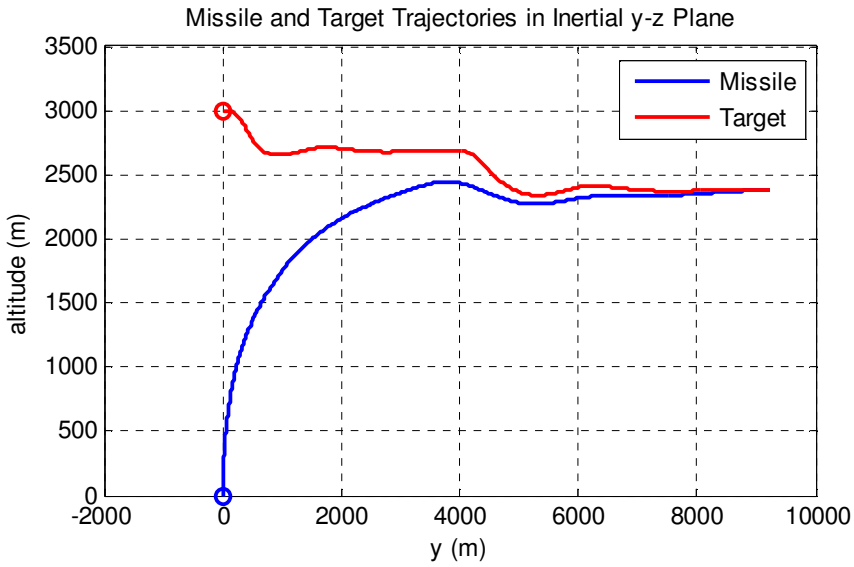

Figure 6-4: Case 11

6.4 Hybrid Proportional Navigation Guidance (HPNG)

PNG and PIDNG methods used in this thesis are based on the utilization of the measured position of the target to calculate the closing velocity and the LOS rate. These methods will suffer from the existence of the noise in the position measurements, especially, when the rms error of measurements are high. Therefore, an update in the calculated values of the closing velocity and the LOS rate is needed to improve the guidance performance of the missile. To decrease the effect of noise in the position measurements, a state estimator based on an Interacting Multiple Model (IMM) via Kalman filtering (KF) approach is used. Since both measurement and estimation values are utilized, this new method is called as "hybrid" PNG method.

Considering the motion of the aircraft, resultant state trajectory of it involves uniform motion and maneuvers. During all of the maneuvers, the missile's tracking performance should be high in order to decrease the miss-distance, the time of flight

and also the control effort used. So, the state estimation process is expected to give better performance in estimated position rms error compared to the measured position rms error. Also, the state estimator provides the velocity and acceleration estimations of the target that are unavailable for PNG and PIDNG cases.

An IMM-KF state estimator can be constructed such that, the uniform motion and the maneuvering motion of the target are modeled with the constant velocity (CV) and constant acceleration (CA) kinematics models [4]. Since the acceleration of the target being tracked is unknown for the missile sensor, it is modeled as a Gaussian noise with zero mean. Variance of the Gaussian noise changes according to the maneuver type being modeled, i.e.: noise with low variance is used for modeling the CV motion whereas noise with higher variance is used for modeling the CA motion. Also, CV and CA models are used in interaction such that the switching between them is a Markov process (Markov chain) with known transition probabilities.

The details of the CV and CA models used in this thesis are formulated in the following sections.

6.4.1 CV Model

The constant velocity (CV) motion model intends to represent the dynamics of a platform in uniform motion that is not maneuvering. The noise term, which is zero-mean white Gaussian, corresponds to the unknown target acceleration. The direct discrete-time kinematics model representing the CV motion is given as follows:

$$\bar{x}_{k+1} = \begin{bmatrix} I_3 & TI_3 \\ 0 & I_3 \end{bmatrix} \bar{x}_k + \begin{bmatrix} \frac{T^2}{2} I_3 \\ TI_3 \end{bmatrix} v_k = F\bar{x}_k + Gv_k \tag{6-12}$$

where, T represents the constant time difference between the steps, I_3 represents the identity vector of dimension 3 and v_k represents the unknown acceleration of the target called process noise. Here, the state vector contains the position in x, y, z

axes and the velocity in x, y, z axes, respectively. Throughout the guidance modeling in this thesis, T is taken as 0.05s which corresponds to sampling with 20Hz.

Since the acceleration is assumed to be an independent (i.e. white noise) process, this relation is also called *white-noise acceleration model* [4].

6.4.2 CA Model

In this model, the unknown target acceleration is assumed to be a process with independent increments [4]. According to [15], CA model is intended to represent the substantial, but transient, accelerations that are present at the beginning and the end of the maneuvers (e.g. the transition from constant velocity motion to a constant acceleration motion). In the discrete-time kinematics formulation of CA model shown below, the accelerations along x, y and z axes also take place as state variables:

$$\bar{x}_{k+1} = \begin{bmatrix} I_3 & TI_3 & \frac{T^2}{2} I_3 \\ 0 & I_3 & TI_3 \\ 0 & 0 & I_3 \end{bmatrix} \bar{x}_k + \begin{bmatrix} \frac{T^2}{2} I_3 \\ TI_3 \\ I_3 \end{bmatrix} v_k = F\bar{x}_k + Gv_k \qquad (6\text{-}13)$$

Note that, the white process noise v_k which is a zero-mean white sequence, representing the acceleration increment during a sampling period.

6.4.3 IMM Filter Structure

For the interacting multiple model (IMM) filter structure used in this thesis, three model matched filters are used, all of which are Kalman filters. One of these filters uses a CV model and the other two use CA models. Since, the unknown acceleration of the target being tracked may take values in a wide range, modeling all the maneuvering motions with only a single process noise rms may give a poor

performance. Instead, it is assumed that the target's uniform motion can be modeled with a single process (low) noise level and the maneuvering motion can be modeled by using two different (higher) noise levels. The following table shows the acceleration levels chosen to model the maneuvers done by the target.

Table 6-2: Process noise levels for the CV and CA models used

a_CV = 0.001 g, **a_CA1 = 0.01 g,** **a_CA2 = 1 g.**
a_CV : Acceleration level for the CV model
a_CAi : Acceleration increment level for the i^{th} CA model, i = 1, 2

More details about the modeling of the IMM filter can be found in [4]. Briefly, the steps used for the IMM filter are shown in the following figure:

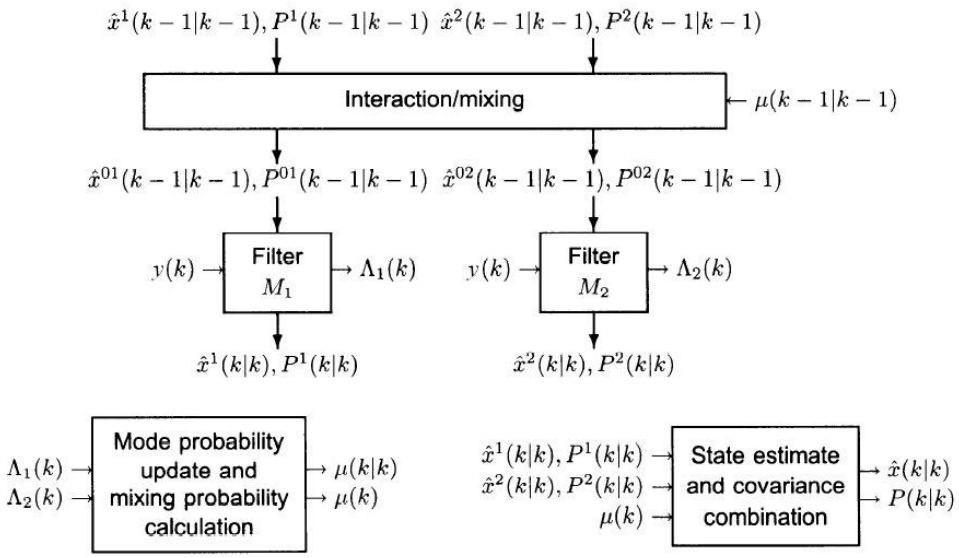

Figure 6-5: One cycle of the IMM Estimator [4].

The mixing of the models is characterized by the Markov transition probabilities. These probability values are assigned according to the properties of the dynamic system (for instance the maneuverability of the target). By considering the maneuvers expected to be done by the target, the Markov transition probabilities can be chosen by the designer. Following matrix shows the Markov transition probabilities that represent the switching between the CV and CA models used:

$$\begin{bmatrix} 0.90 & 0.05 & 0.05 \\ 0.01 & 0.94 & 0.05 \\ 0.01 & 0.01 & 0.98 \end{bmatrix}. \tag{6-14}$$

The first row of this matrix shows the transition probabilities of CV model to stay either in CV mode or switch to any of CA models. The total of these probabilities must be 1. Usually, the diagonal entries of the matrix are chosen between 0.80 and 0.98 that shows the probability of each model to stay in its mode [4].

The IMM filter can be expressed by the following four fundamental steps [4], [15]:

- **Interaction/Mixing:** In order to initialize each filter, the mode-conditioned state estimates and covariance are combined by using the mixing probabilities,

- **Mode-matched filtering:** The mode-conditioned state estimates and covariance are obtained by running the filter bank. Corresponding likelihood functions are also calculated for the next step,

- **Mode probability update:** Mixing and updated mode probabilities are calculated with respect to the likelihoods,

- **Overall state estimate and covariance combination:** The mode-conditioned state estimates and covariance are combined to obtain a joint estimate and covariance for output.

Note that, the Kalman filters using CV and CA models are representing the filters shown in Figure 6-5.

6.4.4 Kalman Filter

In this study, the discrete-time Kalman filter, where the measurements are taken and the state is estimated at every 0.05s in time, is used. The system model for this filter can be formulated as follows:

$$\bar{x}_{k+1} = F\bar{x}_k + B_k u_k + G_k v_k \tag{6-15}$$

$$\bar{z}_k = H_k \bar{x}_k + \bar{w}_k \tag{6-16}$$

where, B_k is the sensor gain matrix that is equal to G_k [15] since the acceleration of the missile itself, u_k, is subtracted from target acceleration in order to have a relative motion. Note that, in the case of a stationary observer, u_k is taken as zero. Also, $\bar{z}_k$ represents the position measurements taken by the sensor on the missile. Throughout the thesis, only the position measurements in 3-D are assumed to be

taken. Note also that, the process noise v_k, the measurement noise $\overline{w}_k$ and the initial state $\overline{x}_0$ have Gaussian distributions [4], [15].

The structure given in the following figure is used to form a Kalman filter model:

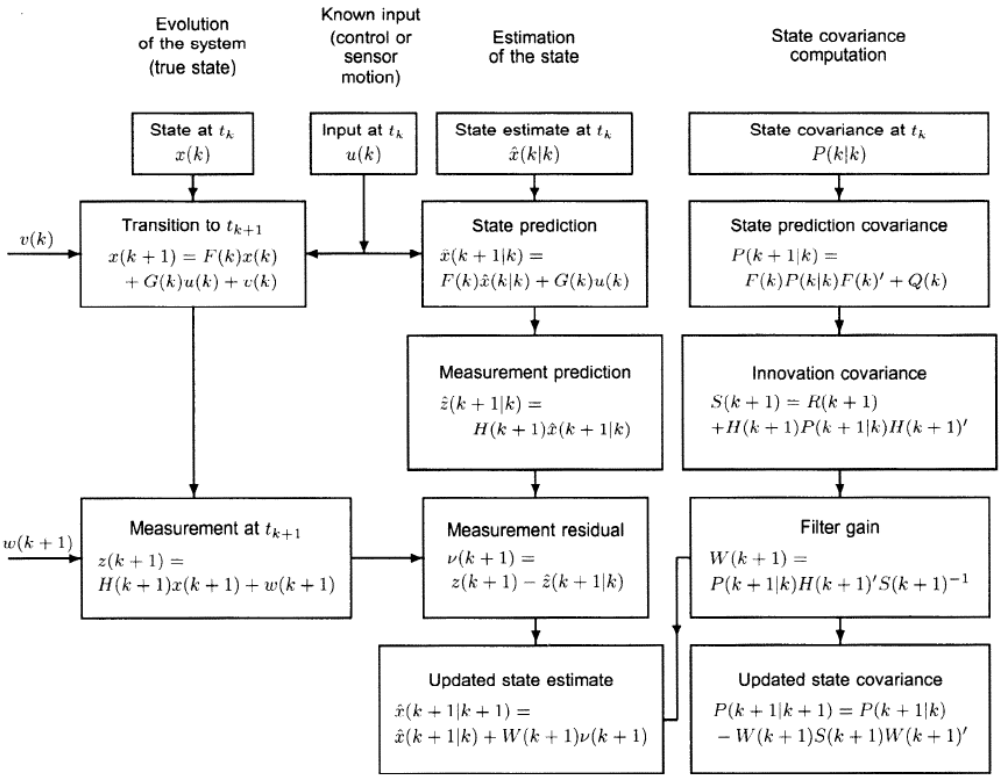

Figure 6-6: One cycle of the KF [4].

More details and examples of different filter designs can be found in [4] and [15].

6.4.5 Formulation of the HPNG Method

The derivation of this new method is based on the PNG method. The only modification to the acceleration commands generated by PNG is given as follows:

$$n_c = N_{meas}\dot{\lambda}_{meas}V_{c,meas} + N_{est}\dot{\lambda}_{est}V_{c,est} \tag{6-17}$$

where, the first part corresponds to the calculated values using the measurement, and the second part corresponds to the calculated values using the estimation. In fact, if the parameter N_{est} is chosen as zero, then this formulation is exactly in the form of a PNG formulation. By modifying the PNG formulation with the results of the estimations, an improvement is done if the estimation rms error is less than the measurement rms error. Throughout this study, the following equation is used in order to compare this new method with PNG fairly:

$$N_{meas} + N_{est} = 4\,, \tag{6-18}$$

where, N_{meas} corresponds to the parameter N that is used in the equations (6-1), (6-6) and (6-7).

If the estimated positions by the IMM filter are closer to the real position values other than the measured position values, then the higher the N_{est} value, the more effective the noise reduction in the signals used by the guidance system. As a consequence, the guidance system that uses HPNG method will perform better than the PNG method.

6.4.5.1 Selection of N_{est}

To select an appropriate value for N_{est}, HPNG method is tested on three different scenarios defined in section 6.5.1. For these scenarios, different measurement noise rms values (σ_w) are used to see the effectiveness of the state estimation process. Here, σ_w represents the noise rms for each of three axes.

Table 6-3: N_{est} selection

		σ_w = 1 m			σ_w = 5 m			σ_w = 10 m		
		S1	**S2**	**S3**	**S1**	**S2**	**S3**	**S1**	**S2**	**S3**
N_{est} = 0	**Miss Dist. (m)**	**10**	**6**	**4**	**675**	**820**	**213**	**3977**	**3506**	**3526**
	Time (s)	44	36	49	37	30	40	8	11	11
N_{est} = 1.0	**Miss Dist. (m)**	**10**	**13**	**2**	**22**	**92**	**133**	**1969**	**684**	**486**
	Time (s)	44	36	49	42	34	41	37	34	39
N_{est} = 2.0	**Miss Dist. (m)**	**10**	**24**	**3**	**54**	**25**	**87**	**409**	**857**	**456**
	Time (s)	44	36	50	42	35	43	38	28	37
N_{est} = 3.0	**Miss Dist. (m)**	**12**	**31**	**5**	**33**	**59**	**134**	**447**	**47**	**393**
	Time (s)	44	36	50	43	35	44	38	34	38
N_{est} = 3.5	**Miss Dist. (m)**	**18**	**34**	**1**	**12**	**148**	**121**	**19**	**196**	**108**
	Time (s)	44	36	50	44	34	45	42	34	42
N_{est} = 3.9	**Miss Dist. (m)**	**19**	**35**	**5**	**131**	**79**	**40**	**21**	**154**	**130**
	Time (s)	44	36	50	43	35	48	43	35	44
N_{est} = 4.0	**Miss Dist. (m)**	**18**	**32**	**11**	**136**	**82**	**27**	**200**	**34**	**51**
	Time (s)	44	36	50	43	35	48	43	145	47

Remark: Throughout the study, miss distance represents the closest distance between the missile and the aircraft trajectories (position states in 3D). Also, the parameter, named "time", given in Table 6-3 represents the time duration after launch up to the instant when the miss distance is reached.

If the miss distance values of the simulations are considered, the higher the N_{est} value, the lower the miss distance for the cases with high rms noise. This result shows that the miss distance obtained by a missile using a PNG based guidance method can be improved with using IMM filter based estimator.

The choice of the N_{est} value depends on the noise level in the measurements. For the simulations done utilizing HPNG method in this thesis, the N_{est} value is used as 3.9. Since the performance of the guidance methods cited here are important in the existence of normal or high level measurement noise, selecting N_{est}=3.9 is expected to result in reasonable miss distance values.

An alternative way of using such an IMM estimator to decrease the noise in the raw measurements is the proper selection of measurement error covariance matrix entries that represent the designer's confidence about the reliability of the measurements. In this case, the N_{est} value is used as 4 to rely only on the estimations other than the measurements. However, our objective is just to decrease the noise in the raw position measurements by using an estimator. The following examples show that the performance of the chosen IMM estimator is satisfactory.

For three of the cases tested above (that are used for the selection of the N_{est} value), position rms errors are shown in the following figures:

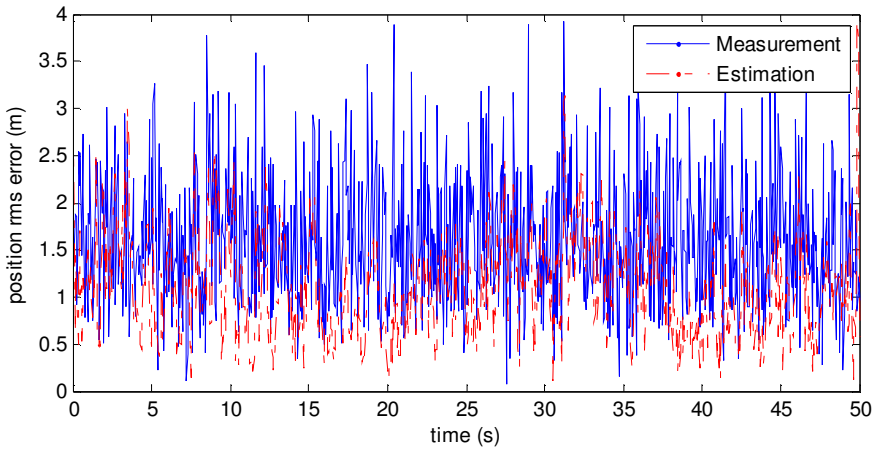

Figure 6-7: Measurement and estimation errors for S3, N_{est}=3.9, σ_w=1 m

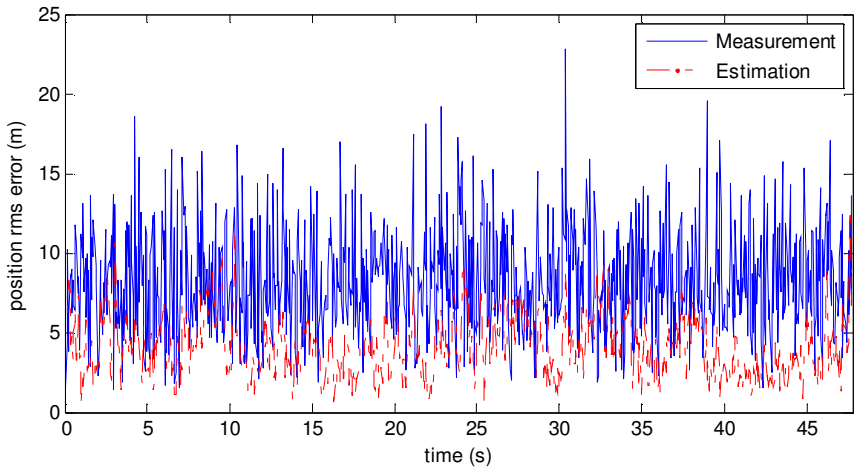

Figure 6-8: Measurement and estimation errors for S3, N_{est}=3.9, σ_w=5 m

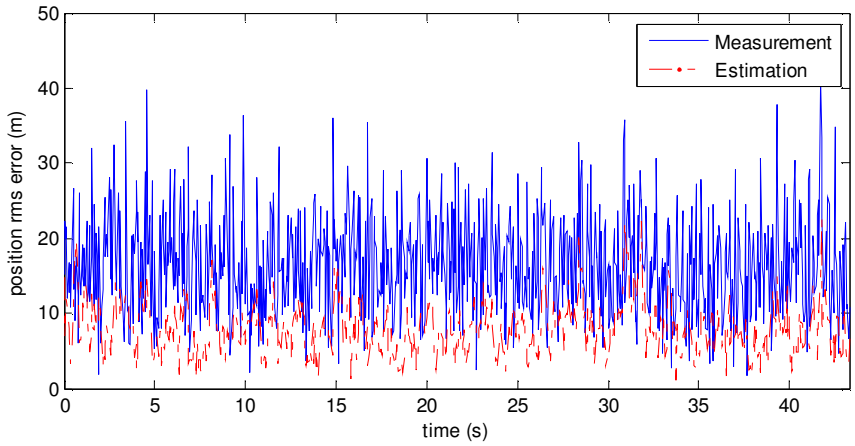

Figure 6-9: Measurement and estimation errors for S3, N_{est}=3.9, σ_w=10 m

It is obvious from the figures above that, the estimation process is successful in decreasing the noise on the position measurements and also, its effect is more clear when the measurement noise level is high.

6.5 Performance Comparison of the Guidance Methods

6.5.1 Scenarios

Basically, there are three main scenarios used for the comparison of the missile guidance systems' performances. For these scenarios, aircraft is used as target for the missile and the trajectory of the target is obtained by applying suitable reference command signals.

For scenarios S1, S2 and S3 defined below, the following initial conditions are used:

Table 6-4: Initial conditions for the scenarios

Initial Conditions for S1, S2 and S3	**Missile**	**Aircraft**
Initial Position (m)	$[0 \quad 0 \quad 0]$	$[4000 \quad 0 \quad -3000]$
Initial Velocity in BCS (m/s)	$[292.4 \quad 0 \quad 0]$	$[199.9 \quad 0 \quad 5.1]$
Initial Euler Angles ϕ_0, θ_0, ψ_0 (deg)	$[0 \quad 37 \quad 0]$	$[0 \quad 0 \quad 30]$

6.5.1.1 Scenario 1 (S1)

For this scenario, there are no reference commands so that, the aircraft has a uniform motion with the given initial conditions. This flight can be called as the straight level flight. There is no maneuvering action for the aircraft during S1 so the resultant trajectory is shown in Figure 6-10, Figure 6-11 and Figure 6-12.

6.5.1.2 Scenario 2 (S2)

During this scenario, only the height and the heading of the aircraft are changed while the speed is kept fixed, so, this scenario can be called as slow maneuvering case. The resultant trajectory is shown in Figure 6-10, Figure 6-11 and Figure 6-12.

6.5.1.3 Scenario 3 (S3)

Compared to the scenarios S1 and S2, this scenario is representing a fast maneuvering action of aircraft since it consists of the speed, height and the heading change during the scenario. Hence, the trajectory obtained is shown in Figure 6-10, Figure 6-11 and Figure 6-12.

Remark: The following 3 figures show the trajectories obtained from a single run of the scenarios S1, S2 and S3 that takes 100 s. In order to show the resultant 3-D

trajectories with a better sense of the maneuvers, output of the single run is given from 3 different view angles.

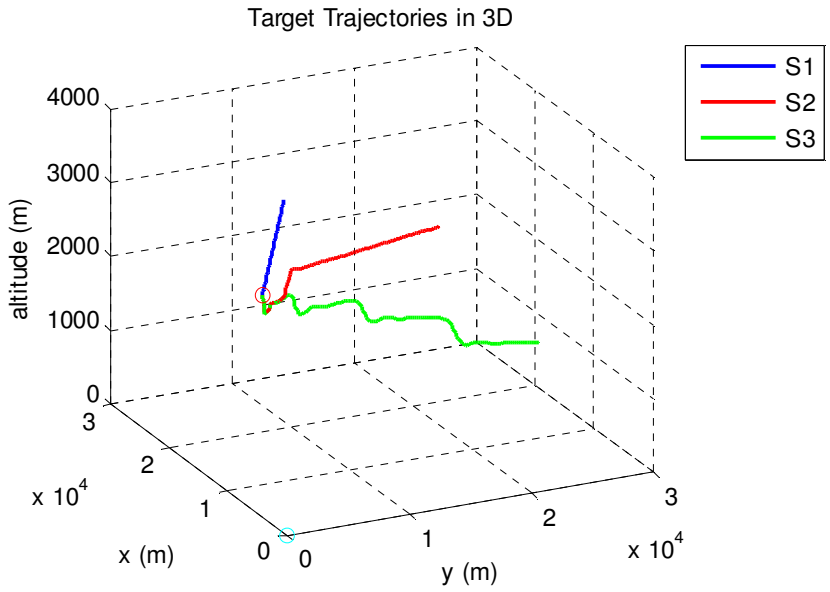

Figure 6-10: Aircraft trajectories for S1, S2 and S3 – 1st view angle

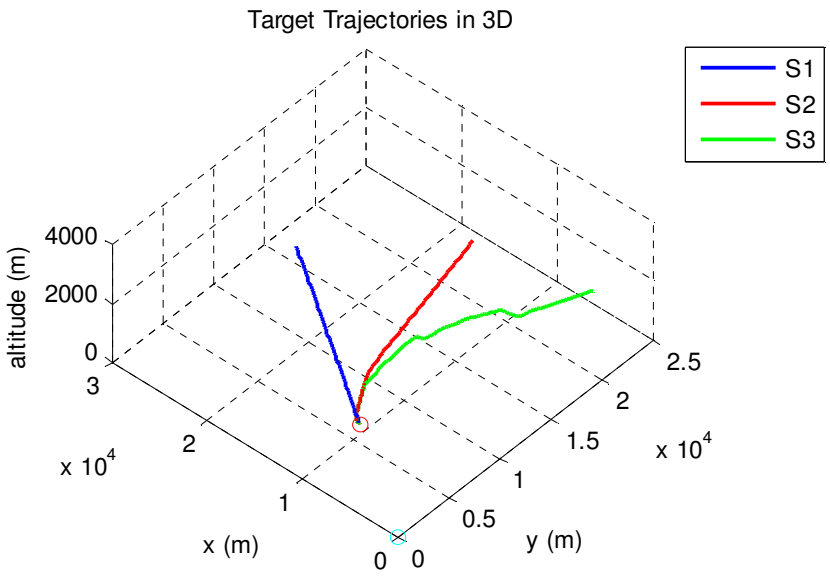

Figure 6-11: Aircraft trajectories for S1, S2 and S3 – 2nd view angle

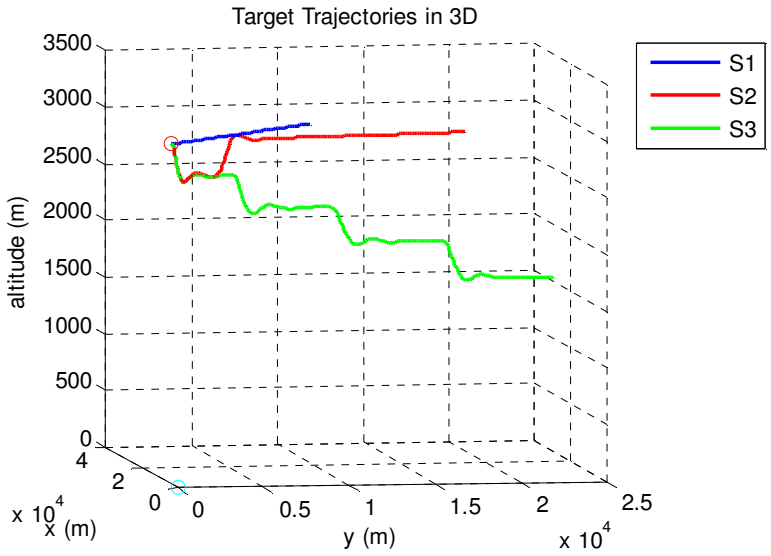

Figure 6-12: Aircraft trajectories for S1, S2 and S3 – 3rd view angle

6.5.2 Simulation Results

In this section, the performance comparison is done for the PIDNG and HPNG methods, since the PNG method performs worse than the HPNG method in the existence of noise on the position measurements (see the section 6.4.5.1).

The three scenarios given in the previous section (S1, S2 and S3) were used with different noise levels on the position measurement. Also, the success criterion is taken as the 50 m kill distance, that is to say, miss distance values that are below 50 m are called as success for the evaluation of the missile guidance methods.

By checking the simulation results given in the following table, although both methods have same success in most of the cases, performance of the new method, HPNG, is higher when the measurement noise level is high. As a result, utilization of the position values estimated by an IMM filter structure and then updating the PNG method by combining the measurement and estimation results give way to a new guidance method, which performs much better than the classical PNG method. This new method, HPNG, even works better than the PIDNG method in some of the scenarios when the measurement noise level is high.

Table 6-5: Comparison of PIDNG and HPNG Methods

Noise rms (m)	Scenario	PIDNG		HPNG		Success
		Miss Distance (m)	Time (s)	Miss Distance (m)	Time (s)	
$\sigma_w = 1$	**S1**	11.1	45.9	18.8	44.5	BOTH
	S2	1.7	36.3	34.7	35.8	BOTH
	S3	0.9	48.3	8.2	50.0	BOTH
$\sigma_w = 5$	**S1**	7.8	44.8	130.7	43.2	**PIDNG**
	S2	17.7	35.8	79.2	35.2	**PIDNG**
	S3	4.7	45.5	39.6	47.8	BOTH
$\sigma_w = 7$	**S1**	12.9	44.1	10.7	43.6	BOTH
	S2	102.0	34.5	369.1	32.8	NONE
	S3	62.6	42.9	22.2	45.6	**HPNG**
$\sigma_w = 9$	**S1**	83.6	44.1	45.0	43.4	**HPNG**
	S2	53.6	35.2	240.0	34.6	NONE
	S3	381.7	40.1	127	43.9	NONE
$\sigma_w = 13$	**S1**	155.5	43.0	160.5	42.1	NONE
	S2	284.6	34.9	544.1	31.4	NONE
	S3	162.6	39.8	195.4	41.6	NONE

CHAPTER 7

GUIDANCE OF THE AIRCRAFT

7.1 Introduction

To guide an aircraft under a missile threat such that the miss distance is maximized, is a difficult problem and there is not a systematic way of solving such a problem. According to some of the states (i.e. speed, direction, range) at the beginning of the engagement scenario and also the dynamic limits of the aircraft and the missile, the effective way of missile evasion technique for the aircraft is expected to change.

In this chapter, the aim is to develop a rule based missile evasion method to guide the aircraft such that, the aircraft is successfully evaded by increasing the miss distance. To do this, first, maximization of the miss distance is expressed as an optimal control problem. After the optimal control problem is formulated and a solution technique is given, this solution technique is applied on 45 cases that have different initial conditions (in terms of the aircraft-missile distance, the relative speed and direction at the beginning of the scenario). Then, by extracting a rule from each of these cases, the reference signals of the aircraft autopilot is determined. It is important to note that, these reference signals are the delta speed, delta height and the delta yaw command signals.

Although these 45 cases are chosen to characterize the typical engagement scenarios, a new optimal control problem with a different initial condition other

than these 45 cases should also be dealt with. Instead of solving the optimal control problem for this new case, an interpolation method is formulated so that a solution to a new case is found by combining the solutions of 45 cases by taking the distance of the new case to all of the 45 cases into consideration. Since finding the solution to an optimal control problem necessitates solving an adjoint system of differential equations backward in time, its online implementation is unrealizable. However, the proposed interpolation algorithm finds a solution online by combining the solutions of the 45 optimal control problems that are solved offline.

Finally, formulation of a PNG-based guidance technique is given in order to evaluate the performance of the proposed rule-based missile evasion method under some simulations (that are given in the next Chapter).

7.2 Rule Based Missile Evasion Method

7.2.1 Miss Distance Maximization as an Optimal Control Problem

The optimal control problem for the miss distance maximization can be formulated as follows:

$$\min_{\bar{u}(t)} J = -\left\| \vec{P}_m(t_{final}) - \vec{P}_a(t_{final}) \right\|, \tag{7-1}$$

subject to the equation (2-37) with the following constraints and the initial condition:

$$\begin{aligned} & G(\bar{x}(t)) \le 0 \\ & \bar{u}_{\min} \le \bar{u}(t) \le \bar{u}_{\max} \ , \\ & \bar{x}(0) = \bar{x}_0 \end{aligned} \tag{7-2}$$

where, $G(.)$ is a vector mapping of state inequality constraints, $\vec{P}_m(t_{final})$ and $\vec{P}_m(t_{final})$ are the position of the missile and the aircraft at $t=t_{final}$, $\bar{u}_{\min}$ and $\bar{u}_{\max}$ are

the bounds of the control input vector. This problem is an optimal control problem (with fixed final time) with state and input dependent inequality constraints. Thus, instead of solving this problem analytically, nonlinear programming and simulation tools are used in this thesis.

7.2.2 Typical Engagement Scenarios

Throughout this study, a typical engagement scenario is defined with the initial distance between missile and aircraft, R (Figure 7-2), and the angle between the initial velocity vectors of the missile and the aircraft, θ (Figure 7-1).

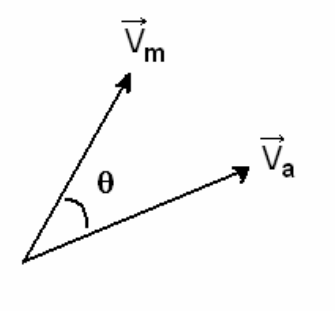

Figure 7-1: Missile and aircraft velocity vectors at the launch time

To illustrate the generic missile-aircraft engagement scenarios, the following figures are given:

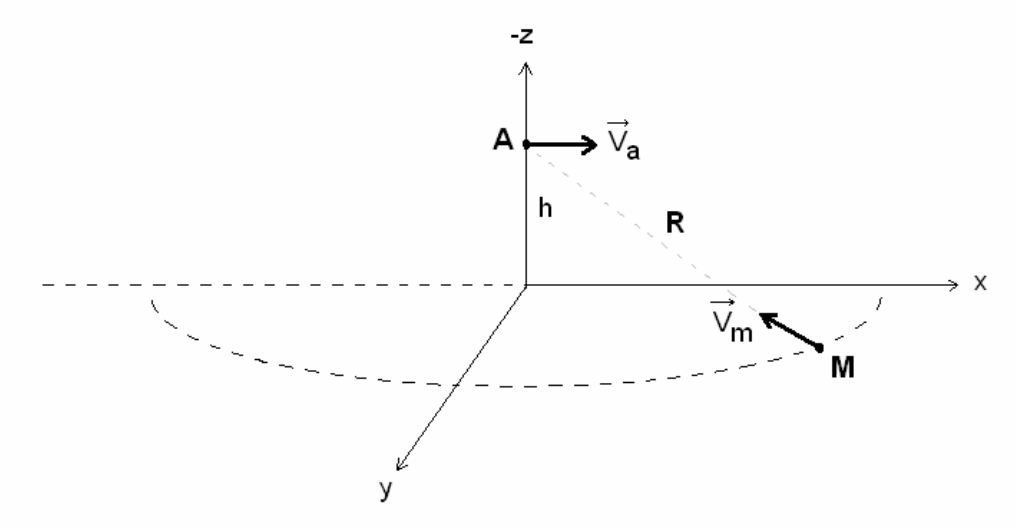

Figure 7-2: Generic engagement scenario for a missile and an aircraft - 1

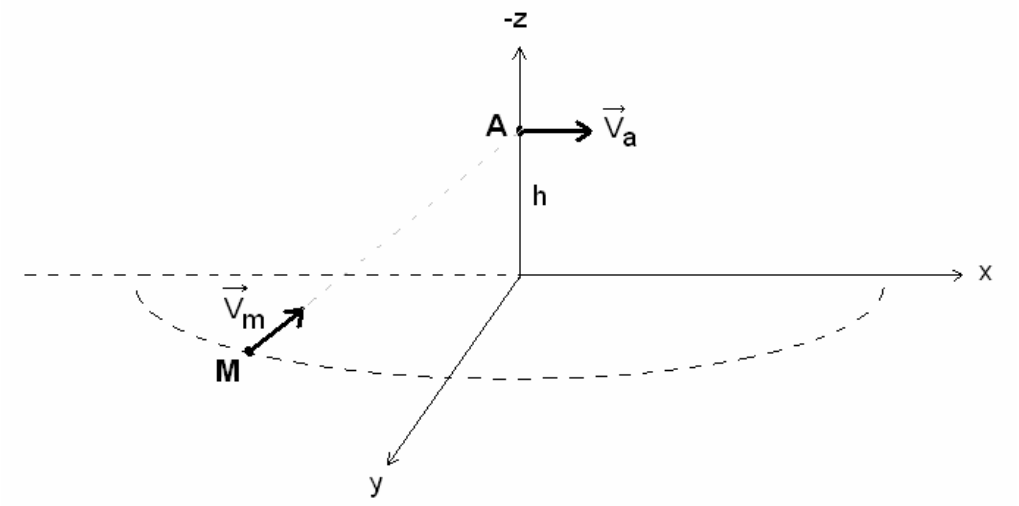

Figure 7-3: Generic engagement scenario for a missile and an aircraft - 2

For all of the cases chosen, the direction of $\vec{V}_a$ is along the x-axis of the ECS. When the distance between the missile and the aircraft, R, the initial altitude of the aircraft, h, and the angle θ are given, the (x_m,y_m) coordinates of the missile launch point are calculated with the following formula, assuming that the missile launch point lies on the horizontal plane of ECS, with z_m = 0 m:

$$\begin{aligned} x_m &= -R\cos\theta \\ y_m &= \sqrt{R^2\sin^2\theta - h^2} \end{aligned}. \tag{7-3}$$

From the formula above, it is seen that the x_m takes both positive and negative values according to the angle θ, however, y_m only takes positive values. This convention is used since (x_m,-y_m) coordinates are just the symmetric points with respect to the x-z plane of the ECS. Using (x_m,-y_m) as the launch point instead of (x_m,y_m) differs only in the lateral plane of the motion due to the symmetry of the aircraft and the missile. The following figure shows the launch point that is symmetric with the one shown in the previous figure.

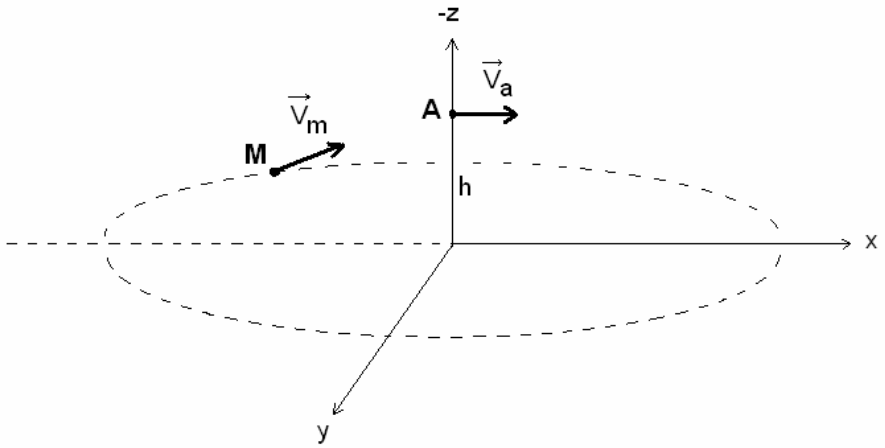

Figure 7-4: Generic engagement scenario for a missile and an aircraft - 3

In order to see the aircraft's maneuvering capability for evasion, 5 different R and 9 different θ values are selected as follows:

$$R = \{500, 1000, 2000, 3000, 3500\}$$
$$\theta = \{10, 30, 50, 70, 90, 110, 130, 150, 170\}' \quad (7\text{-}4)$$

where, R is in meters and θ is in degrees and also total number of (R,θ) combinations is 45.

Bu using the scenario and parameter definitions above, the following table is obtained to summarize the conditions for all of the 45 cases:

Table 7-1: Engagement scenario parameters

Case #	R (m)	θ (deg)	h (m)	x_m (m)	y_m (m)	t_{final} (s)
1	500	10	85	-492	18	3.46
2	500	30	85	-433	235	3.08
3	500	50	85	-321	373	2.55
4	500	70	85	-171	462	2.07
5	500	90	85	0	493	1.71
6	500	110	85	171	462	1.45
7	500	130	85	321	373	1.29
8	500	150	85	433	235	1.18
9	500	170	85	492	18	1.14
10	1000	10	170	-985	35	6.91
11	1000	30	170	-866	470	6.15
12	1000	50	170	-643	747	5.10
13	1000	70	170	-342	924	4.15
14	1000	90	170	0	985	3.42
15	1000	110	170	342	924	2.91
16	1000	130	170	643	747	2.57
17	1000	150	170	866	470	2.37
18	1000	170	170	985	35	2.27
19	2000	10	340	-1970	71	13.82
20	2000	30	340	-1732	940	12.31
21	2000	50	340	-1286	1494	10.21
22	2000	70	340	-684	1848	8.30
23	2000	90	340	0	1971	6.84
24	2000	110	340	684	1848	5.82
25	2000	130	340	1286	1494	5.14

Table 7-2: Engagement scenario parameters – cont'd

Case #	R (m)	θ (deg)	h (m)	x_m (m)	y_m (m)	t_{final} (s)
26	2000	150	340	1732	940	4.74
27	2000	170	340	1970	71	4.54
28	3000	10	510	-2954	106	20.74
29	3000	30	510	-2598	1411	18.46
30	3000	50	510	-1928	2241	15.31
31	3000	70	510	-1026	2773	12.44
32	3000	90	510	0	2956	10.26
33	3000	110	510	1026	2773	8.73
34	3000	130	510	1928	2241	7.72
35	3000	150	510	2598	1411	7.10
36	3000	170	510	2954	106	6.82
37	3500	10	595	-3447	124	18.05
38	3500	30	595	-3031	1646	17.01
39	3500	50	595	-2250	2614	15.34
40	3500	70	595	-1197	3235	13.56
41	3500	90	595	0	3449	11.97
42	3500	110	595	1197	3235	10.72
43	3500	130	595	2250	2614	9.81
44	3500	150	595	3031	1646	9.23
45	3500	170	595	3447	124	8.95

For these 45 cases, the initial speed of the missile is taken as 292.4 m/s, the initial speed of the aircraft for the cases 1-36 is taken as 150 m/s and for the cases 37-45, it is taken as 100 m/s. This difference in the aircraft initial speed stems from the constraint on the final time and the step size of the simulations in order for them to be solvable with a powerful workstation (64 bit, 3.6 GHz processor with 8 MB RAM). In addition, the final time of an engagement is calculated with the following equation:

$$t_{final} = \frac{R}{\left\|\vec{V}_m\right\| - \left\|\vec{V}_a\right\| \cos\theta}, \tag{7-5}$$

where, the distance between the aircraft and the missile (at the launch time) is divided by the difference of the missile and aircraft's initial velocity vector components along the LOS direction.

7.2.2.1 Solutions of the 45 Cases

7.2.2.1.1 Problem Solution Method

The formulation and the solution of the optimal control problem used in this thesis are defined in [19].

The steps of the solution method used here is similar to the one used for the optimization method explained in section 4.3. The basic differences are the state and the input constraints and also the minimization here is applied on the aircraft nonlinear model. So, "fmincon" function is used again to minimize the cost function given in equation (7-1) subject to the following state and input constraints:

$$
\begin{aligned}
&35\,m/s \le V_a \le 270\,m/s \\
&-10^\circ \le \alpha \le 45^\circ \\
&-30^\circ \le \beta \le 30^\circ \\
&0\,m \le h \le 12000\,m \\
&0 \le pow \le 100 \\
&-89^\circ \le \theta \le 89^\circ \\
&-179^\circ \le \phi \le 179^\circ \\
&-179^\circ \le \psi \le 179^\circ \\
&0 \le \delta_{th} \le 1 \\
&-25^\circ \le \delta_e \le 25^\circ \\
&-21.5^\circ \le \delta_a \le 21.5^\circ \\
&-30^\circ \le \delta_r \le 30^\circ
\end{aligned}
\quad . \qquad (7\text{-}6)
$$

Here, the position of the missile is obtained by taking the position states of the missile designed in section 5.2 that uses the PNG method given in section 6.2.

During the simulations, measurement noise is not used, so both the missile and the aircraft are assumed to have each other's position information in the ECS.

Note that, the control input trim values calculated for the speed (V_a) and altitude (h) given for each case (by using the trimming algorithm defined in section 2.3) are used as the initial conditions to start the minimization process.

By choosing a suitable termination condition, (i.e.: the directional derivative = 1e-6, 1-D search step length = 5e-4, maximum number of iterations = 150), the problem is solved for all of the 45 cases successfully. Results of some of the cases are given in the next section.

7.2.2.1.2 Results

All the 45 cases are solved with the proposed solution method given in the previous section. The solution for each case is composed of the optimal control input vector for the aircraft which is given in the equation (2-36). Note that, the time duration of each control input vector is t_{final} seconds, and it changes for each case.

The following 5 example cases show the resulting state trajectories after applying the optimal control input vector to the nonlinear aircraft model:

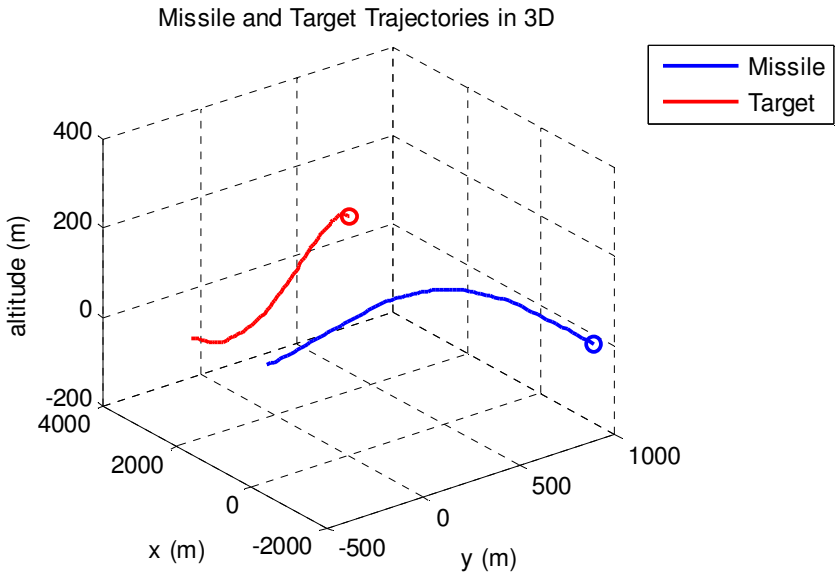

Figure 7-5: Case 20, miss distance = 720 m

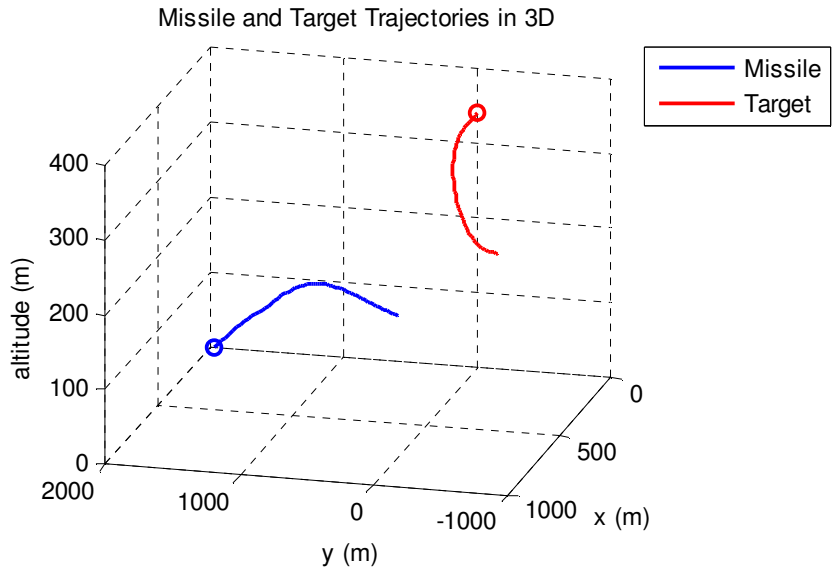

Figure 7-6: Case 23, miss distance = 766 m

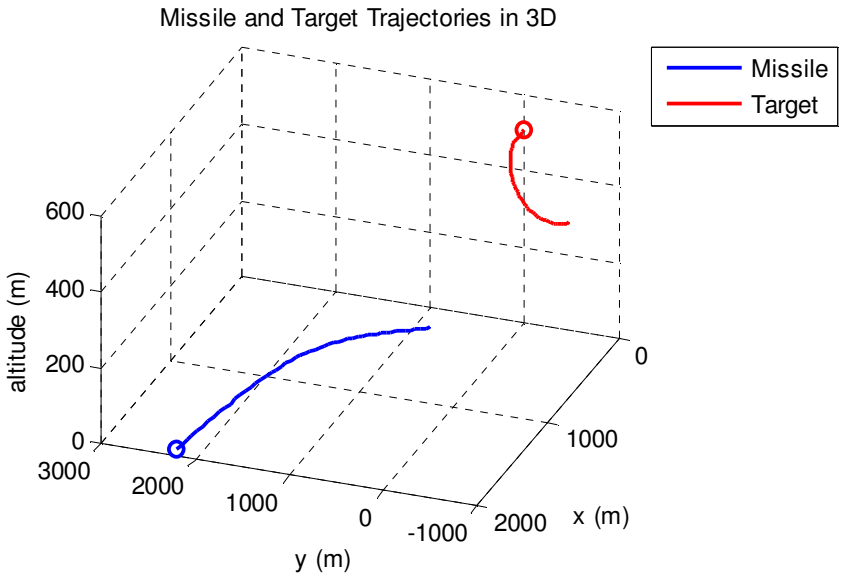

Figure 7-7: Case 34, miss distance = 1208 m

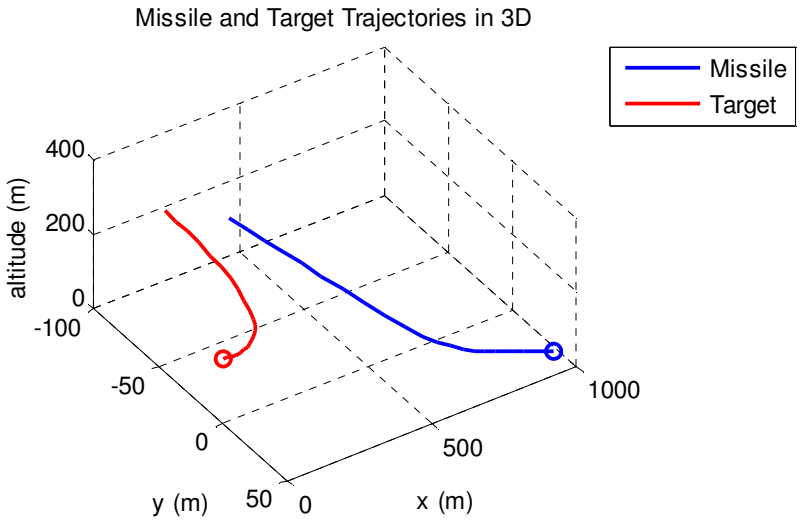

Figure 7-8: Case 18, miss distance = 173 m

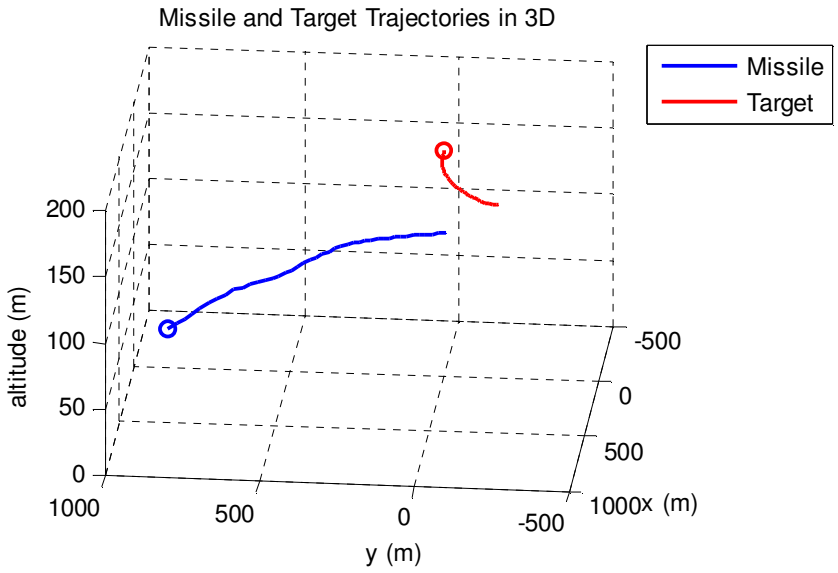

Figure 7-9: Case 13, miss distance = 210 m

7.2.2.2 Rule Extraction

Since the autopilot of the aircraft uses delta speed, delta height and delta yaw as the command signals, the solution of each case, given in the previous section, must be converted to delta speed, delta height and delta yaw commands. To do this, the values of delta speed, delta height and delta yaw at t=0 is subtracted from their values at $t=t_{final}$. So, the optimal control input found for each case, $\bar{u}_i$, is converted to a rule, $\bar{r}_i$, that is composed of the reference command signals of the aircraft autopilot:

$$\bar{r}_i = \begin{bmatrix} \Delta V_i \\ \Delta h_i \\ \Delta \psi_i \end{bmatrix} = \begin{bmatrix} \Delta V_i(t_{final}) - \Delta V_i(0) \\ \Delta h_i(t_{final}) - \Delta h_i(0) \\ \Delta \psi_i(t_{final}) - \Delta \psi_i(0) \end{bmatrix}, \quad i = 1,...,45. \tag{7-7}$$

The rules extracted for the engagement scenarios defined in Table 7-1 are given in the following table:

Table 7-3: Rules for the determination of the aircraft autopilot commands

Case #	ΔV (m/s)	Δh (m)	Δψ (deg)
1	12	1	-1
2	-1	-34	-10
3	-13	25	-9
4	-45	40	-60
5	-10	-10	36
6	-3	13	11
7	-17	6	-45
8	-23	11	46
9	-1	-3	10
10	55	-132	-2
11	45	-80	-30
12	21	-25	-45
13	1	5	-60
14	-14	-53	65
15	-27	-25	79
16	-12	30	1
17	-35	30	-75
18	-63	54	-120
19	120	-340	-5
20	105	-333	-16
21	95	-340	-37
22	58	-174	-69
23	28	-70	-83
24	3	-23	-103
25	-59	21	-114
26	-56	41	-118
27	-84	210	50
28	84	-368	-3
29	92	-505	-31
30	90	-505	-51
31	77	-376	-56
32	66	-300	-88
33	44	-186	-109
34	8	-125	-127
35	-12	-134	-139
36	-73	134	-119
37	124	-595	-2

Table 7-4: Rules for the determination of the aircraft autopilot commands – cont'd

Case #	ΔV (m/s)	Δh (m)	Δψ (deg)
38	133	-592	-25
39	126	-590	-32
40	118	-525	-68
41	83	-392	-83
42	83	-373	-110
43	58	-335	-129
44	33	-330	-142
45	8	-260	-174
Max.	**133**	**210**	**79**
Min.	**-84**	**-595**	**-174**

7.2.3 Interpolation Algorithm

The function of the algorithm given here is to find a rule, $\bar{r}$, for an arbitrary case other than those 45 cases.

First, define the initial condition of each case given in the previous section as an event, $\overline{E}$. Each event can be defined by the initial distance between missile and aircraft, R, and the initial angle between the velocity vectors of the missile and the aircraft, θ:

$$\overline{E}_i = \begin{bmatrix} R_i \\ \theta_i \end{bmatrix}, \quad i = 1,2,3,\ldots,45. \tag{7-8}$$

Then, define the initial condition of an arbitrary case as an input event:

$$\overline{E} = \begin{bmatrix} R \\ \theta \end{bmatrix}. \tag{7-9}$$

After that, distance of the arbitrary event to an event is defined as follows:

$$d_i = \left\| \overline{E} - \overline{E}_i \right\|, \quad i = 1,\ldots,45. \tag{7-10}$$

If $\overline{E}$ is very close to $\overline{E}_i$, then $\bar{r}_i$ is used as the rule for the input event. If not, then $\bar{r}$ can be given as:

$$\tilde{d}_i = \frac{1}{d_i}, \quad i = 1,...,45$$
$$w_i = \frac{\tilde{d}_i}{\sum_{i=1}^{45} \tilde{d}_i} \quad . \tag{7-11}$$
$$\bar{r} = \sum_{i=1}^{45} w_i \bar{r}_i$$

The threshold value to check the closeness of the events can be represented with ε.

Since the units of R and θ are different, normalization must be used at the beginning of the interpolation algorithm:

$$R = \frac{R_{actual}}{R_{\max}}, \quad \theta = \frac{\theta_{actual}}{\theta_{\max}}, \tag{7-12}$$

where, θ_{max}=170°, R_{max}=3500 m, and the subscript "actual" represents the value of the variable before the normalization process. As a consequence, the normalized values of R_{actual} and θ_{actual} are used in the definition of both $\overline{E}$ and $\overline{E}_i$.

Finally, the following equation can be used as the threshold value for the distance:

$$\varepsilon = \left(\begin{bmatrix} \frac{R_{eps}}{R_{\max}} \\ \frac{\theta_{eps}}{\theta_{\max}} \end{bmatrix}^T \begin{bmatrix} \frac{R_{eps}}{R_{\max}} \\ \frac{\theta_{eps}}{\theta_{\max}} \end{bmatrix} \right)^{0.5}, \tag{7-13}$$

where, the subscript "eps" shows the threshold value of the variable, for example: R_{eps}=25 m and θ_{eps}=1°.

7.2.4 Implementation Details

During the implementation of the rule based missile evasion method, the interpolation algorithm defined in the previous section is applied at every time step of the simulation. Note that, the flight simulations throughout this thesis are run with a fixed-step size of 10 ms.

Note that, since the formulated optimal control problem is complex, solving it with a normal PC is not possible even the fixed-step size in the optimization process is chosen large (i.e.: about 100 ms). Thus, a powerful workstation is needed to solve this kind of a problem. It is obvious that, there is a compromise between the duration of the engagement scenarios (t_{final}) and the fixed step size of the simulations. If the duration is increased, then large step size must be chosen to solve it, and by choosing it large, the solution does not always converge.

7.3 Anti-Proportional Navigation Guidance (Anti-PNG)

7.3.1 Formulation

This guidance method is based on the PNG method which is explained in [20]. The formulas given in section 6.2 for the PNG method are generally applicable with a minor change in the sign of the produced acceleration commands. The main idea of the anti-PNG method is to guide the aircraft with a command (n_T in Figure 7-10) which is the negative of the PNG command (n_T' in Figure 7-10). By doing this, the aircraft is forced to evade from the missile instead of having a collision.

A 2-D aircraft-missile engagement geometry which is similar to the one given in Figure 6-1 is given as follows:

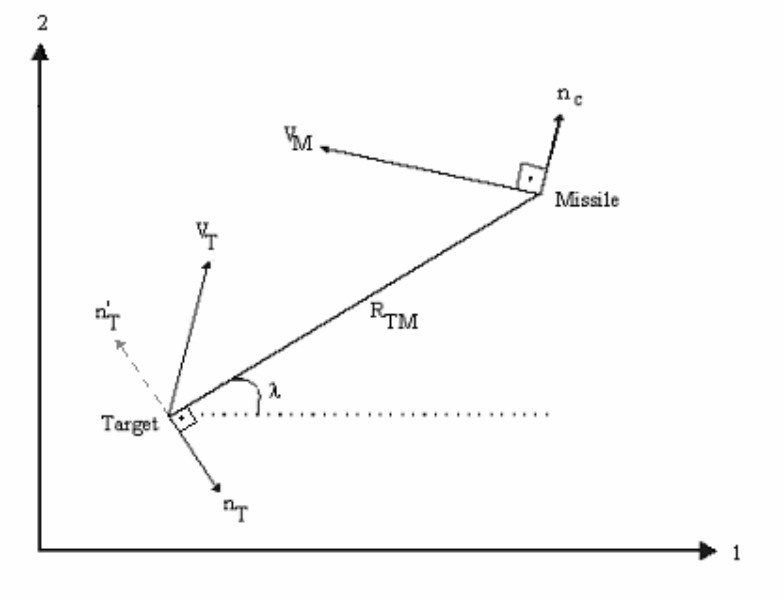

Figure 7-10: Two-dimensional target-missile engagement geometry.

Equations (6-1) to (6-5) are directly used in order to formulate the anti-PNG method. In addition, equations (6-6) and (6-7) are used with a negative sign as shown below to express the guidance commands in the horizontal and vertical frames, respectively:

$$a'_H = -N\dot{\lambda}_{AZ}V_c, \tag{7-14}$$

$$a'_V = -N\dot{\lambda}_{EL}V_c. \tag{7-15}$$

Note that, the proportional navigation ratio (N) is taken as 4 as in the case of PNG method.

7.3.2 Conversion Logic

In order to use the anti-PNG method to guide the aircraft whose autopilot is designed utilizing gain scheduled LQC method as expressed in section 4.2.5, the

outputs of the anti-PNG method, which are the acceleration commands, must be converted to the autopilot reference commands that are delta speed, delta height and delta yaw commands. To do this, the following steps are being followed:

1. The accelerations expressed in the ECS are converted to the delta speed components that are expressed in the ECS:

$$\begin{aligned} \Delta V_y &= \int a'_H dt \\ \Delta V_z &= \int a'_V dt \end{aligned} . \tag{7-16}$$

2. The delta speed components expressed in the ECS are converted to the delta position components that are expressed in the ECS:

$$\begin{aligned} \Delta y &= \int \Delta V_y dt \\ \Delta z &= \int \Delta V_z dt \end{aligned} . \tag{7-17}$$

3. The x-component of the aircraft speed that is expressed in the ECS is assumed to be constant:

$$\begin{aligned} & V_x \approx const. \\ & \Rightarrow \\ & \Delta V_x = 0 \\ & \Delta x = V_x \Delta t \end{aligned} . \tag{7-18}$$

4. The delta speed commands expressed in the ECS are converted to the WCS:

$$\begin{bmatrix} \Delta V_{x_W} \\ \Delta V_{y_W} \\ \Delta V_{z_W} \end{bmatrix} = T_{WB} T_{BE} \begin{bmatrix} \Delta V_x \\ \Delta V_y \\ \Delta V_z \end{bmatrix} . \tag{7-19}$$

Briefly, the autopilot commands that are obtained by using the assumption and the equations above can be summarized as follows:

$$\Delta V = \sqrt{\Delta V_{x_w}^2 + \Delta V_{y_w}^2 + \Delta V_{z_w}^2}$$
$$\Delta h = -\Delta z \quad . \tag{7-20}$$
$$\Delta \psi = \arctan(\frac{\Delta y}{\Delta x})$$

Finally, note that the simulation studies in which the anti-PNG method is used are given in the Chapter 8. There, the performance of the anti-PNG method is tested under some example cases that are also used to test the performance of the rule based missile evasion method given section 7.2.

CHAPTER 8

SIMULATION STUDIES

In this chapter, performances of the proposed aircraft guidance methods in chapter 7, rule-based method and anti-PNG method, are tested under 17 cases. These cases are chosen to cover different ranges and orientations of the missile with respect to the aircraft at the beginning of the engagement scenarios.

For each test case given in, missile-aircraft initial distance (R), initial angle between missile and aircraft velocity vectors (θ), and aircraft height above ground (h) are chosen first. Then, x-y position of the missile on the ground is calculated by using equation (7-3). Note that, aircraft initial velocity vector lies along the x-axis of the ECS and missile initial velocity vector lies along the initial LOS direction (see Figure 7-3). In addition, initial speed of the missile is taken as 292.4 m/s and initial speed of the aircraft is taken as 150 m/s.

Throughout the simulations, the missile is guided by the PNG method given in section 6.2 and controlled by the autopilot that is designed in chapter 5. On the other hand, the gain scheduled LQC structure designed in section 4.2.5 is used as the aircraft autopilot. It is important to note that, both the aircraft and the missile are assumed to know each other's position during an engagement.

Results of the simulations are given in Table 8-2. Here, if a test scenario ends up with a miss distance of 50 m or higher, the guidance method used is assumed to be the successful, that is to say, the kill distance is chosen as 50 m.

Table 8-1: Initial conditions of the test scenarios

Test Case #	R (m)	θ (deg)	h (m)	x_m (m)	y_m (m)
1	600	10	100	-591	29
2	800	30	100	-693	387
3	1000	50	100	-643	759
4	1200	70	100	-410	1123
5	1400	90	200	0	1386
6	1600	110	200	547	1490
7	1800	130	200	1157	1364
8	2000	150	200	1732	980
9	2200	170	300	2167	237
10	2400	20	300	-2255	764
11	2600	40	300	-1992	1644
12	2800	60	300	-1400	2406
13	3000	80	400	-521	2927
14	3200	100	400	556	3126
15	3400	120	400	1700	2917
16	3600	140	400	2758	2279
17	3800	160	500	3571	1200

Table 8-2: Simulation results

Test Case #	ANTI-PNG		RULE-BASED		Success
	Miss Distance (m)	Time (s)	Miss Distance (m)	Time (s)	
1	8.3	3.83	150.6	3.46	Rule-Based
2	43.2	3.67	182.9	4.29	Rule-Based
3	115.5	3.72	146.8	5.64	BOTH
4	116.8	3.93	64.5	5.75	BOTH
5	32.0	4.86	61.3	5.52	Rule-Based
6	247.8	4.87	84.3	5.11	BOTH
7	342.1	4.54	62.7	4.81	BOTH
8	218.1	5.11	50.4	4.81	BOTH
9	13.6	5.06	25.7	5.04	NONE
10	185.0	15.70	202.4	11.23	BOTH
11	592.6	9.29	55.7	9.79	BOTH
12	243.9	9.99	210.1	11.07	BOTH
13	20.4	11.42	496.5	10.38	Rule-Based
14	20.4	15.00	102.2	12.57	Rule-Based
15	110.5	12.02	90.8	12.04	BOTH
16	15.7	14.05	94.4	11.96	Rule-Based
17	1070.0	7.16	131.9	13.12	BOTH

By checking the results given in Table 8-2, it is seen that there is only one critical scenario (test case #9) in which both of the guidance methods are said to fail. But for the rest of the test scenarios, the rule based method is successful to guide the aircraft by evading the missile, whereas for the 6 of the scenarios, anti-PNG method is said to fail. However, for 8 of the scenarios at which both of the methods are said to be successful, miss distance values obtained by the anti-PNG method are higher than the values obtained by the rule-based method. This result shows that the anti-PNG method may also be used as an effective guidance method for some specific scenarios.

If the kill distance of 50 m is used as the only success criterion, following generalizations can be deduced:

- For the short range engagements (500-1500 m), and the long range engagements (3000-4000 m) rule based method performs better than the anti-PNG method,

- For the mid-range engagements (1500-3000 m), both methods perform well except a specific case which is test case #9 (a mid-range, nearly head-on engagement).

In order to make more generalizations, the test case parameter resolutions may be increased and also different PNG ratios can be used for the anti-PNG method to check its effect on the evasion capability of the aircraft.

The missile and the aircraft trajectories in 3-D, obtained for both guidance methods applied on each test case (given in Table 8-2) are shown as follows:

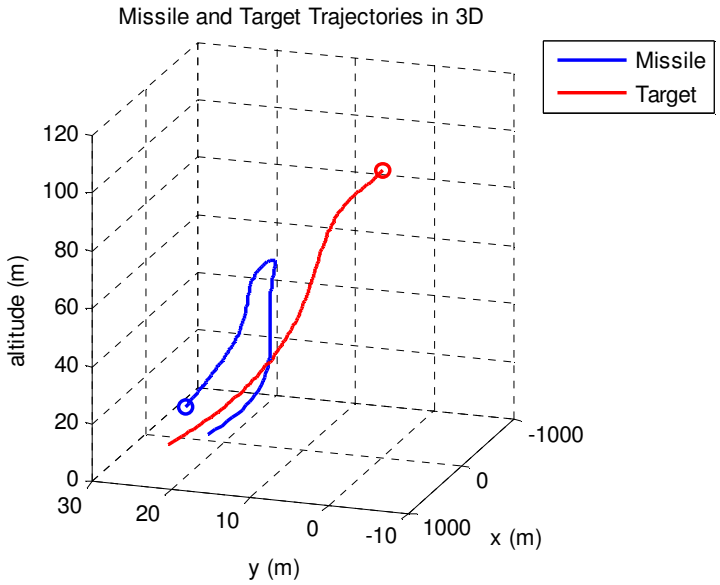

Figure 8-1: Anti-PNG method – case 1

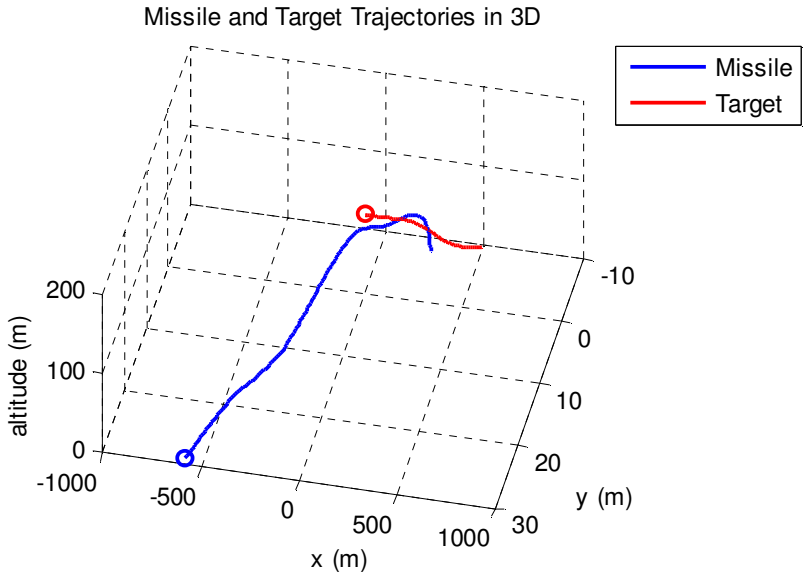

Figure 8-2: Rule based method – case 1

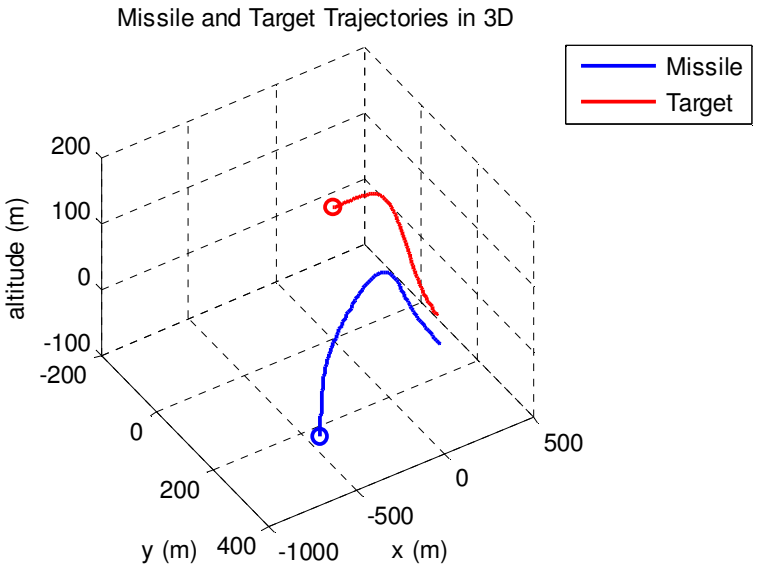

Figure 8-3: Anti-PNG method – case 2

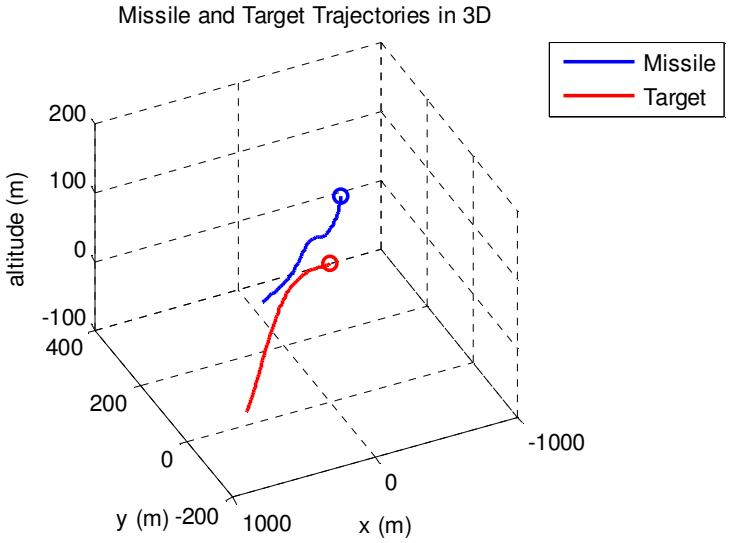

Figure 8-4: Rule based method – case 2

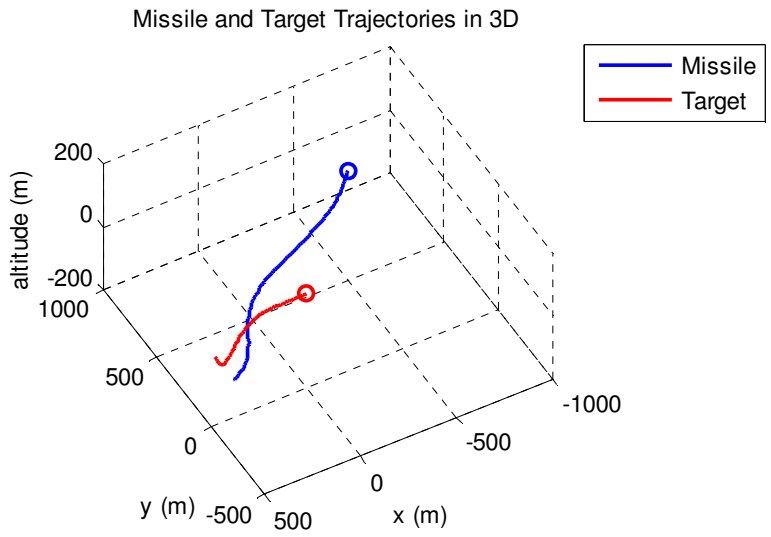

Figure 8-5: Anti-PNG method – case 3

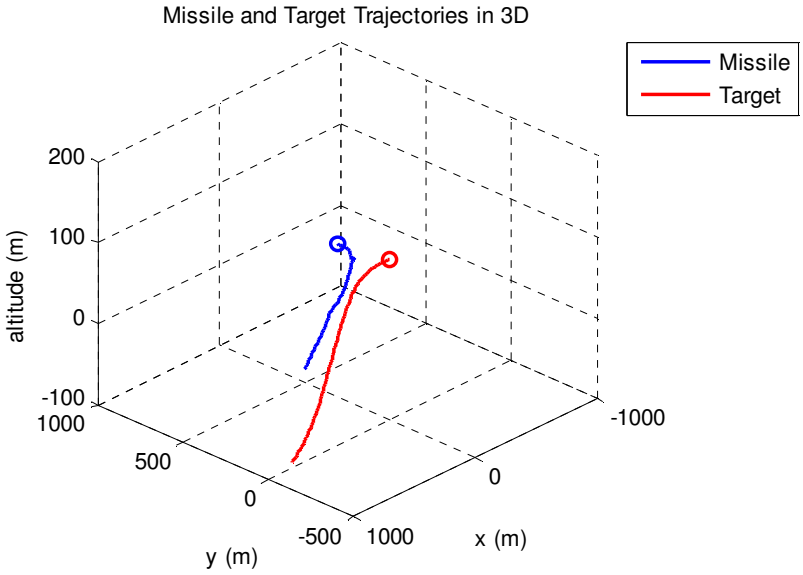

Figure 8-6: Rule based method – case 3

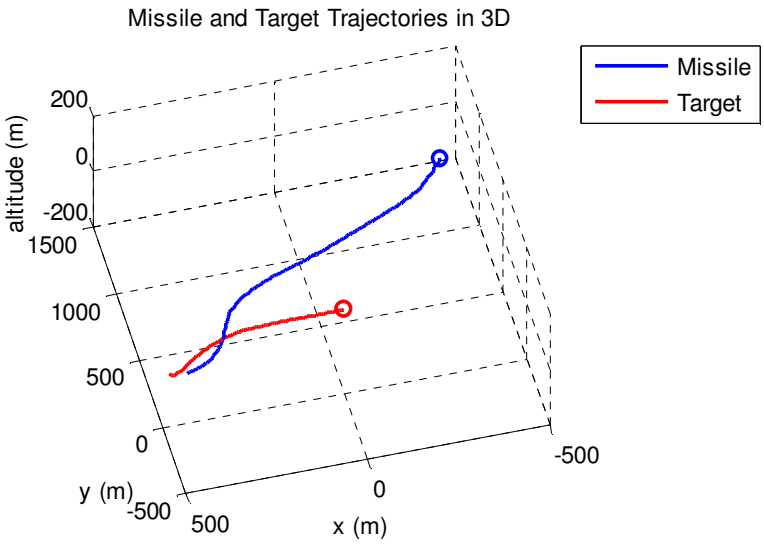

Figure 8-7: Anti-PNG method – case 4

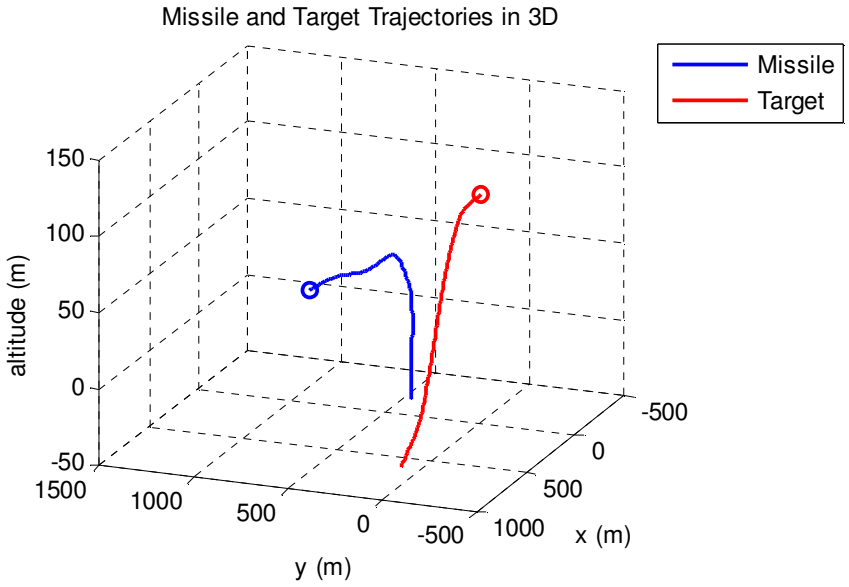

Figure 8-8: Rule based method – case 4

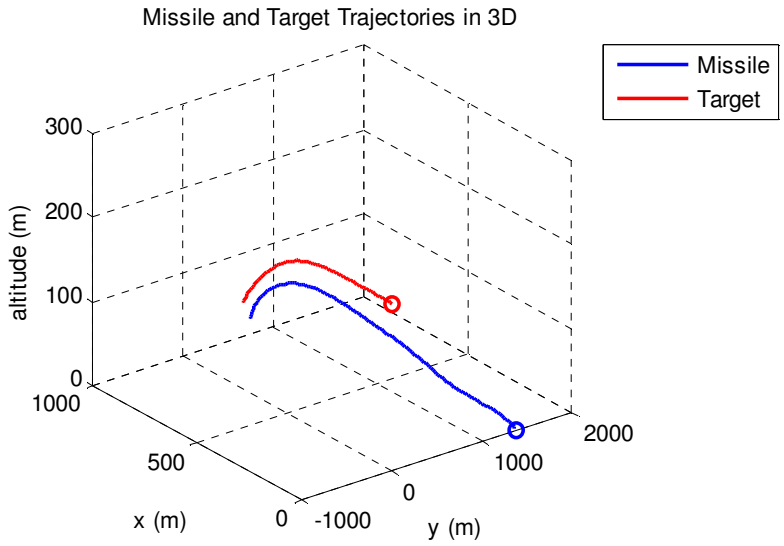

Figure 8-9: Anti-PNG method – case 5

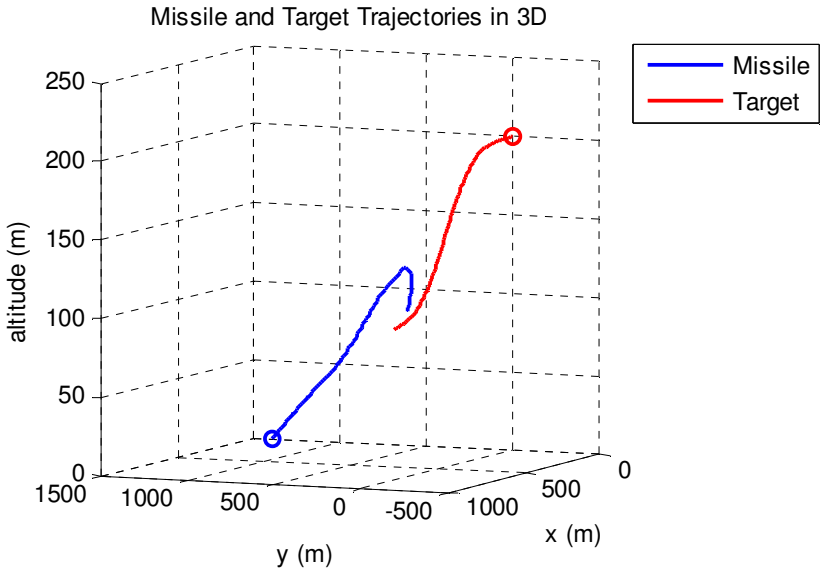

Figure 8-10: Rule based method – case 5

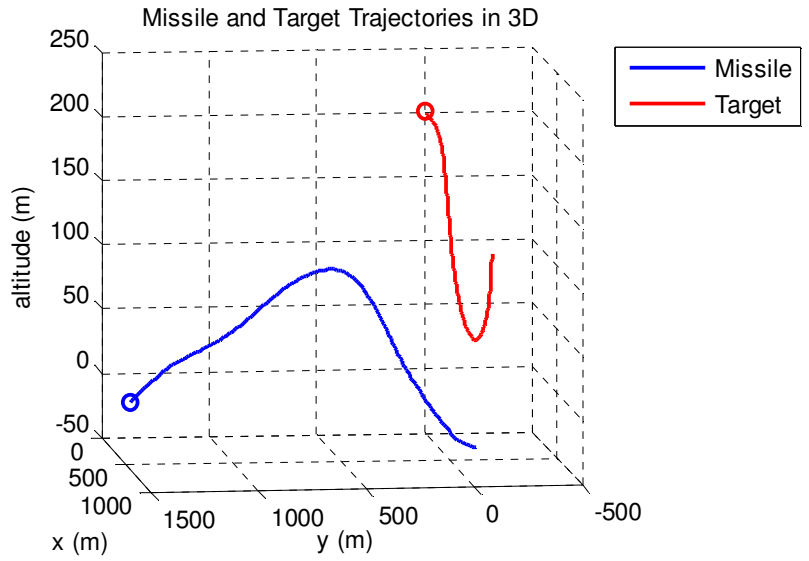

Figure 8-11: Anti-PNG method – case 6

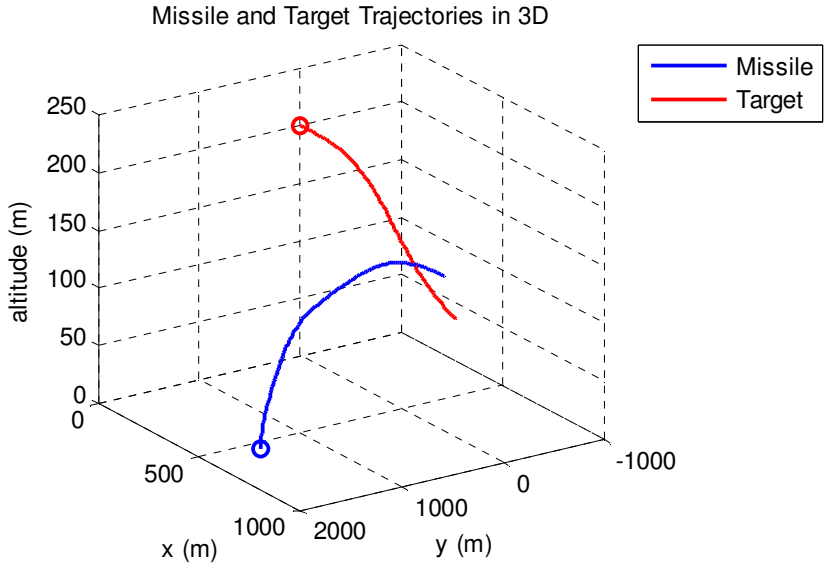

Figure 8-12: Rule based method – case 6

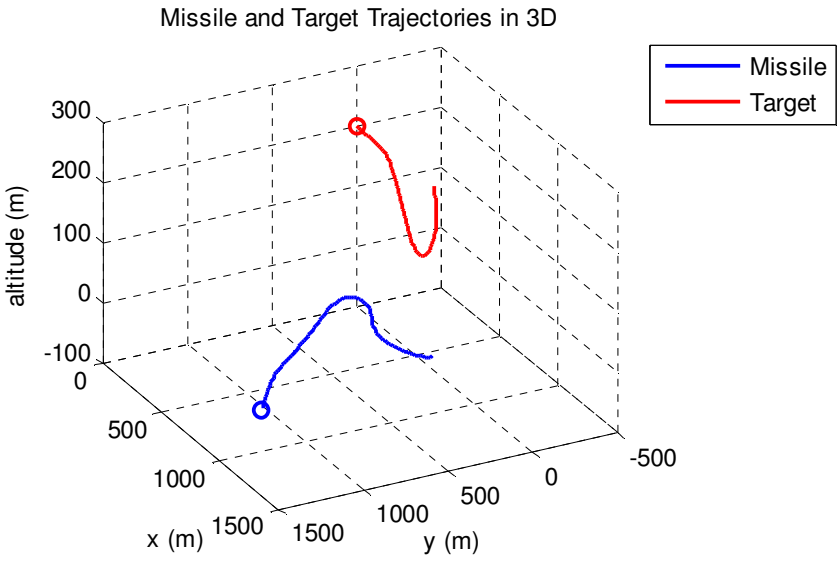

Figure 8-13: Anti-PNG method – case 7

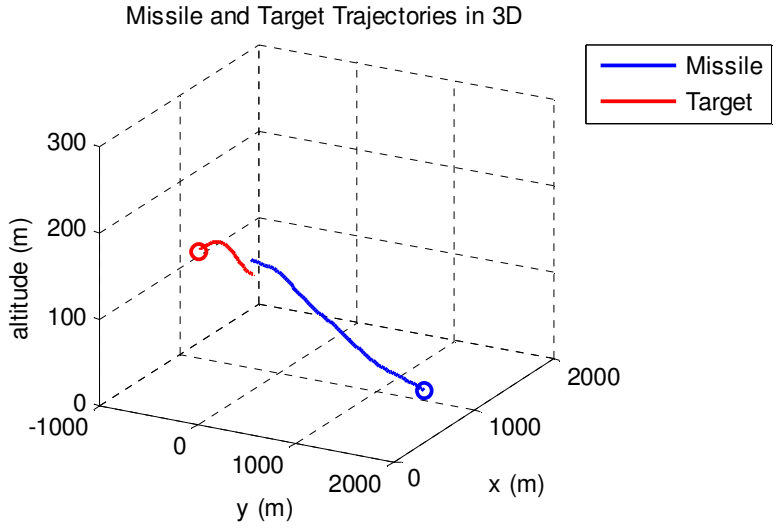

Figure 8-14: Rule based method – case 7

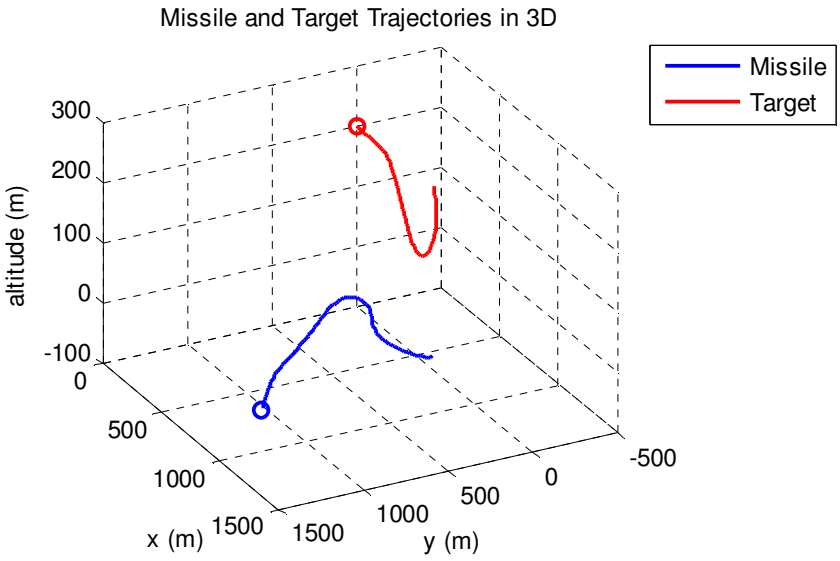

Figure 8-15: Anti-PNG method – case 8

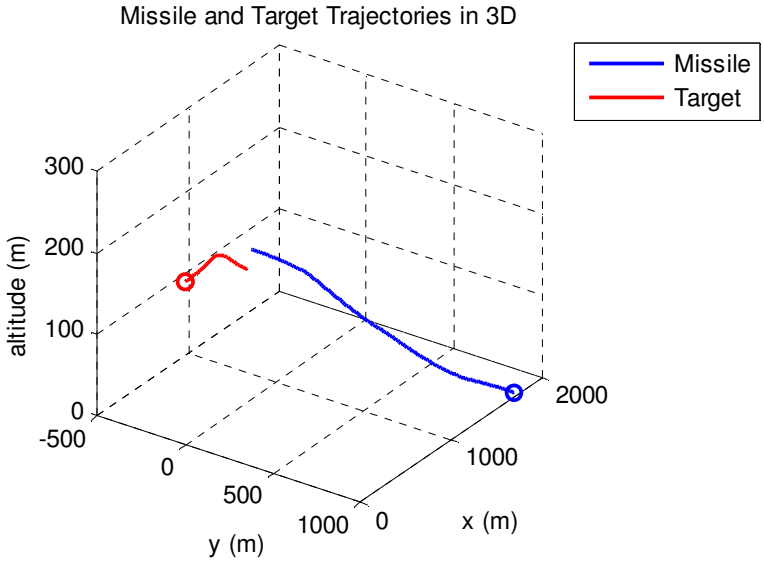

Figure 8-16: Rule based method – case 8

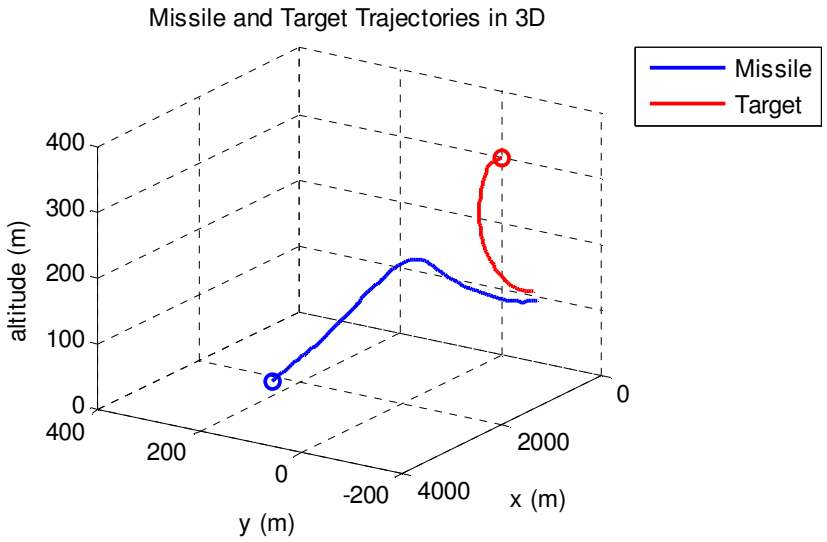

Figure 8-17: Anti-PNG method – case 9

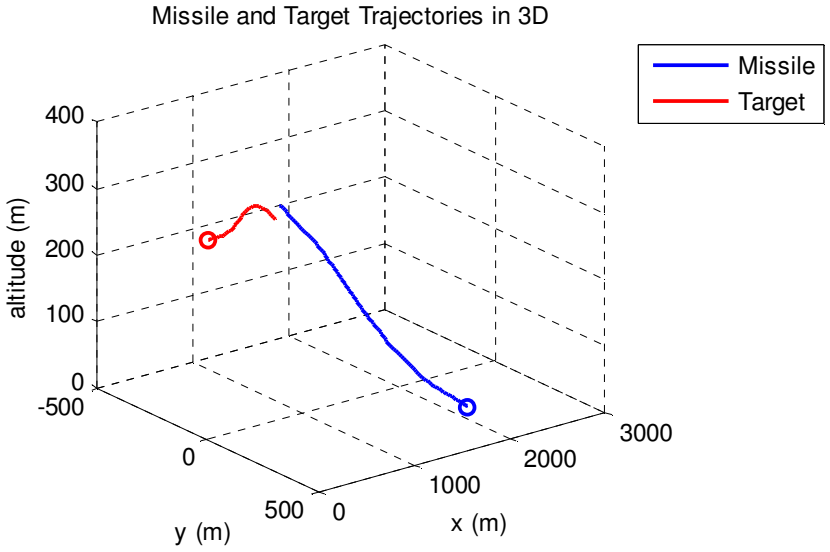

Figure 8-18: Rule based method – case 9

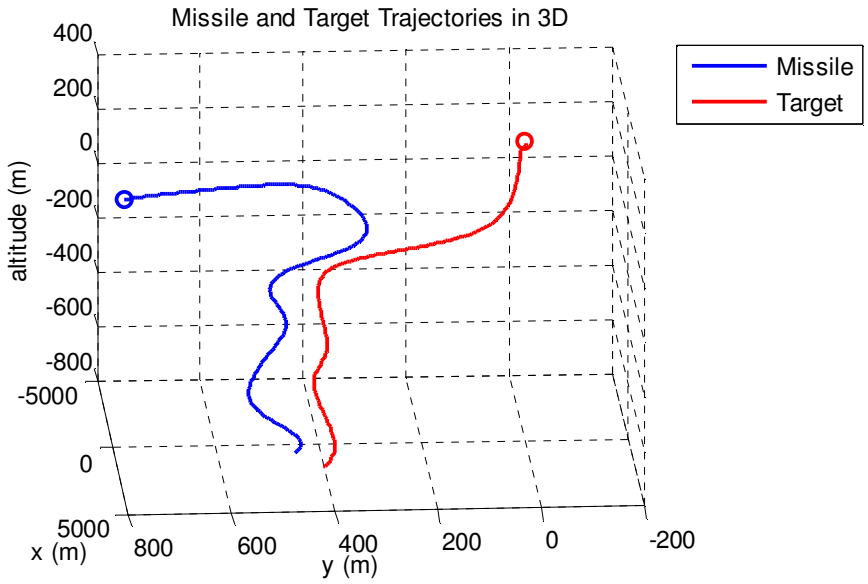

Figure 8-19: Anti-PNG method – case 10

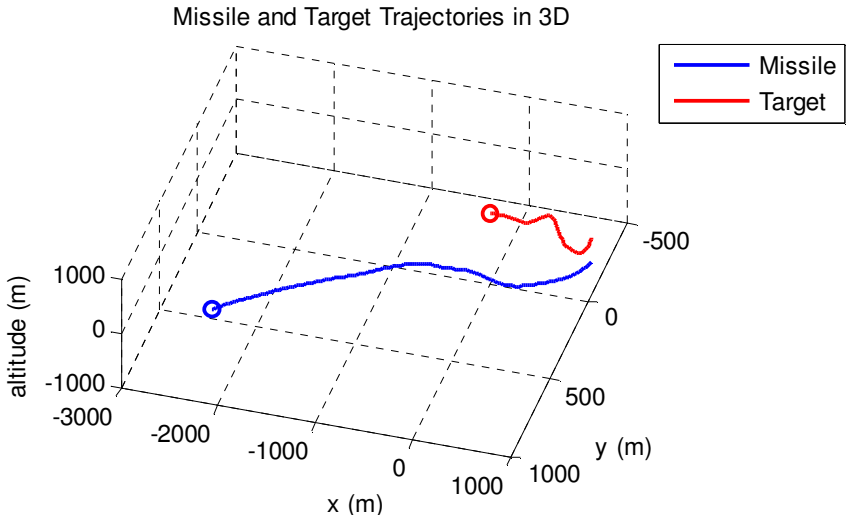

Figure 8-20: Rule based method – case 10

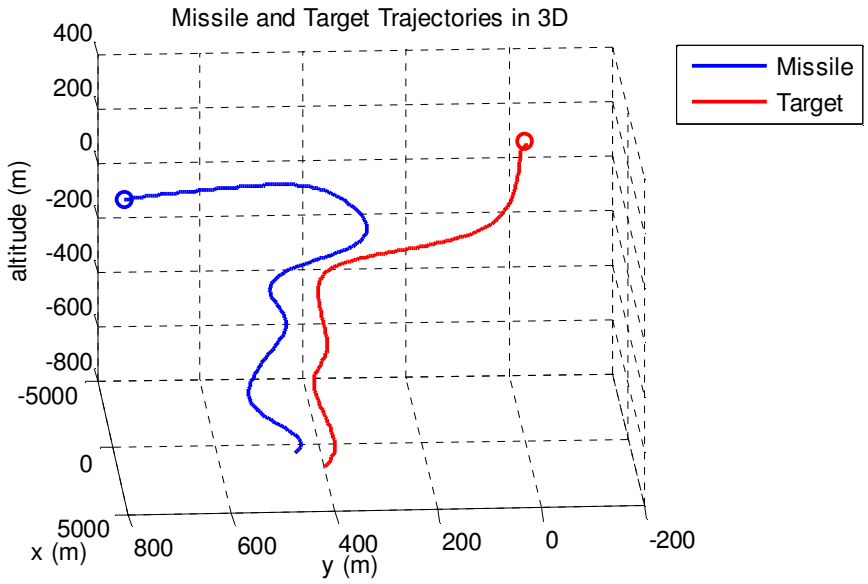

Figure 8-21: Anti-PNG method – case 11

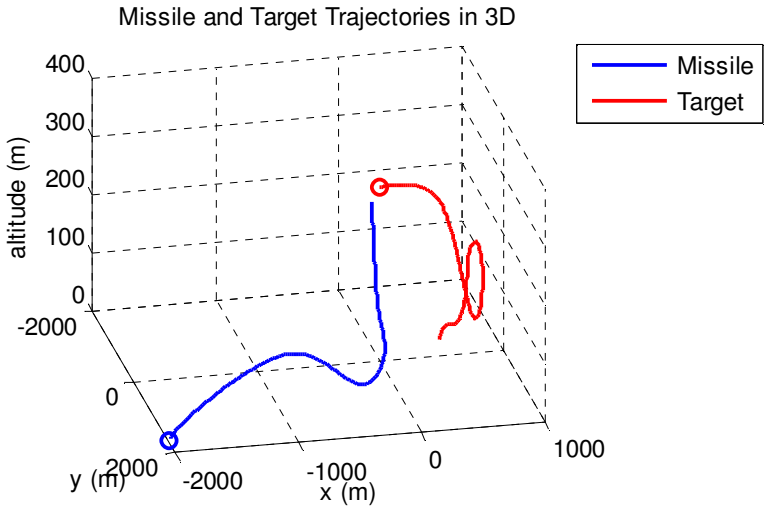

Figure 8-22: Rule based method – case 11

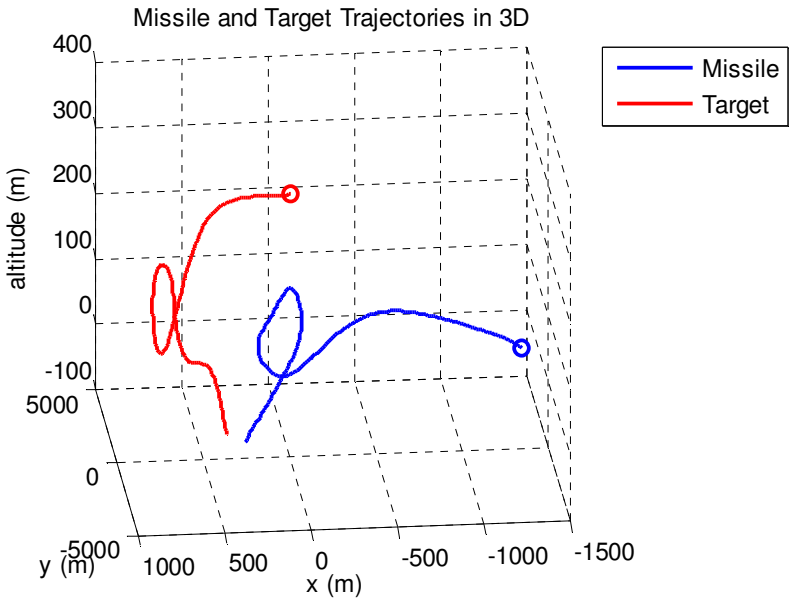

Figure 8-23: Anti-PNG method – case 12

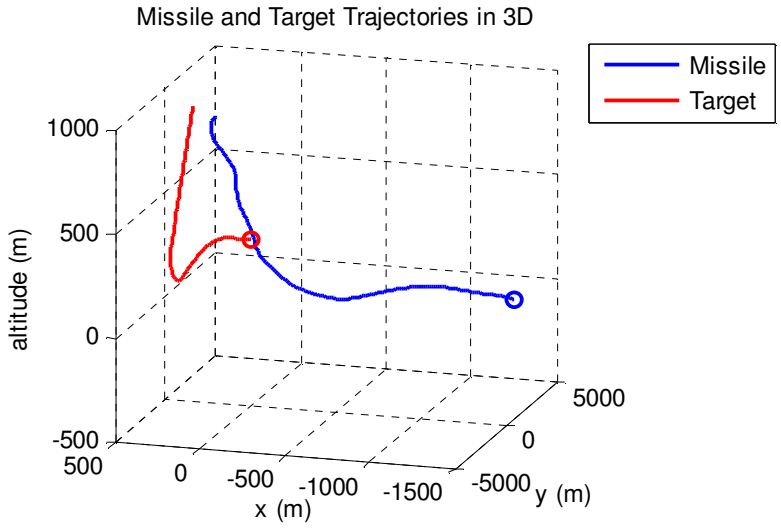

Figure 8-24: Rule based method – case 12

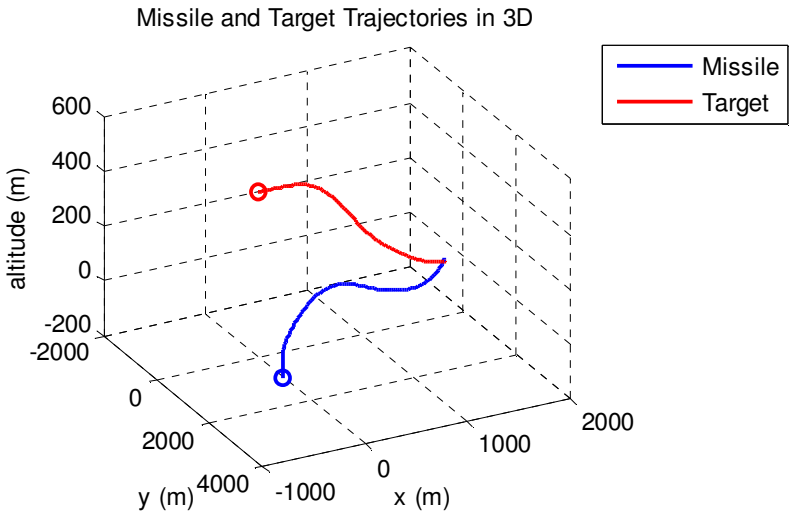

Figure 8-25: Anti-PNG method – case 13

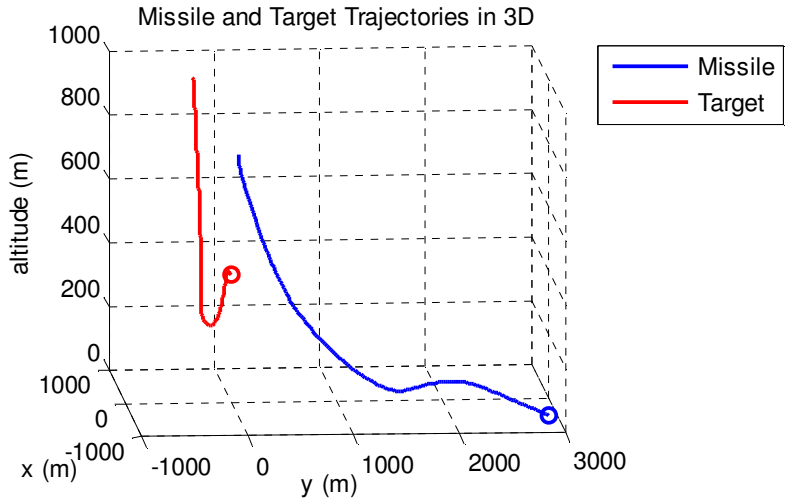

Figure 8-26: Rule based method – case 13

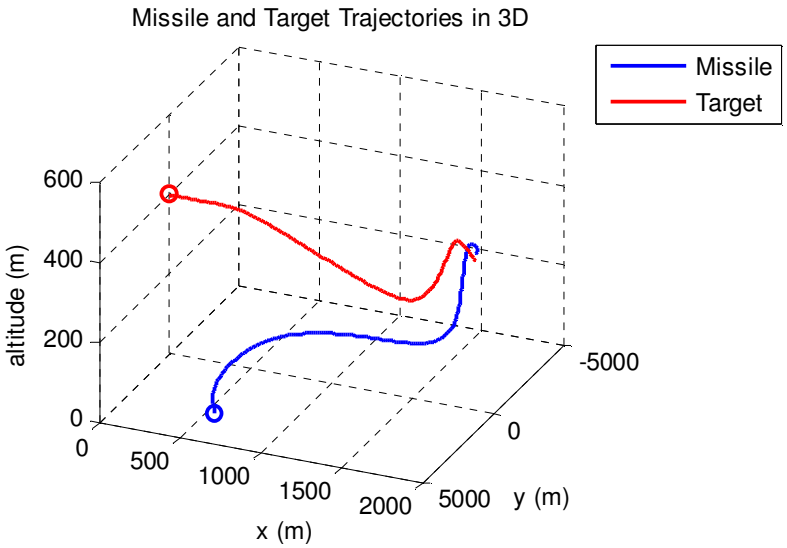

Figure 8-27: Anti-PNG method – case 14

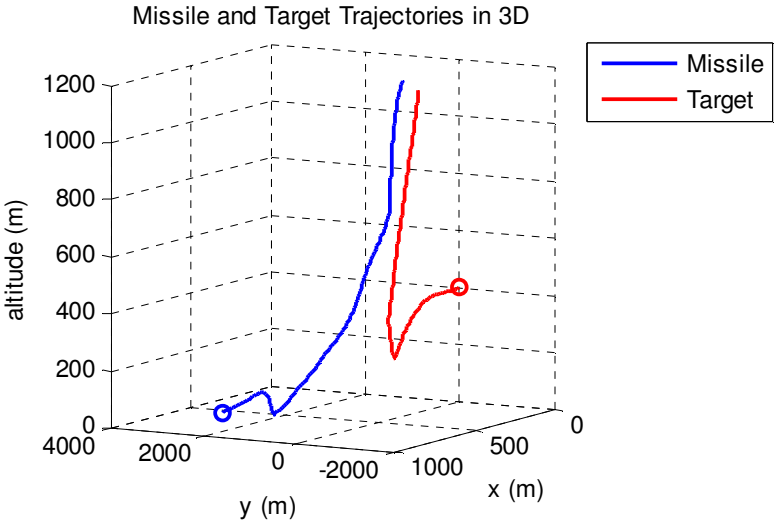

Figure 8-28: Rule based method – case 14

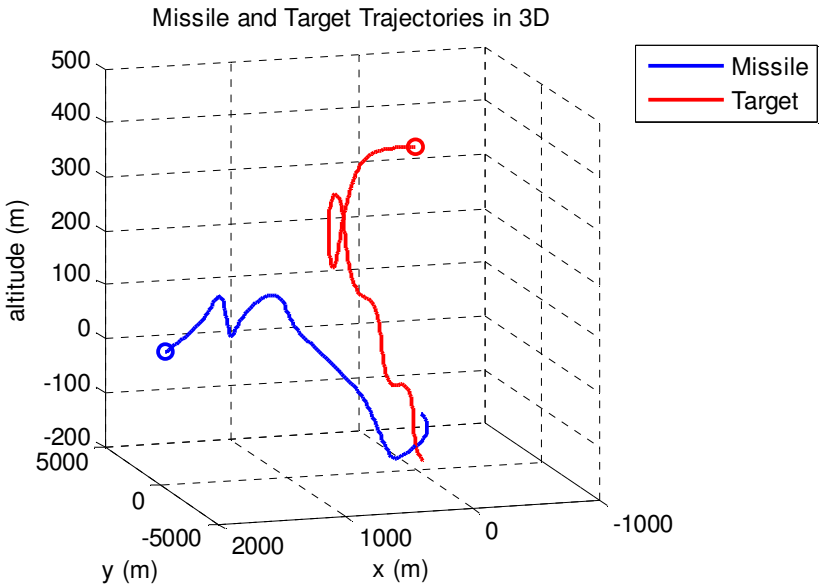

Figure 8-29: Anti-PNG method – case 15

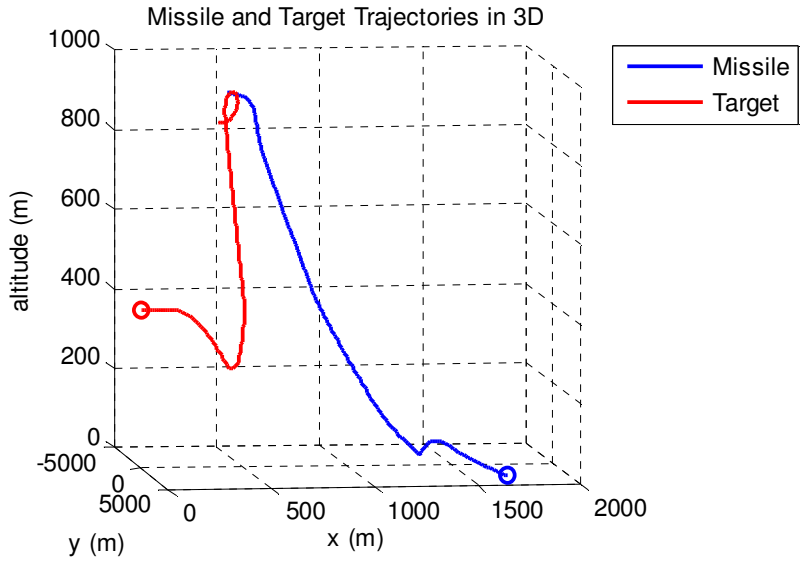

Figure 8-30: Rule based method – case 15

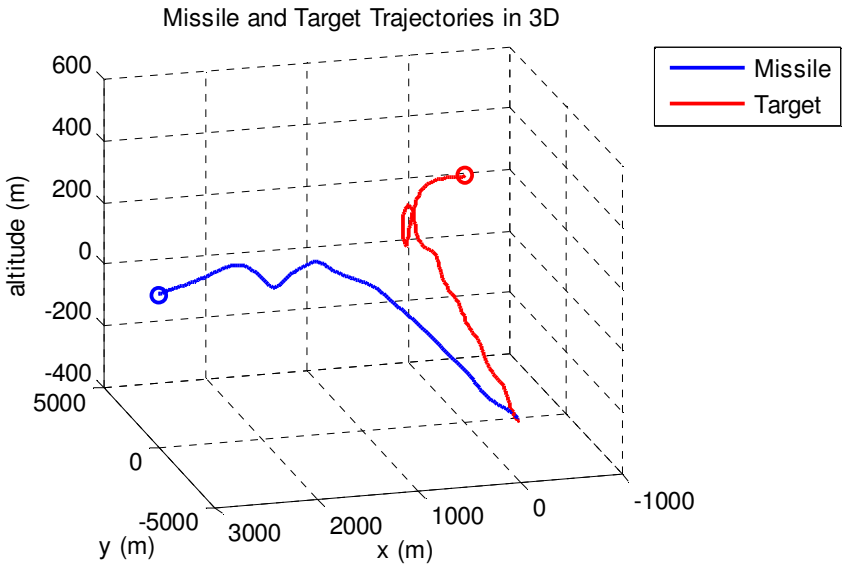

Figure 8-31: Anti-PNG method – case 16

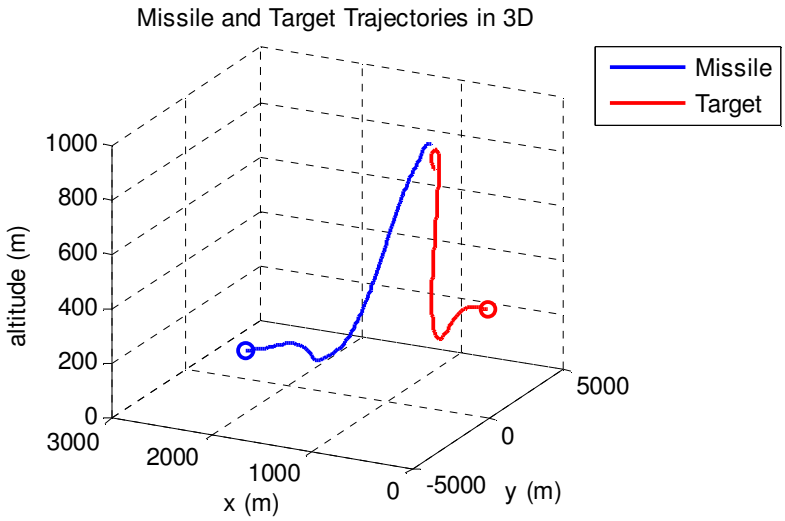

Figure 8-32: Rule based method – case 16

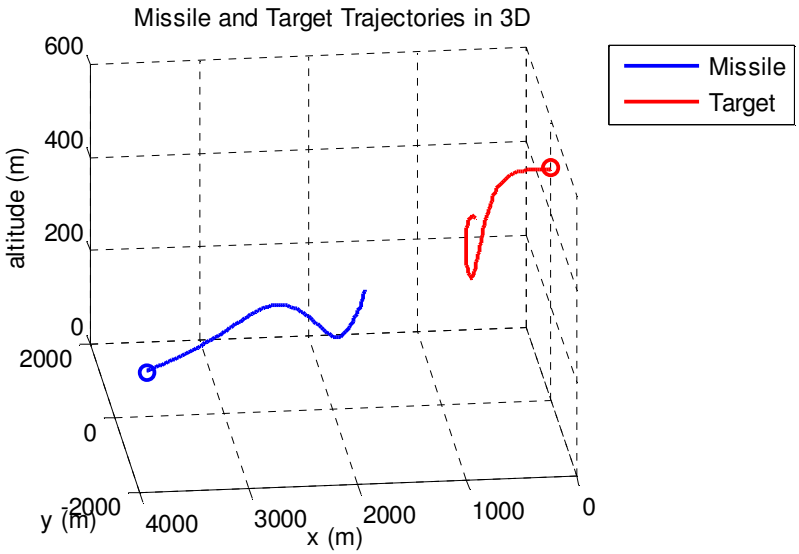

Figure 8-33: Anti-PNG method – case 17

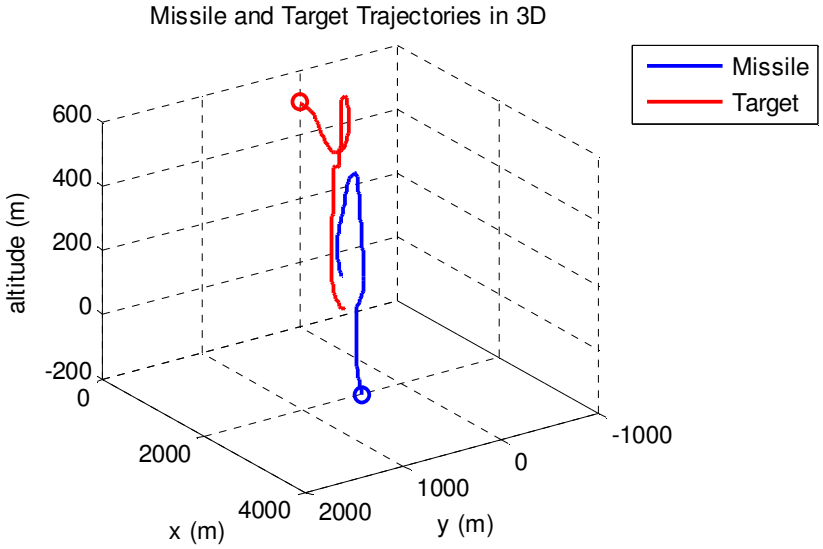

Figure 8-34: Rule based method – case 17

CHAPTER 9

CONCLUSION AND FUTURE WORK

In this thesis, in order to develop a guidance system for a missile and an aircraft, first, the derivations of EOM of a missile and an aircraft are given. Then, linearization, trimming and decoupling processes of the nonlinear EOM are explained. After having the linearized models, the controllers are designed based on the lateral and the longitudinal LTI models separately. The aircraft controllers are tested on both LTI system and NL system, whereas, the missile controllers are only tested on the LTI system. Then, the guidance system designs for a missile and an aircraft are explained. Finally, simulation studies are given in order to compare the performances of the proposed aircraft guidance methods.

The main contribution of this thesis to the literature is two new guidance methods, one of which is developed for a missile and the other is developed for a fighter aircraft. Although the new missile guidance method, HPNG, is based on the classical PNG method, its performance is much better than the performance of the PNG method, especially when there is noise in the position measurements. Performance of the HPNG method may further be improved by using more complex Kalman filter structures that are suppressing the measurement noise more and also modeling the target maneuvers better.

The aircraft guidance method developed for this study is the rule based missile evasion method that suggests a way of using the results of the miss distance

maximization problem online, although the problem is formulated as an optimal control problem and the online implementation of solving such a problem is unrealizable. Therefore, an interpolation algorithm finds a solution online by combining the solutions of the 45 optimal control problems that are solved offline. Hence, the aircraft is guided online by using the interpolated rule derived from the solution of lots of miss distance maximization problems that are constructed taking the typical engagement scenarios into account.

A relatively new guidance method used for the aircrafts given in [20], called anti-PNG, is utilized for this study with a suitable conversion logic. This guidance method is used to evaluate the performance of the rule based method by comparing them under some generic engagement scenarios. The main idea of the anti-PNG method is to guide the aircraft with a command which is the negative of the PNG command. By doing this, the aircraft is forced to evade from the missile instead of having a collision.

Simulation studies given in chapter 8 shows that the rule based missile evasion algorithm performs better than the anti-PNG method. However, the simulation results also show that the anti-PNG method may also be used as an effective guidance method for some specific scenarios.

In addition to the studies done in this thesis, both of the proposed aircraft guidance methods may further be improved. For example, the rule based method developed here is used to extract general rules (change in speed, height and yaw). An improvement can be made such that a collection of some special purpose rules that behaves as a general purpose rule is found for a more complex engagement scenario that includes CMs (such as a flare) and CCMs (such as a tracker that discards the CMs). Another improvement may be made by solving much more optimal control problems to increase the resolution in the rule extraction process. On the other hand, the conversion logic used for the anti-PNG method may be improved to evade from a proportional navigation guided threat in a more effective way.

Finally, all the suggested improvements for the given guidance methods may be considered as a future work that constitutes the parts of a doctoral study.

REFERENCES

[1] K. Ogata, “Modern Control Engineering”, Prentice Hall, NJ, 2002

[2] B. Stevens, and F. Lewis, “Aircraft Control and Simulation”, Wiley Interscience, NY, 1992

[3] P. H. Zipfel, “Modeling and Simulation of Aerospace Vehicle Dynamics”, AIAA Education Series, VA, 2000

[4] Y. Bar-Shalom, X. R. Li, and T. Kirubarajan, “Estimation with Applications to Tracking and Navigation”, John Wiley & Sons, NY, 2001

[5] P. Zarchan, “Tactical and Strategic Missile Guidance”, Volume 199, Progress in Astronautics and Aeronautics, Massachusetts, 2002

[6] L. T. Nyugen, M. E. Ogburn, W. P. Gilbert, K. S. Kibler, P. W. Brown, and P. L. Deal, “NASA Technical Paper 1538 – Simulator Study of Stall / Post-Stall Characteristics of a Fighter Airplane With Relaxed Longitudinal Static Stability”, NASA, Langley, 1979

[7] F. R.Garza, and E. A. Morelli, “A Collection of Nonlinear Aircraft Simulations in MATLAB”, NASA/TM-2003-212145, Virginia, 2003

[8] Y. Huo, “Model of F-16 Fighter Aircraft”, http://www.usc.edu/dept/ee/catt/soft.htm, June 10th 2007, Last date accessed: January 15th 2008

[9] R. S. Russell, “Nonlinear F-16 Simulation Using Simulink and Matlab”, Technical Report, Department of Aerospace Engineering and Mechanics, University of Minnesota, 2003,

http://www.aem.umn.edu/people/faculty/balas/darpa_sec/SEC.Software.html, February 10th 2007, Last date accessed: January 15th 2008

[10] Ç. Evcimen, and K. Leblebicioğlu, "An Optimal Proportional-Integral Guidance for Missiles", 4. Ankara International Aerospace Conference, 10-12 September 2007

[11] M. Rauw, S. Bennani, H. van der Vaart, "An Integrated Approach to the Design of Flight Control Systems using CAD Tools", 3rd ESIEE Congress, France, November 17-18, 1994

[12] http://www.mathworks.com, February 1st 2007, Last date accessed: May 2nd 2008

[13] R. Ö. Doruk, "Missile Autopilot Design by Projective Control Theory", M. S. Thesis in METU, Department of Electrical and Electronics Engineering, August 2003

[14] K. D. Şahin, "A Pursuit Evasion Game Between a Missile and an Aircraft", M. S. Thesis in METU, Department of Electrical and Electronics Engineering, December 2002

[15] B. Yıldırım, "A Comparative Evaluation of Conventional and Particle Filter Based Radar Target Tracking", M. S. Thesis in METU, Department of Electrical and Electronics Engineering, November 2007

[16] J. H. Blakelock, "Automatic Control of Aircraft and Missiles", John Wiley & Sons, NY, 2nd Edition, 1991

[17] D. E. Kirk, "Optimal Control Theory: An Introduction", Prentice-Hall, NJ, 1970

[18] C. T. Chen, "Linear System Theory and Design", 3rd Ed, Oxford University Press, NY, 1999

[19] V. M. Becerra, “Solving Optimal Control Problems with State Constraints Using Nonlinear Programming and Simulation Tools”, IEEE Transactions on Education Vol. 47, No. 3, August 2004

[20] B. Jung, K. S. Kim, Y. Kim, “Guidance Law for Evasive Aircraft Maneuvers”, AIAA Guidance, Navigation and Control Conference and Exhibit, Austin, Texas, 11-14 August 2003

APPENDIX A. AIRCRAFT DESIGN PARAMETERS

A.1 Aerodynamic Model and Coefficients

Aerodynamic forces and moments stem from the air diverted by the aircraft in different directions, depending on the following factors:

- the airspeed V_T (or Mach number M) and density of the airflow ρ,
- the geometry of the aircraft: wing area S, wing span b and mean aerodynamic chord $\bar{c}$,
- the orientation of the aircraft relative to the airflow: angle of attack α and angle of sideslip β,
- the chord surface deflections δ,
- the angular rates p, q , r.

As a result of these dependencies, non-dimensional aerodynamic force and moment coefficients of the aircraft vary nonlinearly with angle of attack and sideslip, angular velocity components and control surface deflections. There are other variables such as the time derivatives of the angle of attack and sideslip that also play a role, but this effect is neglected because of the **Assumption 1**. Detailed information about the aerodynamic forces and moments is given in [2].

Briefly, the standard way of modeling the aerodynamic forces and moments can be given as follows:

$$
\begin{aligned}
X &= \bar{q}SC_{X_T}(\alpha,\beta,p,q,r,\delta,...) \\
Y &= \bar{q}SC_{Y_T}(\alpha,\beta,p,q,r,\delta,...) \\
Z &= \bar{q}SC_{Z_T}(\alpha,\beta,p,q,r,\delta,...)
\end{aligned}, \tag{A-1}
$$

$$
\begin{aligned}
\bar{L} &= \bar{q}SbC_{l_T}(\alpha,\beta,p,q,r,\delta,...) \\
\bar{M} &= \bar{q}S\bar{c}C_{m_T}(\alpha,\beta,p,q,r,\delta,...) \\
\bar{N} &= \bar{q}SbC_{n_T}(\alpha,\beta,p,q,r,\delta,...)
\end{aligned}, \tag{A-2}
$$

where, $\bar{q}$ is the aerodynamic pressure (see Appendix A.2). Instead of the BCS force coefficients C_{X_T}, C_{Y_T} and C_{Z_T}, the WCS force coefficients C_D, C_Y and C_L can be used, where C_D is called drag, C_Y is side-force and C_L is lift coefficient [2]. All of these aerodynamic coefficients can be obtained by wind-tunnel experiments and flight tests. The aerodynamic data used for the aircraft in this thesis were derived from wind-tunnel tests conducted with sub-scaled models of a jet fighter aircraft, which is F-16 [6].

Below, formulations of total coefficient equations are shown that are formed by summation of various aerodynamic contributions to a given coefficient [2]:

The x-axis force coefficient C_{X_T}:

$$
C_{X_T} = C_x(\alpha_d,\delta_e) + \frac{q\bar{c}}{2V_T}C_{X_q}(\alpha_d). \tag{A-3}
$$

The y-axis force coefficient C_{Y_T}:

$$
C_{Y_T} = -0.02\beta_d + 0.021\frac{\delta_a}{20} + 0.086\frac{\delta_r}{30} + \frac{b}{2V_T}\left[C_{Y_r}(\alpha_d)r + C_{Y_p}(\alpha_d)p\right]. \tag{A-4}
$$

The z-axis force coefficient C_{Z_T}:

$$
C_{Z_T} = C_{z,1}(\alpha_d,\beta_d) + \frac{q\bar{c}}{2V_T}C_{Z_q}(\alpha_d) - 0.19\frac{\delta_e}{25}. \tag{A-5}
$$

The rolling-moment coefficient C_{l_T} :

$$C_{l_T} = C_{l,1}(\alpha_d, \beta_d) + \frac{b}{2V_T}\left[C_{l_r}(\alpha_d)r + C_{l_p}(\alpha_d)p\right] + C_{l,2}(\alpha_d, \beta_d)(\frac{\delta_a}{20}) + C_{l,3}(\alpha_d, \beta_d)(\frac{\delta_r}{30}). \quad \text{(A-6)}$$

The pitching moment coefficient C_{m_T} :

$$C_{m_T} = C_m(\alpha_d, \delta_e) + C_{Z_T}(x_{cgr} - x_{cg}) + \frac{q\bar{c}}{2V_T}C_{m_q}(\alpha_d). \quad \text{(A-7)}$$

The yawing moment coefficient C_{n_T} :

$$\begin{aligned} C_{n_T} = {} & C_{n,1}(\alpha_d, \beta_d) + \frac{b}{2V_T}\left[C_{n_r}(\alpha_d)r + C_{n_p}(\alpha_d)p\right] - \frac{\bar{c}}{b}C_{Y_T}(x_{cgr} - x_{cg})... \\ & + C_{n,2}(\alpha_d, \beta_d)(\frac{\delta_a}{20}) + C_{n,3}(\alpha_d, \beta_d)(\frac{\delta_r}{30}) \end{aligned}, \quad \text{(A-8)}$$

where, α_d and β_d represent α and β in degrees. Note that, x_{cgr} is the reference center of gravity as a fraction of $\bar{c}$ and x_{cg} is the center of gravity as a fraction of $\bar{c}$, whose values are taken as 0.35 and 0.30, respectively [2].

The data for the aerodynamic coefficients are given as look-up tables in [2], and it is valid for the following flight envelope for the F-16 [6], [2] and [7]:

- $-10° \le \alpha \le 45°$
- $-30° \le \beta \le 30°$
- $0.1 \le M \le 0.6$
- $0 \text{ m} \le h \le 15{,}239 \text{ m}$

where, M is the Mach number (see Appendix A.2) and h is the altitude. During the aircraft flight simulations, a linear interpolation algorithm is used to calculate the

coefficients within the flight envelope that also extrapolates beyond the look-up table boundaries, however, the results are more likely to be unrealistic.

A.2 Atmospheric Model

Air density and speed of sound are calculated using relations that formulate the U.S. Standard Atmosphere [2], [8]. Required quantities that depend on these atmospheric properties, namely, Mach number M and dynamic pressure $\bar{q}$ are also calculated. The relationships are:

$$\begin{aligned} T &= 1 - 0.703\times10^{-5} h \\ \rho &= 0.002377\times T^{4.14} \\ M &= \begin{cases} \dfrac{V_T}{\sqrt{1.4\times1716.3\times390}} & h \geq 35{,}000\,ft \\ \dfrac{V_T}{\sqrt{1.4\times1716.3\times519\times T}} & h < 35{,}000\,ft \end{cases}, \\ \bar{q} &= 0.5\rho V_T{}^2 \end{aligned} \tag{A-9}$$

where, T is the temperature in Kelvin, h is the height in feet, ρ is the air density in slug/ft^3, V_T is the true airspeed in ft/s and $\bar{q}$ is in lbf/ft^2.

A.3 Engine Model

The jet fighter aircraft is powered by an afterburning turbofan jet engine, which is modeled taking throttle gearing and engine power level lag into account. Thrust response is modeled with a first-order lag, and lag time constant τ_{eng} is modeled as a function of the actual engine power level P_a and the commanded power, P_c. The commanded power level changes linearly with the throttle position up to the level of 0.77 and then the change of the slope causes nonlinearity as seen below [6]:

$$P_c(\delta_{th}) = \begin{cases} 64.94\delta_{th} & if \quad \delta_{th} \leq 0.77 \\ 217.38\delta_{th} - 117.38 & if \quad \delta_{th} > 0.77 \end{cases}. \tag{A-10}$$

Note that, the throttle position is limited to the range $0 \le \delta_{th} \le 1$. As mentioned before, engine power level dynamic response is modeled using a first-order lag. Therefore, actual power level derivative $\dot{P}_a$ is given by [6]:

$$\dot{P}_a = \frac{1}{\tau_{eng}}(P_c^* - P_a), \tag{A-11}$$

where

$$P_c^* = \begin{cases} P_c & if \quad P_c \ge 50 \quad and \quad P_a \ge 50 \\ 60 & if \quad P_c \ge 50 \quad and \quad P_a < 50 \\ 40 & if \quad P_c < 50 \quad and \quad P_a \ge 50 \\ P_c & if \quad P_c < 50 \quad and \quad P_a < 50 \end{cases}, \tag{A-12}$$

$$\frac{1}{\tau_{eng}} = \begin{cases} 5.0 & if \quad P_c \ge 50 \quad and \quad P_a \ge 50 \\ \dfrac{1}{\tau_T} & if \quad P_c \ge 50 \quad and \quad P_a < 50 \\ 5.0 & if \quad P_c < 50 \quad and \quad P_a \ge 50 \\ \dfrac{1}{\tau_T} & if \quad P_c < 50 \quad and \quad P_a < 50 \end{cases}, \tag{A-13}$$

$$\frac{1}{\tau_T} = \begin{cases} 1.0 & if \quad (P_c^* - P_a) \le 25 \\ 0.1 & if \quad (P_c^* - P_a) \ge 50 \\ 1.9 - 0.036(P_c^* - P_a) & if \quad 25 < (P_c^* - P_a) < 50 \end{cases}. \tag{A-14}$$

Engine thrust data for idle T_{idle}, military T_{mil} and maximum power settings $T_{\max}$ are given in look-up table format as a function of altitude and Mach number over ranges 0 m < h < 15,239 m and $0 \le M \le 1$ and the resulting force produced by the thrust is computed according to the actual engine power level as follows [6]:

$$F_T = \begin{cases} T_{idle} + (T_{mil} - T_{idle})(\dfrac{P_a}{50}) & if \quad P_a < 50 \\ T_{mil} + (T_{\max} - T_{mil})(\dfrac{P_a - 50}{50}) & if \quad P_a \ge 50 \end{cases}. \tag{A-15}$$

To calculate the thrust data from the look-up tables, a linear interpolation algorithm is used [2]. But when the altitude or Mach number or both goes beyond the table limits, the linear interpolation algorithm may extrapolate an unrealistic value as a result.

A.4 Control Variables and Actuators

The aircraft model allows for control over throttle, elevator, ailerons and rudder. All the control surface deflections are defined positive in the conventional way, i.e. a positive throttle setting causes an increase in acceleration along the body x-axis, a positive elevator deflection results in a decrease in pitch rate, a positive aileron deflection gives a decrease in roll rate and a positive rudder deflection decreases the yaw rate.

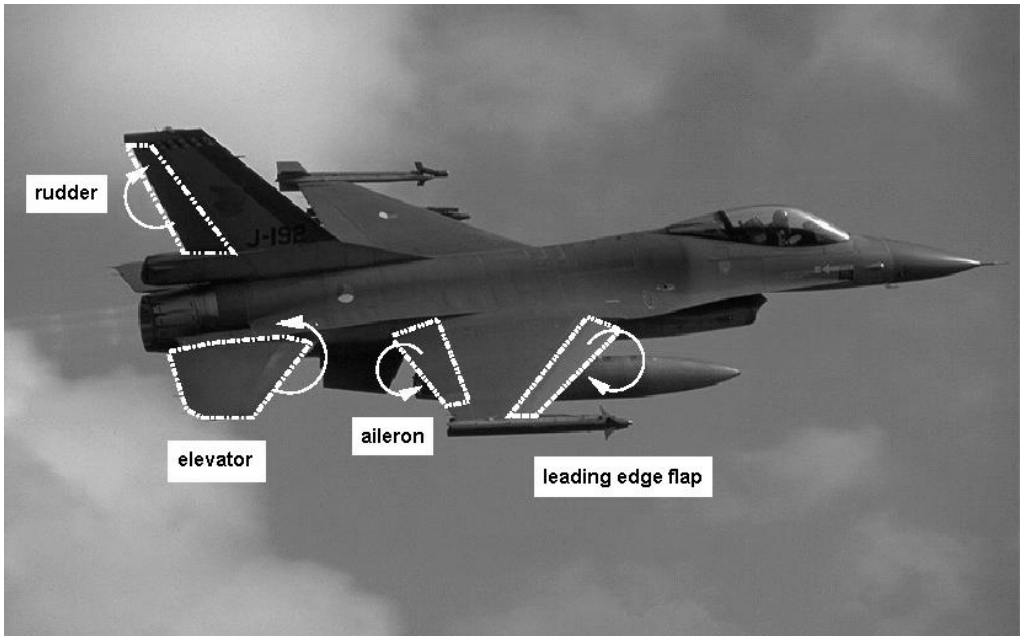

Figure A-1: Control surfaces of F-16.

Aileron, elevator and rudder are driven by servo-controlled actuators to produce deflections commanded by flight control system. Actuators of the control surfaces are modeled as first-order low-pass filters with certain gain and saturation limits in deflection angle and rate.

Table A-1: Control surface actuator models [2]

Symbol	Command Name	Deflection Limit	Rate Limit	Time Constant	Positive Sign Convention	Effect
δ_e	Elevator	± 25.0°	60°/s	0.0495s lag	Trailing edge down	Negative pitching moment
δ_a	Ailerons	± 21.5°	60°/s	0.0495s lag	Right-wing trailing edge down	Negative rolling moment
δ_r	Rudder	± 30.0°	60°/s	0.0495s lag	Trailing edge left	Negative yawing moment, positive rolling moment

Throttle position input has only an upper saturation limit of 1 and lower as 0 [2], [8]. Instead, the lag caused by the engine response is explained in Appendix A.3.

A.5 Sensor Model

Control system design for the aircraft necessitates measurement of the state variables in order to use them in the feedback loop. For the autopilot designs of the aircraft, all the state variables are assumed to be measurable with a time lag of 0.1s and so, transfer function of the simple sensor model that behaves as a LPF is given as follows:

$$G_F(s) = \frac{1}{1+0.1s}. \tag{A-16}$$

This LPF type sensor works as a noise filter that is used to remove the high frequency components of the signal being measured.

In addition to a sensor, a washout circuit is used on the output of the yaw rate sensor, in order to filter the steady-state component of the yaw rate during turns [2]. As a result, transfer function of the washout circuit is given below as a HPF whose time constant is 1s:

$$G_W(s) = \frac{s}{1+s}. \tag{A-17}$$

This kind of an HPF passes the signal changes that are faster than the time constant of the filter itself. More information about the sensor and the washout circuit and some implementations can be found in [2].

A.6 Additional Parameters for F-16 Model

Table A-2: Other parameters used in the model

Symbol	Parameter	Value	Unit
x_{cg_r}	Reference center of gravity location	1.2	m
g	Gravitational constant	9.8	m/s^2
h_{eng}	Engine angular momentum	216.9	$kg.m^2/s$
d_r	Radian-to-degree conversion factor	57.3	-

Table A-3: Mass and geometry properties

Symbol	Parameter	Value	Unit
W	Vehicle weight	9295.4	kg
b	Reference wing span	9.1	m
S	Reference wing area	27.9	m^2
$\bar{c}$	Mean aerodynamic chord	3.5	m
I_x	Roll moment of inertia	12874.8	$kg.m^2$
I_y	Pitch moment of inertia	75673.6	$kg.m^2$
I_z	Yaw moment of inertia	85552.1	$kg.m^2$
I_{xz}	Product moment of inertia	1331.4	$kg.m^2$
I_{xy}	Product moment of inertia	0	$kg.m^2$
I_{yz}	Product moment of inertia	0	$kg.m^2$

APPENDIX B. MISSILE DESIGN PARAMETERS

B.1 Actuators

Aileron, elevator and rudder are driven by servo-controlled actuators to produce deflections commanded by flight control system. Actuators of the control surfaces are modeled as first-order systems with the parameters and the structure shown in the table and the figure, respectively:

Table B-1: Control surface actuator models

Symbol	Command Name	Deflection Limit	Rate Limit	Time Constant
δ_e	Elevator	±10°	1200°/s	0.02s lag
δ_a	Ailerons	± 5°	1200°/s	0.02s lag
δ_r	Rudder	± 10°	1200°/s	0.02s lag

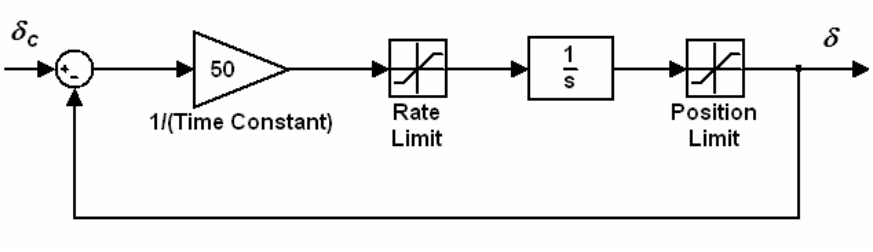

Figure B-1: Nonlinear control actuation system model

B.2 Sensor Model

Control system design for the missile necessitates measurement of the state variables in order to use them in the feedback loop, as in the case of aircraft. For the autopilot designs of the missile, all the state variables are assumed to be measurable with a time lag of 0.02 s and so, the transfer function of the simple sensor model that behaves as a LPF is given as follows:

$$G(s) = \frac{50}{s + 50}. \tag{B-1}$$

This LPF type sensor works as a noise filter that is used to remove the high frequency components of the signal being measured.